Modified Asymmetrically Clipped Optical Orthogonal Frequency Division Multiplexing (MACO-OFDM) System

Salma Darwish Abd Elaziz Mohamed

Department of Electronic and Electrical Engineering, University of Strathclyde

This dissertation is submitted for the degree of

Doctor of Philosophy

August 2015

I would like to dedicate this thesis to my lovely angel Habeeba ...

DECLARATION

This Thesis is the result of the author's original research. It has been composed by the author and has not been previously submitted for examination which has led to the award of a degree.

Salma Darwish Abd Elaziz Mohamed

August 2015

ACKNOWLEDGEMENTS

In the beginning, I would like to thank ALLAH for giving me the ability and strength to finish my work as without this I wouldn't have acheived this thesis.

First, I would like to dedicate this thesis to my dear father and mother for their support, love, and encouragement. They believed in me and devote their life to help me to succeed.

My inexplicable apperciation to my dear husband and my sweet little angel Habeeba for their continuous support, love, encouragement and motivation. Words are insufficient to explain how I am grateful for their presence in my life.

My deep gratitude to my supervisor, Prof. Ivan Andonovic, for his great help and support. He supported and encouraged me to pursuit my research. Many thanks to my supervisor, Prof. Hossam Shalaby, for his advices, patience and guidance which helped me through my study. Also, I would like to thank my third supervisor, Prof. Moustafa Hussein, for his help.

I would like to acknowledge Prof. Harald Haas, from the Institute for Digital Communications (IDCOM) at the University of Edinburgh, UK, and his research group especially Dobroslav for their continuous help.

Finally, I would like to thank Prof. Ihab Badran, and Dr. Heba Shaban, from college of engineering, at Arab Academy for Science, Technology and Maritime Transport, Egypt, for their help and guidance.

ABSTRACT

A modification to the Asymmetrically Clipped Optical OFDM (ACO-OFDM) technique, a well reported non-coherent optical implementation is proposed. A Modified ACO-OFDM (MACO-OFDM) system is developed to improve system performance at the expense of spectral efficiency. A MACO-OFDM system model is defined underpinned by a detailed mathematical framework verified through Monte Carlo simulations. System performance is compared to that of conventional ACO-OFDM. A 1.5 dB saving is achieved in the Bit Error Rate (BER) performance of 4-QAM ACO-OFDM after applying the proposed modification; the theoretical and simulation results are in good agreement. As the constellation size increases, the improvement in BER performance decreases.

The research then treats the impact of atmospheric turbulence on the performance of both conventional ACO-OFDM and the proposed MACO-OFDM system. A Single Input Multiple Output (SIMO) approach using multiple receivers is employed to mitigate the impact of atmospheric turbulence. The performance of MACO-OFDM outperforms that of ACO-OFDM by nearly 3 dB, 4 dB, and 5 dB as the number of receiving apertures (nRx) increases as 1, 2, and 4 respectively in weak atmospheric turbulence; in moderate turbulence the performance is improved by 2 dB, and 4.5 dB for nRx=2, and nRx=4; and in strong turbulence, the BER performance is enhanced by nearly 2 dB and 4 dB for nRx=2 and nRx=4.

The channel capacity of MACO-OFDM has been shown to be half that of conventional ACO-OFDM. The capacity of SIMO MACO-OFDM architecture in atmospheric turbulent channel is evaluated.

TABLE OF CONTENTS

LIST OF FIGURES

LIST OF TABLES

LIST OF ABBREVIATIONS

ACO-OFDM	Asymmetrically-Clipped Optical Orthogonal Frequency Division Multiplexing
AWGN	Additive White Gaussian Noise
BER	Bit Error Rate
BPSK	Binary Phase Shift Keying
CLT	Central Limit Theorem
CO-OFDM	Coherent Optical Orthogonal Frequency Division Multiplexing
DCO-OFDM	DC- Biased Optical Orthogonal Frequency Division Multiplexing
DDO-OFDM	Direct Detection Optical Orthogonal Frequency Division Multiplexing
DSP	Digital Signal Processing
FDM	Frequency Division Multiplexing
FFT	Fast Fourier Transform
ICI	Inter-Carrier Interference
IFFT	Inverse Fast Fourier Transform
IID	Independent and Identically Distributed
IQ	Inphase and Quadrature
IR	Infrared
ISI	Inter-Symbol Interference
LOS	Line-of-Sight
MACO-OFDM	Modified Asymmetrically-Clipped Optical Orthogonal Frequency Division Multiplexing

MRC	Maximal Ratio Combining
NLD	Nonlinear Distortion
OFDM	Orthogonal Frequency Division Multiplexing
O-OFDM	Optical Orthogonal Frequency Division Multiplexing
OTR	Optical to RF
pdf	Probability Density Function
PSK	Phase Shift Keying
QAM	Quadrature Amplitude Modulated
RF	Radio Frequency
RTO	RF to Optical
SIMO	Single Input Multiple Output
SISO	Single Input Single Output
SNR	Signal to Noise Ratio
U-OFDM	Unipolar Orthogonal Frequency Division Multiplexing

LIST OF SYMBOLS

f_c	Carrier Frequency
A_k^m	Square M-QAM symbols of the k^{th} subcarrier
x_n^m	IFFT output time domain signal
σ_x^2	Variance of the time domain bipolar MACO-OFDM
μ_{np}	Covariance of two samples of MACO-OFDM
σ_s^2	Average power of MACO-OFDM signal
R_b	Bit rate of MACO-OFDM signal
σ_n^2	AWGN power
$m_{correct}$	Mean of the correct detected sample
$v_{correct}$	Variance for correctly detected sample
m_{wrong}	Mean of the wrong detected sample
$\sigma_{n_{correct}}^2$	Variance of the noise due to the non-linear transformation in case of correct detection
$\sigma_{n_{wrong}}^2$	Variance of the noise due to the non-linear transformation in case of wrong detection
$P_{correct}$	Probability of correct detection
P_{wrong}	Probability of erroneous detection
$g_{average}$	Average gain factor
$N_{average}$	Average noise variance
l_o	Inner scale eddies
L_o	Outer scale eddies
C_n^2	Index of refraction structure parameter
I_o	Irradiance intensity in no turbulence

σ_l^2	Log irradiance variance
L_p	Link length
R_F	Fresnel zone
$K_n(..)$	Modified bessel function of the second kind of order n
$\tilde{H}_n$	Gamma-gamma channel coefficient matrix
$\tilde{H}_n^H$	Hermitian transpose of gamma-gamma channel coefficient matrix
M_t	Number of transmitting source
C	Shannon's Channel Capacity
I	Irradiance intensity
K	Wave number
N	Size of IFFT/FFT
R	Average number of bits
α	Effective number of large eddies
B	Effective number of small eddies
$\Gamma(\ldots)$	Gamma function

CHAPTER 1

INTRODUCTION

1.1 Motivation

Wireless optical communications is fast becoming a viable alternative to Radio Frequency (RF) implementations due to, in addition to provisioning very high data in the order of G/bits per second, licence-free spectrum operation which facilitates rapid, low cost deployments. Wireless optical implementations operate at visible or invisible eye-safe light using low power lasers.

Each optical wireless unit consists of a transceiver comprising an optical source plus a lens or a telescope transmitting light signals through air to another lens within the receiver. The receiving telescope is the front-end to a high-sensitivity receiver connected via an optical fibre. Full duplex i.e. bi-directional data flow is provided. The laser beam is engineered to be low divergence and for optimum performance, it is advantageous to operate Line-of-Sight (LOS) between wireless transceivers for maximum data rate provisioning (Figure 1.1). In this research LOS is considered between the transmitter and receiver. Optical wireless systems have been reported to function over distances of several kilometres at acceptable data rates [1].

Like optical fibre systems, optical wireless utilises lasers as the carrier of data, but instead of enclosing the data stream in a glass fibre enjoying constant, well understood channel characteristics, signals are transmitted through air. Light travels through air faster than through glass, so it is fair to classify wireless optical technology as communications at the speed of light [1, 2].Viable wireless optical data transport occurs as long as there is a clear path between source/destination and sufficient power at the transmitter. Given the nature of light, interception stealthily is difficult, providing a certain level of data security[2]. Data can also be transmitted encrypted enhancing the degree of security [2].

Wireless optical requires no spectrum license to operate. As the optical signal propa-

Fig. 1.1 Line of sight (LOS) optical system :http://www.google.co.uk/imgres?imgurl=http://www.wavecomgroup.com/images/beam21.gif&imgrefurl=http://www.wavecomgroup.com/Cablefree_FreeSpace.htm&h=245&w=401&tbnid=jNHSFLM--PYUDM:&zoom=1&docid=QwvHOWKXoV1G-M&itg=1&ei=wXveVJTUMePg7Qa_rIDQAg&tbm=isch&ved=0CFoQMygvMC8 .

gates in air, the performance is highly impacted by the prevailing atmospheric conditions. The atmospheric channel is dynamic and the optical signal is affected by rain, fog, temperature and dust [2, 3]. One of the major atmospheric effects is scintillation [2, 3], random fluctuations in the receiving optical signal level arising from atmospheric turbulence. The turbulence strength and hence its impact on system performance is measured by a factor referred to as the 'scintillation index'; the turbulence strength is classified as weak, moderate, or severe [2–4]. It is worth noting that the performance of wireless optical systems in weak and moderate turbulence has been studied in the literature. However, little has been reported for the case of severe turbulence even though it is important to evaluate the upper bound on system performance.

One of the most recently developed multi-carrier modulation schemes is Orthogonal Frequency Division Multiplexing (OFDM). OFDM has been successfully adopted in many wired and wireless communications systems because of a number of advantages; OFDM is spectrally efficient, has an inherent robustness against narrowband interference, employs relatively simple equalization techniques compared to single-carrier systems and provides excellent robustness in multipath environments [5–8]. The addition of a cyclic prefix to the beginning of the OFDM symbol improves system robustness to both inter-symbol and inter-carrier interference as the prefix preserves orthogonality between sub-carriers. Inter-symbol interference is a distortion in a signal caused when symbol interferes with subsequent symbols; inter-carrier interference arises from carrier frequency offsets owing to the Doppler spread due to channel time variation.

In spite of the widespread analysis of OFDM in wireless communications and its recorded advantages, it has only recently been the focus of serious commercial development as latterly, the maturity and functionality of Digital Signal Processing (DSP) technologies makes its implementation is feasible and cost effective. OFDM has also been proven to be effective in combating dispersion in optical transmission media, allowing the transmission at very high data rates through optical fibre [9]. In terms of optical OFDM (O-OFDM), two classes of systems have been defined; Coherent Optical OFDM (CO-OFDM) and Direct Detection (incoherent) Optical OFDM (DDO-OFDM) (Figure 1.2).

The former draws on classical coherent techniques with an additional laser source at the

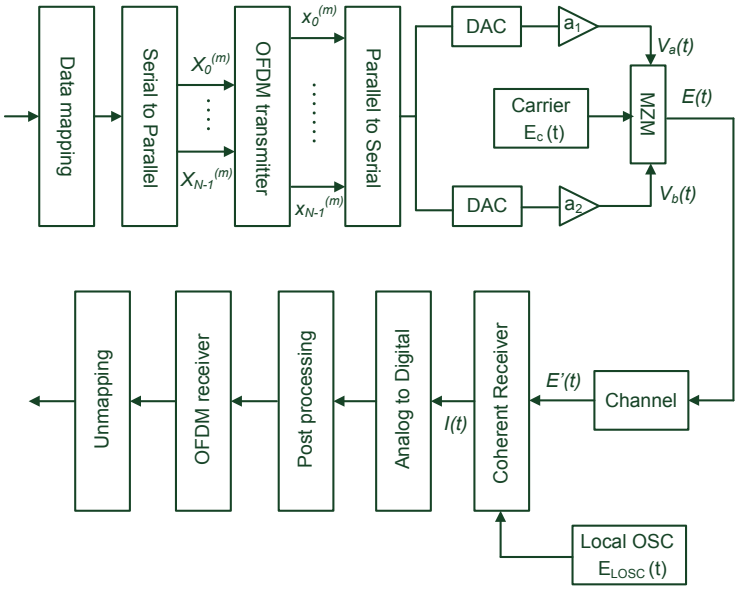

Fig. 1.2 Block diagram of Coherent Optical OFDM [10].

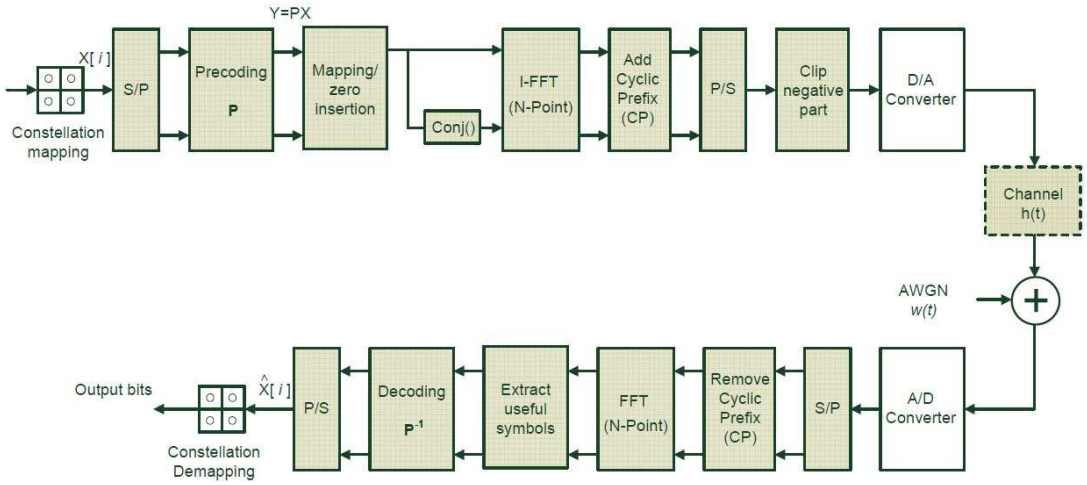

Fig. 1.3 Block diagram of DDO-OFDM system .

receiver to locally generate the carrier; like past coherent systems, performance is governed highly by the coherence of the laser i.e. it is sensitive to phase noise. In the case of DDO-OFDM, the OFDM signal is transmitted as an intensity level on the optical carrier which translates into a much simpler receiver but at the expense of more optical power and the use of guard bands between the optical carrier and the OFDM sub-carriers (Figure 1.3).

The research focusses on DDO-OFDM as the phase and irradiance fluctuation suffered by the traversing beam through air makes optical coherent detection more onerous, sensitive to both signal amplitude and phase fluctuations [4].

Table 1.1 summarises the advantages and disadvantages of the two regimes of operation.

Table 1.1 Comparison between CO- OFDM and DD-OFDM systems.

OFDM System type	Advantages	Disadvantages
CO-OFDM	high spectral efficiency , high receiver sensitivity , and robustness against polarization dispersion	sensitive to phase noise , needs additional laser at the receiver, and 3- complexity of receiver.
DD-OFDM	simpler receiver	more optical power and the use of gaurd band between the optical carrier and the subcarriers

1.2 Contributions

A number of contributions can be identified arising out of the research;

- A modification to Asymmetrically Clipped Optical Orthogonal Frequency Division Multiplexing (MACO-OFDM) using unipolar encoding is developed to improve the Bit Error Rate (BER) performance of the ACO-OFDM technique.
- the BER performance of MACO-OFDM is analysed mathematically and validated through Monte Carlo simulations assuming Additive White Gaussian Noise (AWGN). The performance is compared with analytical results
- A comparison of BER performance between MACO-OFDM and ACO-OFDM is carried out

- The BER performance of both systems is investigated in an atmospheric turbulent channel

- The use of maximal ratio combining receiver is proposed to mitigate the impact of atmospheric turbulence on the performance of both systems; their performance is compared

- The capacity of MACO-OFDM is evaluated assuming the channel is subject to AWGN, atmospheric turbulence and with receiver diversity

1.3 Thesis Outline

The Dissertation is organised as follows. Chapter 2 introduces the history of optical wireless communications. The principles of OFDM are presented, the system configuration under evaluation is defined followed by a description of the foundation of optical OFDM supported by a summary of the range of implementations.

A modification to ACO-OFDM (MACO) that improves system performance is proposed in Chapter 3. The MACO-OFDM system model is presented and the mathematical framework established to analyse system performance is introduced. The BER performance of MACO-OFDM is then estimated and compared to conventional ACO-OFDM.

MACO-OFDM performance subject to atmospheric turbulence is then discussed in Chapter 4. An introduction on atmospheric turbulence, and the validity of both the log normal and gamma-gamma models are presented. A summary of reported research on O-OFDM system performance under atmospheric turbulence and ACO-OFDM and MACO-OFDM system performance in the range of weak to strong atmospheric turbulence is estimated.

Chapter 5 introduces the use of Multiple-Input-Multiple-Output (MIMO) techniques in conjunction with OFDM systems to improve system performance impacted by a turbulent channel. A range of diversity techniques is introduced and a Single-Input-Multiple-Output (SIMO) O-OFDM system model is developed. A performance analysis comparison owing to the introduction of SIMO is presented.

The capacity of MACO-OFDM is discussed in Chapter 6. MACO-OFDM capacity subject to AWGN is evaluated and compared to that of ACO-OFDM. The capacity of SIMO MACO-OFDM under different atmospheric turbulence regimes is estimated.

Chapter 7 concludes on the findings of the research and the potential range of future work is discussed.

1.4 Publications

The following publications arose out of the research;

- Salma D. Mohamed, Ivan Andonovic, Hossam Shalaby, Moustafa Hussien, "Modified Asymmetrically-Clipped Optical Orthogonal Frequency-Division Multiplexing System Performance," IEEE Photonics Conference (IPC), pp. 289-290, 8-12th Sept. 2013, Bellevue, WA.
- Salma D. Mohamed, Haitham Khallaf, Hossam Shalaby, Ivan Andonovic, Moustafa Hussien," Two Approaches for the Modified Asymmetrically Clipped Optical Orthogonal Frequency Division Multiplexing System," Electronics, Communications and Computers (JEC-ECC), 2013, 17-19th Dec. 2013, Egypt.

CHAPTER 2

BACKGROUND

2.1 Introduction

Optical wireless communications is gaining popularity as a viable approach to provisioning data. Research and development in the discipline has accelerated recently due to the huge growth in the number of information terminals and portable devices in outdoor as well as indoor environments[11].

Optical wireless has a number of advantages, offering an abundance of unregulated bandwidth, 200 THz in the 700 nm - 1500 nm wavelength range. The system components are small, light and relatively low cost. The implementation is considered as 'health friendly' since issues of RF interference are obviated, there are no RF radiation hazards which in turn opens up the applications spectrum and it is relatively easy to install (an advantage with any wireless system). Optical wireless implementations operate at visible or invisible eye-safe light levels, so interception stealthily is difficult, providing a certain level of data security and robustness to classical anti-jamming. In the case of outdoor wireless optical, the optical transceiver is highly directional, utilising cone shaped laser beams mounted at heights to provide Line-of-Sight (LOS) clearance between transceivers [2]. In the case of RF links, the signal radiates in all directions providing a wide receiving range. When using the near infrared (near-IR) range of 750nm - 950 nm, the transmitted signal intensity has to be limited by eye safety standards; the eye safety requirement is relaxed at the higher wavelength range of 1550 nm as the human eye is less sensitive to light [4].

2.2 History of Optical Communications

Information transmission using optical signal has been in use since ancient times [3]. Message transmission using optical signals were recorded during the Grecian siege of Troy in

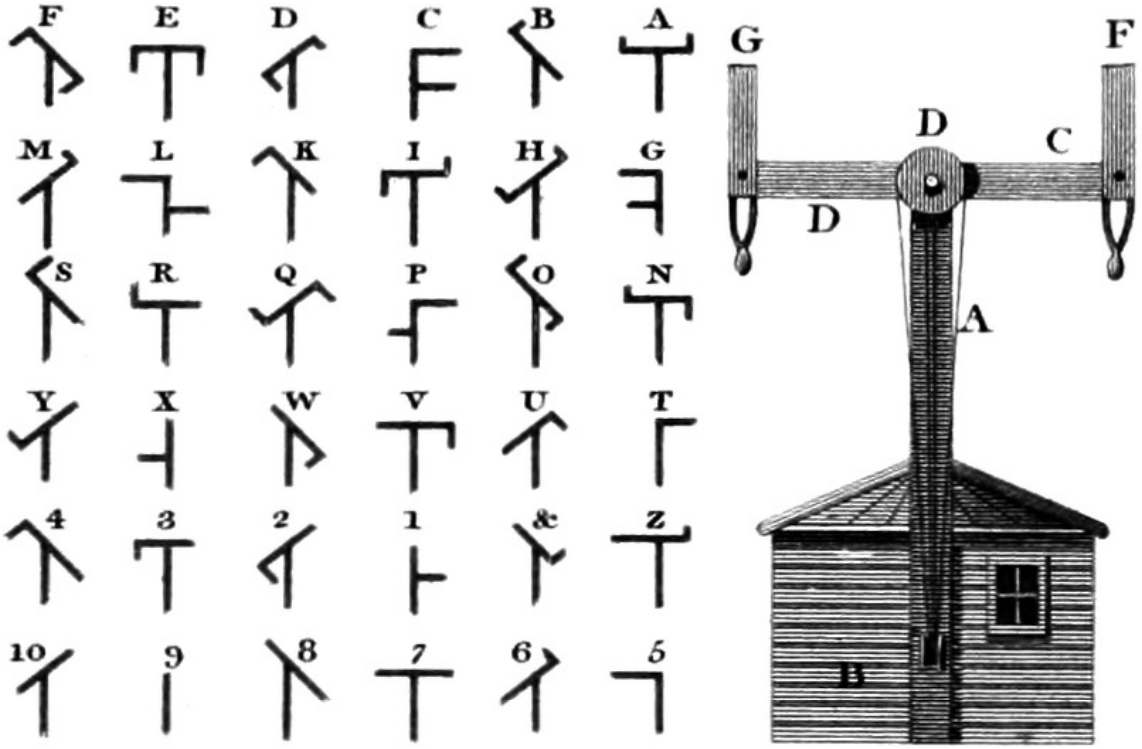

Fig. 2.1 A semaphore tower invented by Claude Chappe in 1972 [12]

1200 BC [3]. In 150 BC, smoke signals were used commonly by American Indians to transmit messages [4]. Optical telegraphy was invented by Claude Chappe in early 1790's [12], enabling the transmission of messages over distances of hundreds of kilometres in minutes by changing the orientation of the signalling "arms" on a large tower (Figure 2.1).

In 1880, Alexander Graham Bell invented the photo-phone recognised as the first optical communication through an unguided channel (Figure 2.2). The system used sun radiation to carry a voice signal over a distance of 200 m. The receiver comprised a parabolic mirror with a selenium photo-cell located at its focal length. The experiment was compromised due to the materials of the devices used and the absence of sun radiation [3, 4].

Lightwave communications experiments were conducted during both world wars [3], but more striking success with radio and radar arrested any further developments. It was not until the invention of the laser, new suites of semiconductor devices and optical fibres in the 1960s that optical communications finally became the subject of massive research and development [13]. The modern era of indoor optical communication can be traced back to 1979 to the work of Gfeller and Bapst who used diffuse emission in the infrared band as the carrier source [3].

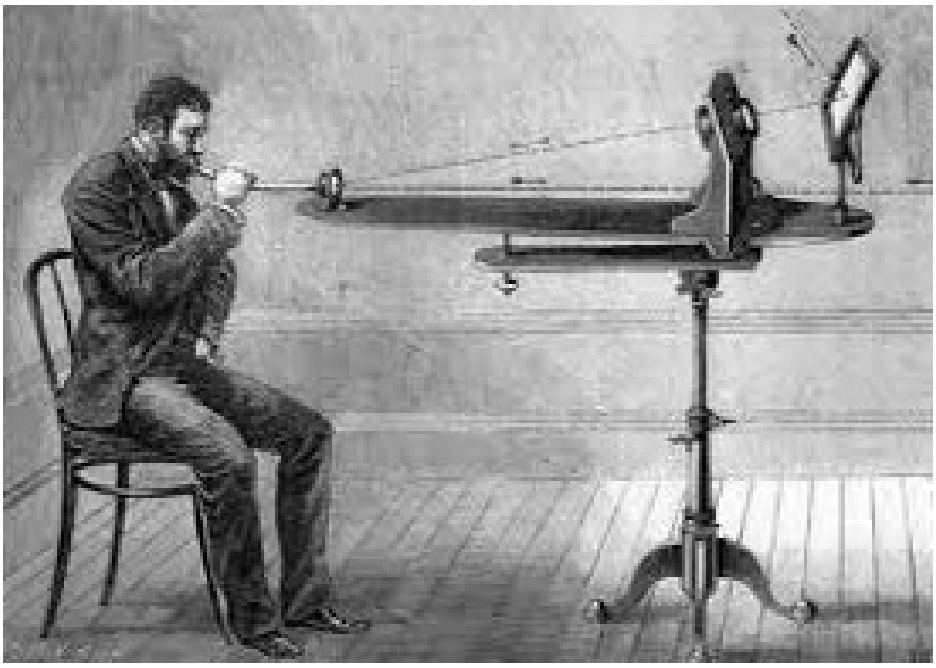

Fig. 2.2 The photophone by Alexander Graham Bell and Charles Sumner Tainter, [3]

During the last thirty years great strides have been made in electro-optics. Light beam communications devices are now finding their way into many common appliances, telephone equipment and computer systems [13]. On-going defence research programs have led to some major breakthroughs in long range optical communications. Ground-station to orbiting satellite optical links are already transporting key data as well as very long range satellite to satellite communications [13]. Today, with the ever decreasing cost of critical components, a system to transmit and receive audio, television or even high speed computer data over long distances can be realised for use in many consumer–led applications [4].

2.3 Orthogonal Frequency Division Multiplexing (OFDM)

Although the concept of Orthogonal Frequency Division Multiplexing (OFDM) has been the subject of extensive research for several decades, only recently has it been integrated into modern communications system implementations [5]. Owing to a compelling list of advantages, OFDM has been successfully adopted in a range of wired and wireless communications systems. OFDM is spectrally efficient, has an inherent robustness against narrowband interference, employs a simple equalisation technique compared to single-carrier systems, and is highly robust to multi-path environments. Further, the simple addition of a cyclic prefix to the start of the OFDM symbol can mitigate the impact of both inter-symbol and

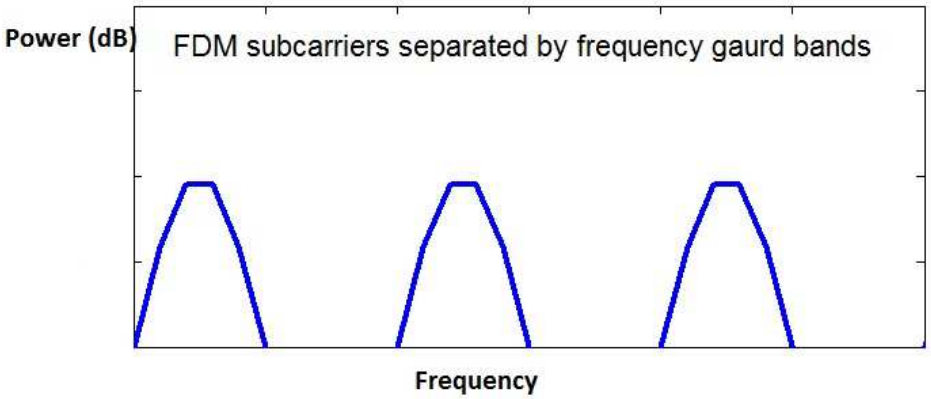

Fig. 2.3 Spectrum of FDM signals .

inter-carrier interferences as the cyclic prefix preserves orthogonality between sub-carriers [5–8]. Recently, a cyclic prefix in some OFDM systems is not used as it reduces the effective data capacity and overall data rate.

2.3.1 OFDM Principles

To better understand the principles of OFDM, it is important to introduce Frequency Division Multiplexing (FDM), a single carrier modulation [5] which then allows the differences with multi-carrier variants such as OFDM to be accentuated.

Single carrier modulation transmits information on only one carrier by modulating its amplitude, phase, or frequency. In the case of digital signals, data is transmitted in the form of bits; each group of bits are referred to as symbols [14]. For high data rates, the duration of one symbol becomes small, rendering it more susceptible to impulse noise and other impairments [15, 16]. These impairments degrade the performance of the system, hindering the recovery of the original data. As the bandwidth of the single carrier increases, the system becomes subjected to increased levels of interference from other constituent signals; this interference is referred to as frequency or carrier wave [8].

FDM extends the concept of single carrier modulation through the use of multiple sub-carriers. The total data rate is now divided amongst different subcarriers; the data does not have to be divided equally or to be from the same data source. FDM has many advantages over single carrier modulation. Narrowband frequency interference only affects one of the sub-carriers not the entire signal. As each sub-carrier supports a lower data rate, the symbol duration is much longer, in turn increasing robustness to impulse noise and reflections [5, 14] (Figure 2.3).

FDM systems use guard bands to prevent interference between the spectrums of adjacent

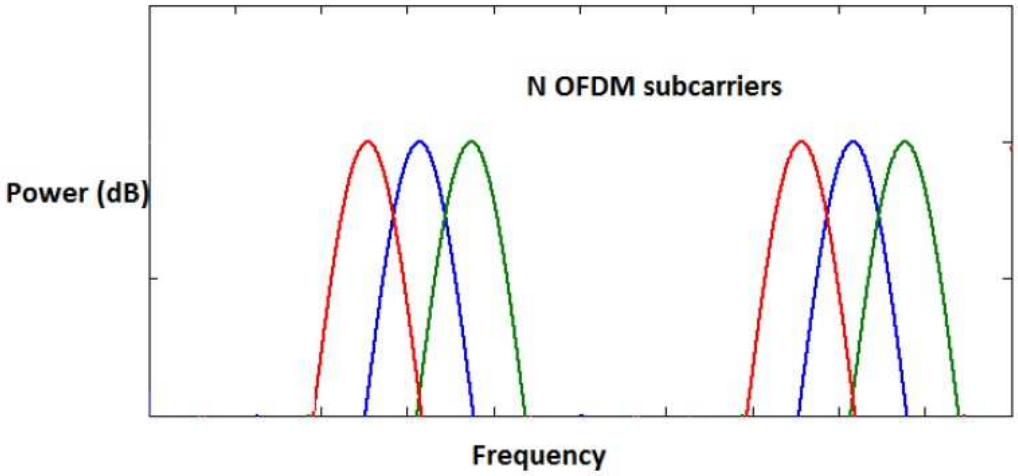

Fig. 2.4 Spectrum of OFDM signals .

sub-carriers, thus lowering the effective data rate in comparison to single carrier systems with the same modulation.

2.3.1.1 Orthogonality and FDM

An increase in the spectral efficiency of systems results if FDM utilises orthogonal sub-carriers [5]. The use of guard bands between subcarriers is now removed as the spectrum of sub-carriers can overlap without compromising the demodulation as long orthogonality is maintained (Figure 2.4). Orthogonality is defined as when the dot product of two deterministic signals is equal to zero or if two random processes are uncorrelated [5]. Routinely, the Inverse Fast Fourier transform (IFFT) is employed to obtain orthogonal sub-carriers [6, 9] (Figure 2.4).

The sinusoids of the IFFT form an orthogonal basis set, and a signal in vector space is expressed as a linear combination of orthogonal sinusoids. The input signal is correlated with each of the IFFT basis functions. If the input signal has energy at a certain frequency, then the correlation between the signal and the basis functions have a peak value at the corresponding frequency [5]. This process takes place at the OFDM transmitter to map an input signal onto a set of orthogonal sub-carriers viz. the IFFT basis functions.

The same transform takes place at the OFDM receiver to process the received sub-carriers. The signals from different sub-carriers are then combined to form an estimation of the original signal. As the basis functions are orthogonal, the correlation yields peak values only at the corresponding frequency. The other sub-carriers are uncorrelated and consequently do not contribute energy to the signal; thus the sub-carrier spectrums can overlap without creating interference [5, 6, 9].

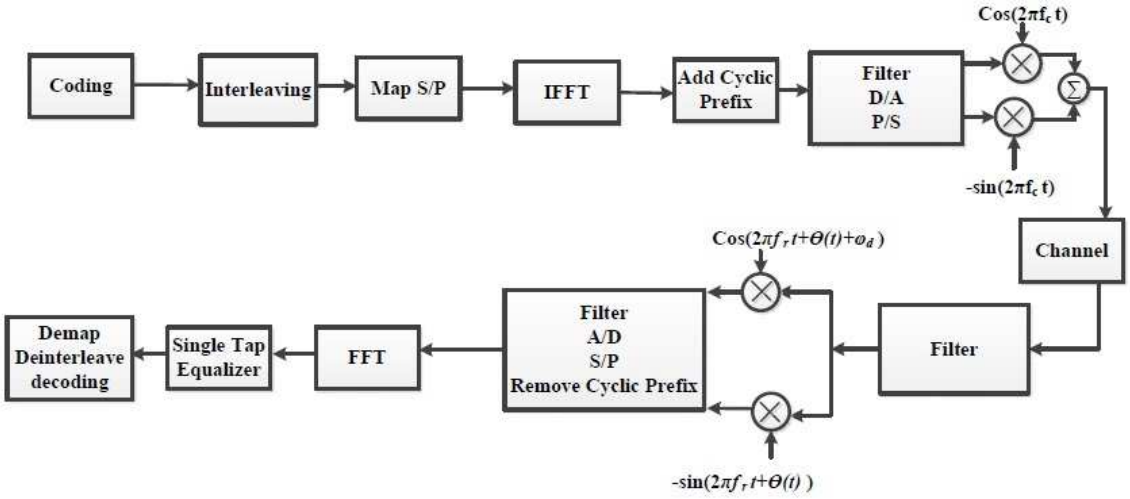

Fig. 2.5 Block diagram of an OFDM comminucation system for RF wireless systems.

2.3.2 OFDM System Configuration

Figure 2.5 shows a block diagram and the main components of a typical wireless OFDM system.

The blocks within the transmitter execute coding and interleaving. Usually, all OFDM systems employ error correction as frequency selective fading in the channel results is some parallel data streams creating deep fading. After coding, the data is Quadrature Amplitude Modulated (QAM) [9] modulated, in so doing mapping the signal onto complex samples. The output of the modulator block comprises serial to parallel converted streams for input to the IFFT. A cyclic prefix is then added to the output of IFFT block. The output of the stage that merges filtering, parallel-to-serial and digital-to-analogue conversion is a band-limited signal consisting of sinusoids of the baseband sub-carriers frequencies. The In-phase Quadrature (IQ) modulator [9] is used for up-conversion to the carrier frequency of f_c and f_r at the transmitter and the receiver respectively. Usually both frequencies are equal but in practice there may be some difference. At the receiver, the signal is down-converted by mixing the IQ components with a locally generated carrier. Any constant error in the absolute phase in the $\theta(t)$ at this stage can be corrected through the use of single tap equaliser [9].

2.3.2.1 Fast Fourier Transform (FFT) and Inverse Fast Fourier Transform (IFFT)

The main difference between OFDM compared to a single carrier system is the Inverse Fast Fourier Transform (IFFT) and Fast Fourier Transform (FFT) [9] at the transmitter and receiver respectively. In spite of the fact that Phase Shift Keying (PSK) [9] is compatible

with OFDM, it is rarely used as for large constellations the points are closer to each other and consequently subject to more noise. Also, a constant signal envelope is not presented. Thus, QAM [6, 9, 14] is usually most often used with OFDM, thus the input X to the IFFT block is complex such that $X = [X_0 X_1 X_2 .....X_{N-1}]$. The length of X is N, where N is the size of IFFT. Every element of X has a specific subcarrier to be carried on, such that X_k represents the data to be carried on the k_{th} subcarrier.

The output of IFFT is $x = [x_0 x_1 x_2 .....x_{N-1}]$ where the definition of the inverse discrete Fourier transform is [9];

$$x_m = \frac{1}{\sqrt{N}} \sum_{k=0}^{N-1} X_k exp\left(\frac{j2\pi km}{N}\right) \tag{2.1}$$

where $0 \leq m \leq N-1$ and $0 \leq k \leq N-1$. .

The forward Discrete Fourier transform can be defined as;

$$X_k = \frac{1}{\sqrt{N}} \sum_{m=0}^{N-1} x_m exp\left(\frac{-j2\pi km}{N}\right) \tag{2.2}$$

The IFFT/FFT pair ensures that the total energy and the average power of every OFDM frame at the input and the output of the transform is kept the same [9].

At the receiver, a FFT is carried out on the received sampled data for each symbol;

$$Y_k = \frac{1}{\sqrt{N}} \sum_{m=0}^{N-1} y_m exp\left(\frac{-j2\pi km}{N}\right) \tag{2.3}$$

where $0 \leq k \leq N-1$, $y_m = [y_0 y_1 y_2 .....y_{N-1}]^T$ is the input time domain received sampled data at the receiver FFT block, and $Y_k = [Y_0 Y_1 Y_2 .....Y_{N-1}]^T$ is the discrete frequency domain vector at the output of FFT. If there is no noise or distortion, then $Y = X$ as FFT and IFFT are transform pair.

If the signal is not distorted but subject to Additive White Gaussian Noise (AWGN) [6, 7, 9, 14], then the signal takes the form;

$$y_m = x_m + w_m \tag{2.4}$$

where w_m is a AWGN sample.

By substituting Equation 2.4 into Equation 2.3 then Y_k takes the form;

$$Y_k = \frac{1}{\sqrt{N}} \sum_{m=0}^{N-1} y_m exp\left(\frac{-j2\pi km}{N}\right) = X_k + W_k \tag{2.5}$$

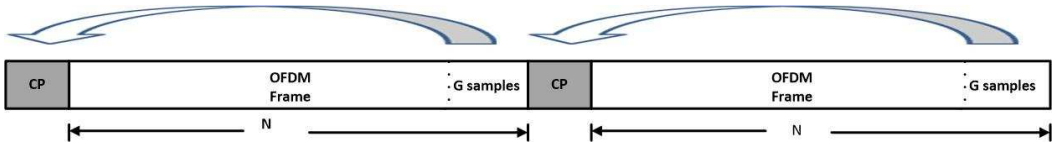

Fig. 2.6 Time domain sequence of OFDM frames showing the cyclic prefix.

where

$$W_k = \frac{1}{\sqrt{N}} \sum_{m=0}^{N-1} w_m exp\left(\frac{-j2\pi km}{N}\right) \tag{2.6}$$

For $0 \leq k \leq N-1$, W_k is the k_{th} noise component at the receiver FFT output. W_k is the sum of N independent white Gaussian Noise samples w_m, and is considered as independent Gaussian process. w_m does not have to follow a Gaussian distribution; however W_k follows a Gaussian distribution owing to the central limit theorem (C.L.T) [7, 9, 14, 17].

2.3.2.2 Cyclic Prefix

A cyclic prefix x is normally used within an OFDM symbol as it mitigates both inter-symbol interference (ISI) and inter-carrier interference (ICI) whilst easing equalisation as it is only single tap[9, 14, 15]. The cyclic prefix is implemented by adding a number of the samples from the end of each frame to the start of the time domain frame before transmission; in Figure 2.6, G samples are added to the start of each OFDM frame.

2.3.3 RF OFDM System Performance

The BER performance of Binary Phase Shift Keying $(BPSK)$ [18]and QAM OFDM [19] are presented in Figure 2.7 and Figure 2.8 to illustrate the differences in performance of these systems and for future reference, serving to aid a comparison with the optical implementations developed in the research.

The BER performance of BPSK OFDM is inferior to that of M-QAM OFDM. As expected, the latter's performance degrades as the modulation order increases.

2.4 Optical Orthogonal Frequency Division Multiplexing (O-OFDM)

Despite of the widespread use of OFDM in RF wireless communications, it has only recently been the subject of development in respect of optical links [9]. The evolution of the

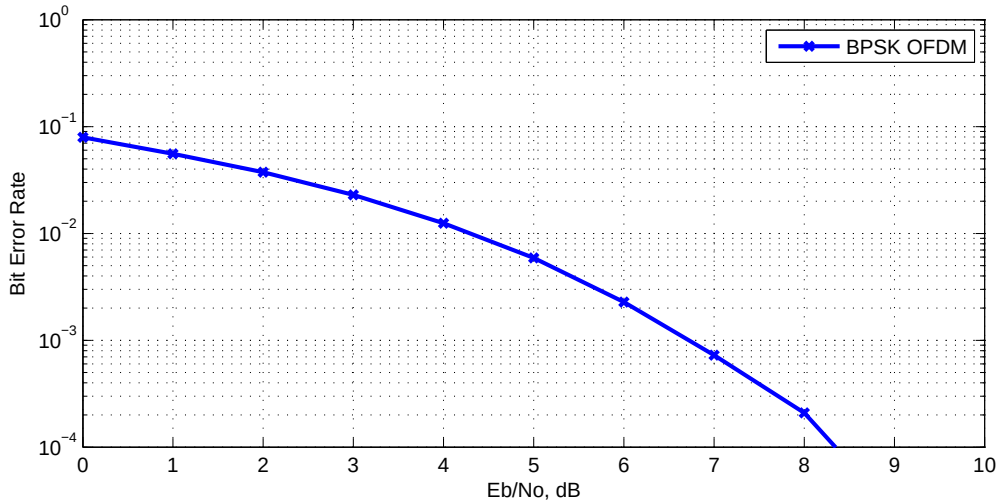

Fig. 2.7 BER performance of BPSK OFDM.

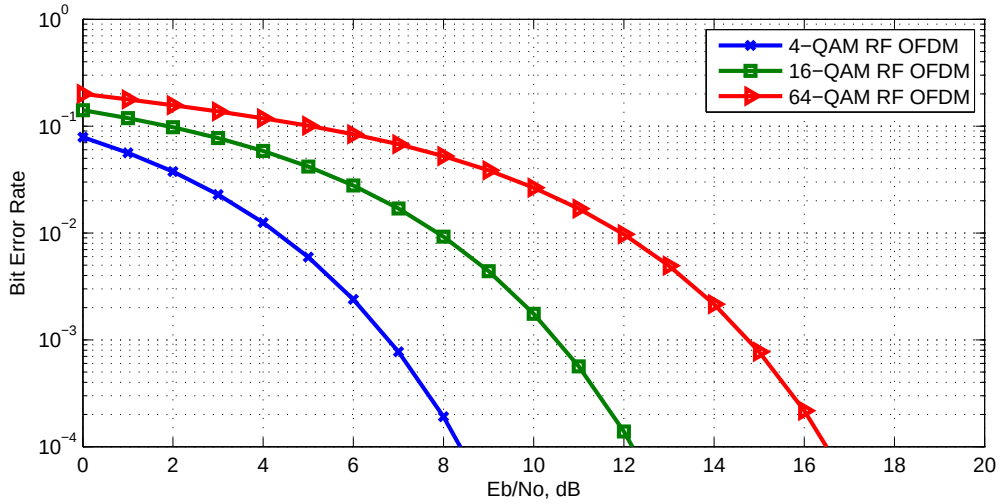

Fig. 2.8 BER performance of M-QAM OFDM.

discipline has to a great extent, been gated by developments in digital signal processing (DSP) technologies, enabling highly complex processing to be executed to manage system impairments at low cost e.g. combatting the effect of dispersion in optical media especially in multi-carrier scenarios such as OFDM which in turn facilitates transmission at very high data rates [9].

In terms of optical OFDM ($O-OFDM$), two classes of systems have been defined; coherent optical OFDM ($CO-OFDM$) and direct detection, non-coherent optical OFDM ($DDO-OFDM$). The former draws on classical coherent techniques with a laser source at the receiver to locally generate a carrier; like RF systems, performance is governed significantly by the coherence of the laser i.e. it is sensitive to phase noise. CO-OFDM provides high spectral efficiency, enhanced receiver sensitivity and robustness against polarisation dispersion. To achieve high spectral efficiency, the spectrum of sub-carriers is over-lapped by avoiding interference through the use of coherent detection and signal orthogonality. A typical CO-OFDM consists of five main components: RF OFDM signal transmitter, RF to optical (RTO) up-converter, fibre link, optical to RF (OTR) down-converter, and RF OFDM receiver. The complexity of CO-OFDM makes it less attractive [20].

In the case of DDO-OFDM, the OFDM signal is transmitted as an intensity level on the optical carrier which translates into a much simpler receiver implementation but at the expense of more optical power and the use of guard bands between the optical carrier and the OFDM sub-carriers [9, 14]. In this research, the focus is on DD-OOFDM. Table 2.1 summarises the main differences between DDO-OFDM and RF-OFDM systems.

Table 2.1 Comparison between a typical OFDM system and IM/DD optical system.

IM/DD Optical System	Typical OFDM System
Unipolar	Bipolar
Information carried on optical intensity	Information carried on electrical field
No local oscillator (laser) at the receiver	Local oscillator at the receiver
Direct detection	Coherent detection

2.4.1 O-OFDM Techniques

Since intensity modulation and direct detection is the basis of any incoherent optical system and due to the fact that OFDM signal is complex, several techniques have been developed to convert the signal into the real, positive domain to modulate the source for onward transmission through an optical channel. Hermitian symmetry is employed to ensure that the OFDM

signal is real but the signal still retains its bipolar information [15, 16, 21–28].

Many techniques have been proposed in literature to make the signal positive such as, DC- Biased Optical OFDM $(DCO-OFDM)$ [15, 16, 21, 22], Asymmetrically-Clipped Optical OFDM $(ACO-OFDM)$ [15, 16, 21–28], Unipolar OFDM (U-OFDM) [29] and Flip OFDM [30, 31].

2.4.1.1 DCO-OFDM

With intensity modulation/direct detection, a complex signal has to be represented as real and positive. Any method selected has an associated set of conditions which in turn impose a level of degradation on performance. In O-OFDM implementations, Hermitian symmetry is invoked in most cases such that the output of the IFFT is real but not necessarily positive.

One approach to obtaining a positive signal is to add a suitable DC bias and the elements of the signal that remain negative are clipped to zero level (DCO-OFDM). The processed OFDM signal then intensity modulates the source for transmission. On reception, the DC bias is subtracted from the received signal after photo-detection at the receiver. The processed signal is then input to a FFT. Nonlinear distortion (NLD) noise is introduced due to clipping [15, 16, 21, 22].

2.4.1.1.1 System Model

Figure 2.9 shows the DCO-OFDM block diagram. Assuming QAM modulation, let A_k^m represents data samples from square QAM constellation[15, 16, 21, 22]. m represents the OFDM symbol number, while $k = 0,1,2,3,.....,N-1$ denotes the subcarrier number in each OFDM frame. Hermitian symmetry is imposed to obtain a real time domain signal after the IFFT operation as shown in Figure 2.10 such that for $k \neq 0, N/2$ [21]

$$A_k^m = \left(A_{N-k}^m\right)^* \tag{2.7}$$

Also, the subcarriers at $k = 0, N/2$ are set to zero such that;

$$A_0^m = A_{N/2}^m = 0 \tag{2.8}$$

Each OFDM frame is then inputted to the IFFT to transform N complex samples to N real samples. The IFFT output time domain signal x_n^m is;

$$x_n^m = \frac{1}{\sqrt{N}} \sum_{k=0}^{N-1} A_k^m exp\left(\frac{j2\pi kn}{N}\right) \tag{2.9}$$

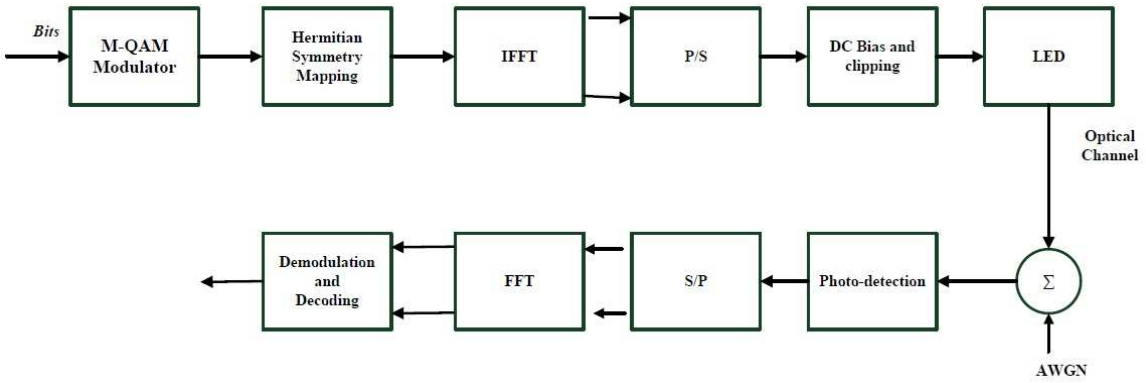

Fig. 2.9 Block diagram of an DCO-OFDM comminucation system .

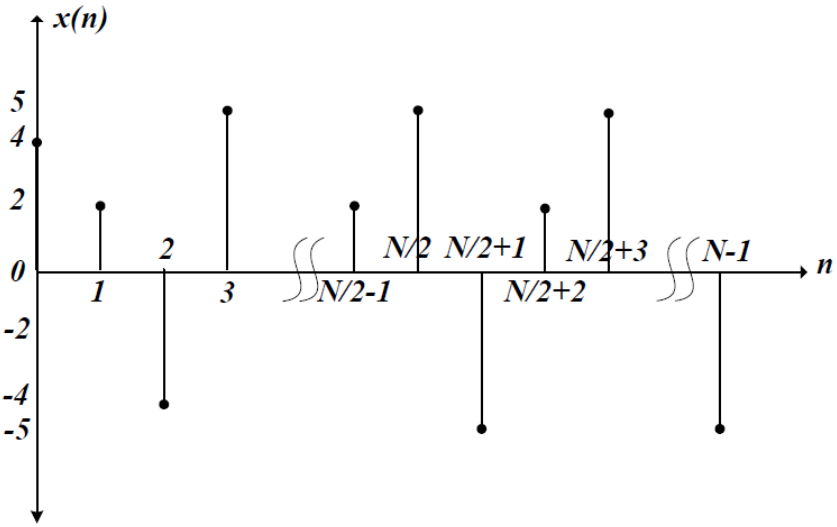

Fig. 2.10 Bipolar time domain DCO-OFDM signal.

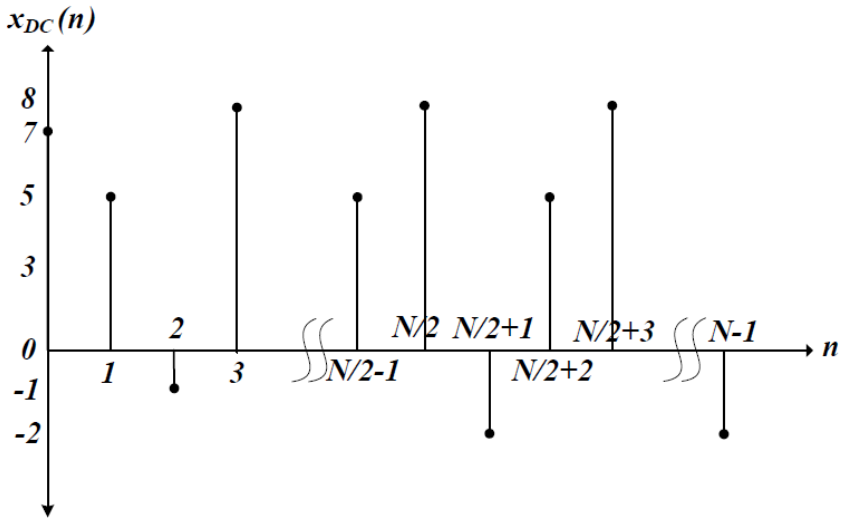

Fig. 2.11 Bipolar time domain signal plus the DC bias.

where$n = 0,1,2,.....,N-1$. x_n^m follow a Gaussian distribution due to the Central Limit Theorem (CLT) as N is sufficiently large. All x_n^m samples are real but not all are positive and thus not suitable for intensity modulation. To achieve a positive OFDM time domain signal, a suitable DC bias B_{DC} is added to x_n^m to obtain $(x_{DC})_n^m$ (Figure 2.11);

$$(x_{DC})_n^m = x_n^m + B_{DC} \tag{2.10}$$

B_{DC} in dB is defined as [22];

$$B_{DC}(dB) = 10Log_{10}\left[\frac{E\left[[(x_{DC})_n^m]^2\right]}{E\left[(x_n^m)^2\right]}\right] \tag{2.11}$$

After the addition of B_{DC} to x_n^m, some samples of $(x_{DC})_n^m$ may still be negative; these negative samples are clipped and set to zero (Figure 2.12. Clipping introduces distortion due to the loss of information; so regardless to any other kind of noise and distortion, the received signal at the receiver is a noisy version of the original signal impacting on system performance manifest through an increase in the Bit Error Rate (BER).

To decrease clipping noise, the value of the DC bias has to increase. However an increase in the DC bias translates into an increase in the transmitted power. Thus a trade-off exists between the transmitted power and the BER performance. Figure 2.13 shows the BER

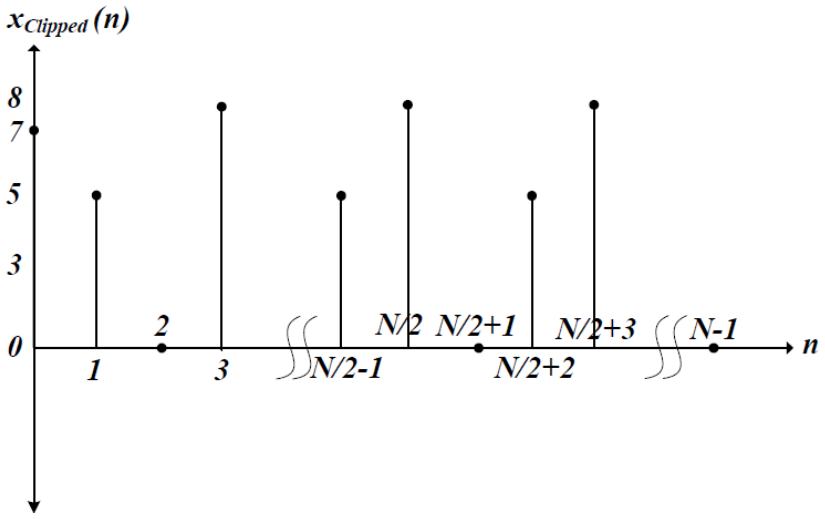

Fig. 2.12 DCO-OFDM time domain signal.

performance variation as a function of the added DC bias. The assumption is that the OFDM time domain signal modulates an ideal optical source producing a linear transformation between the input signal and the output optical power; the system is subject to AWGN and ideal photo-detection is assumed at the receiver. Post receiver, the DC bias is subtracted from the signal and fed to the FFT block.

2.4.1.2 ACO-OFDM

ACO-OFDM has been proven to be more power efficient than DCO-OFDM because it does not rely on a DC bias, consequently reducing the transmitter power requirement [26].

In ACO-OFDM, data is mapped to the odd sub-carriers only, the even sub-carriers being set to zero. In addition, the negative parts of the IFFT output are clipped to zero. Thus clipping noise falls on the even sub-carriers and does not impact the odd sub-carriers. Conversely, transmitting data on the odd sub-carriers only decreases the data rate by half and hence the implementation provides have half the spectral efficiency of DCO-OFDM for the same order M-QAM [15, 16, 21–28]. As expected, a 3 dB difference in BER performance exists between ACO-OFDM and Bipolar OFDM for the same M-QAM modulation order.

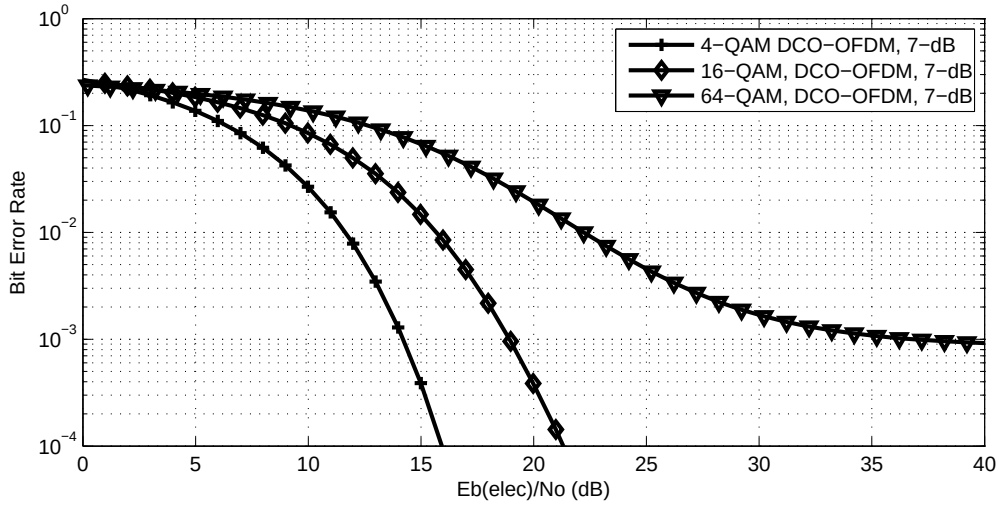

Fig. 2.13 DCO-OFDM BER performance with DC bias of 7 dB.

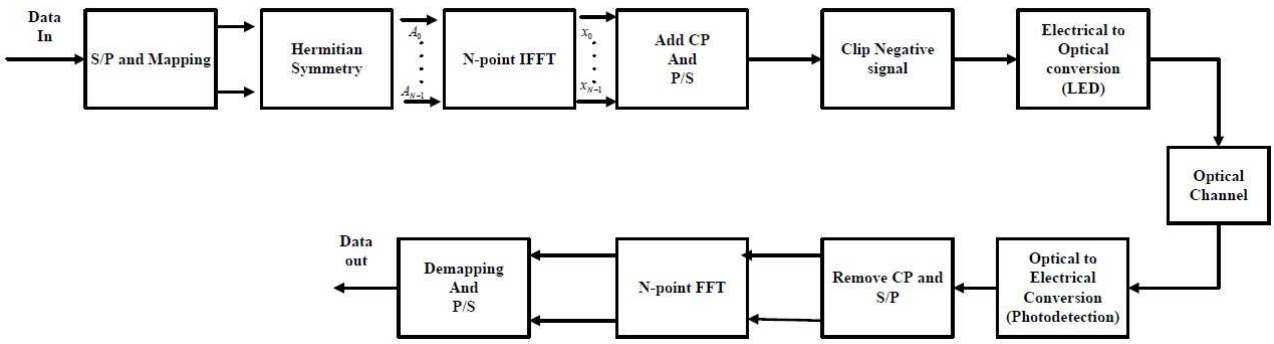

Fig. 2.14 Block diagram of an ACO-OFDM communication system.

2.4.1.2.1 System Model

Figure 2.14 shows the ACO-OFDM system block diagram. The input at the transmitter is first mapped to complex M-QAM symbols $A(l)$ which are then input to the IFFT block, generating a complex and bipolar output. As the system is intensity based, the time domain signal has to be real and positive and in this case the frame mapping has to be done before the IFFT block. Block diagram of an ACO-OFDM communication system .

Data is only mapped on the odd sub-carriers and the even ones are set to zero such that only $N/4$ symbols of $A(l)$,$l = 0,1,2,3,...N/4-1$ are mapped onto half of the odd sub-carriers. Hermitian symmetry [15, 16, 21–28] is then imposed on the other half of the sub-carriers to ensure that the output of the IFFT is real. The ACO-OFDM vector $A_{frame}(k)$

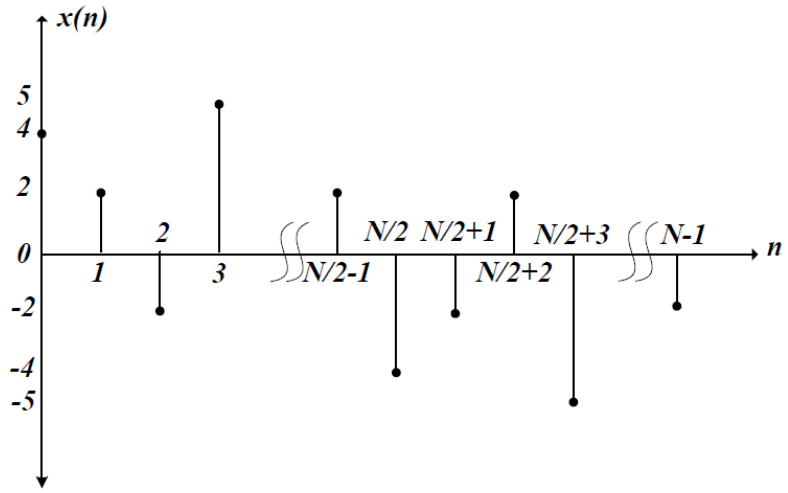

Fig. 2.15 IFFT output time domain signal.

has the following form ;

$$A_{frame}(k) = [0A_1 0A_3 0A_5 0.....A_{N/2-1} 0A^*_{N/2-1} 0.....0A^*_3 0A^*_1] \tag{2.12}$$

where

$$A_k = A^*_{N-k} \tag{2.13}$$

and $k = 1,3,5,7,.....N/2-1$.

After the Hermitian symmetry is imposed, the ACO-OFDM signal is passed through the IFFT; the output time domain signal $x(n)$ is real but bipolar and anti-symmetric around the element $N/2$ as (Figure 2.15)[28];

$$x(n) = \frac{1}{\sqrt{N}} \sum_{k=0}^{N-1} A_{frame} exp\left(\frac{j2\pi kn}{N}\right) \tag{2.14}$$

such that

$$x(n) = -x(n+N/2) \tag{2.15}$$

The bipolar real time domain signal $x(n)$ is clipped at a zero level to ensure that it is positive producing $x_{ACO-OFDM}$ after passing through the negative signal clipper block (Figure

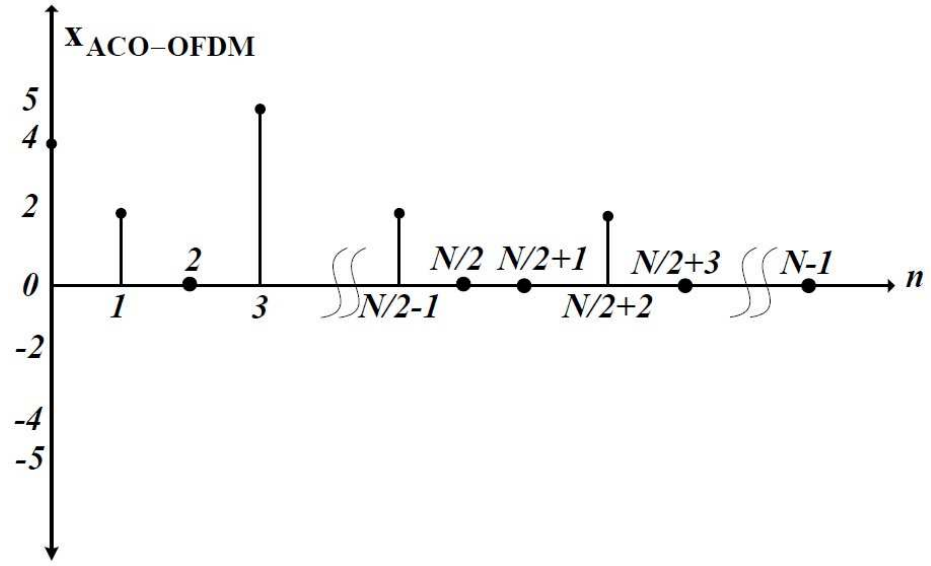

Fig. 2.16 Time domain ACO-OFDM signal .

2.16). The optical source is intensity modulated by the ACO-OFDM signal, $x_{ACO-OFDM}$.

It is assumed that the optical source is ideal producing a linear transformation between the input and output optical power. The optical signal transmitted through the optical channel is subject to AWGN. On reception, the signal becomes bipolar owing to the noise added in the electrical domain [27]. This model and assumptions are most often used to estimate the performance of wireless optical systems where signal degradation owing to high levels of ambient infrared radiation producing shot noise at the receiver is modelled as AWGN [23, 24, 26, 27].

At the receiver, clipping of the received signal at the zero level takes place. As is the case for intensity modulation, the transmitted signal is real and positive and thus the received signal without the noise has to be also real and positive, reducing the impact of noise. Half of the transmitted ACO-OFDM signal is clipped to zero and every positive sample has a mirrored negative sample. Assuming AWGN, half of the transmitted signal is of zero value, and nearly half of the zero valued samples will effectively be converted to negative values by noise [24–26]. Clipping the received signal to zero thus removes 1.25 dB of noise. Higher levels of additional noise can be removed if it is sufficiently large to convert a positive signal value to a negative value. The signal is then input to the FFT block followed by QAM demodulation [26].

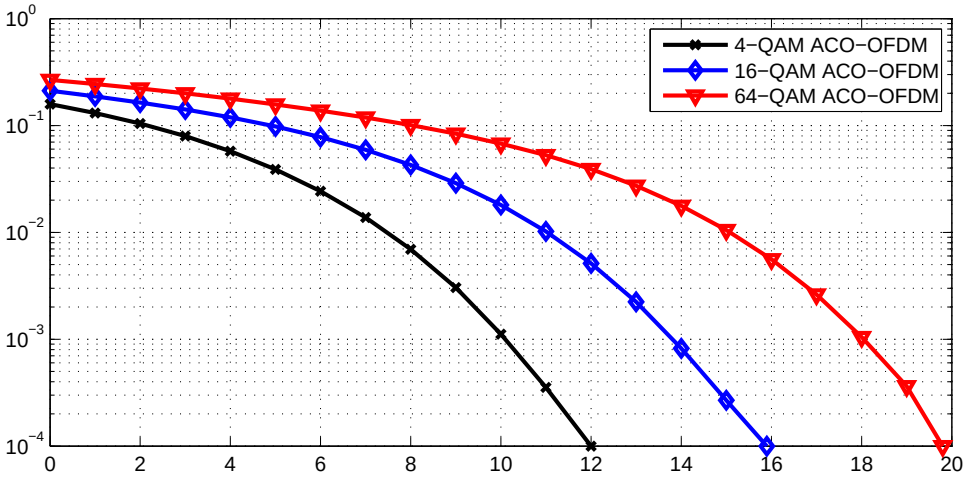

Fig. 2.17 ACO-OFDM BER performance vs. signal energy to noise ratio.

2.4.1.2.2 ACO-OFDM BER performance

Figure 2.17 shows the BER performance of ACO-OFDM as a function of the signal Energy-to-Noise (E_b/N_o) ratio for different QAM modulation indices whilst Figure 2.18 shows a comparison between the BER performance of both ACO-OFDM and bipolar OFDM; ACO-OFDM performance is $3dB$ worse.

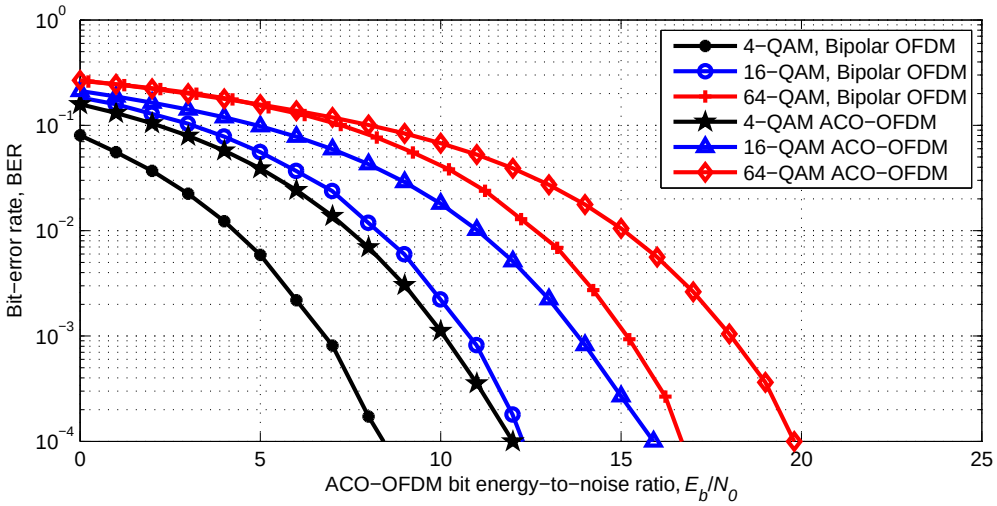

Fig. 2.18 Comparison of BER performance vs. signal energy to noise ratio for ACO-OFDM and Bipolar OFDM .

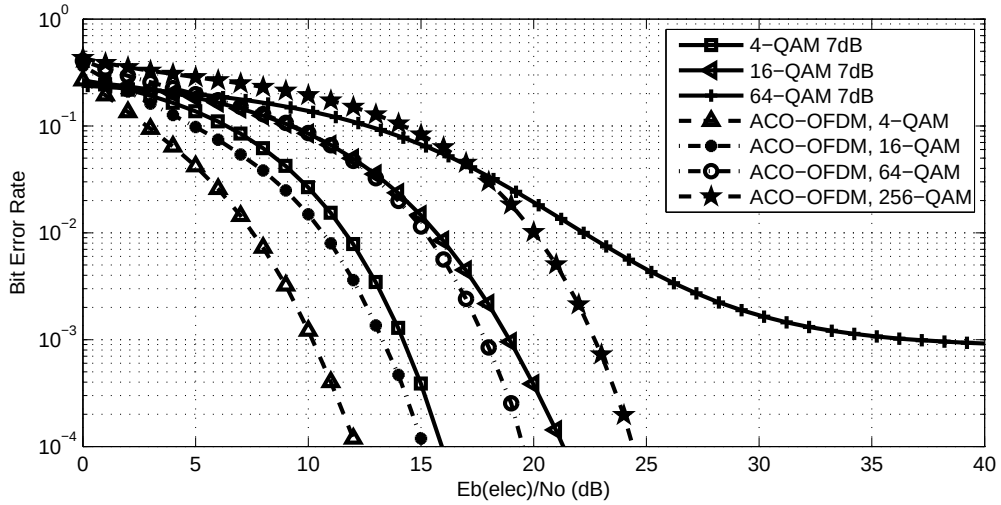

Fig. 2.19 Comparison of BER performance vs. signal energy to noise ratio for ACO-OFDM and DCO-OFDM .

2.4.1.2.3 Comparison of key parameters

A comparison between DCO-OFDM and ACO-OFDM is carried out with reference to two major system metrics viz. spectral efficiency and BER performance.

a) Spectral efficiency:

Spectral efficiency is defined as the number of information bits per unit bandwidth, measured in $bits/Hz$ [22]. Both systems sacrifice half of the OFDM frame to obtain a real, bipolar time domain signal through employing Hermitian symmetry. ACO-OFDM uses only odd sub-carriers, so ACO-OFDM requires twice the size of a standard OFDM frame to transmit the same information content as DCO-OFDM. The spectral efficiency of ACO-OFDM is thus half that of DCO-OFDM.

b) BER performance:

The BER performance of ACO-OFDM is better than that of DCO-OFDM with DC bias of 7 dB (Figure 2.19). For a fair comparison, 4-QAM DCO-OFDM is compared to 16-QAM ACO-OFDM and 16-QAM DCO-OFDM is compared to 256-QAM ACO-OFDM. In the first case, ACO-OFDM BER performance is better than that of DCO-OFDM by nearly 1 dB; however in the second case, as the constellation size increases, the ACO-OFDM BER performance degrades and DCO-OFDM performance is superior by nearly 3.5 dB. Increasing the DC bias in DCO-OFDM, results in a degradation in performance with respect to ACO-OFDM.

2.4.1.3 Flip OFDM

Flip OFDM (FO-OFDM) aims to for a similar performance as that of ACO-OFDM but at less complexity.

2.4.1.3.1 System Model

Figure 2.20 shows the block diagram of the F-OFDM system [30, 31]. The F-OFDM frame mapping block relies on Hermitian symmetry and a 'flipping' process explained below.

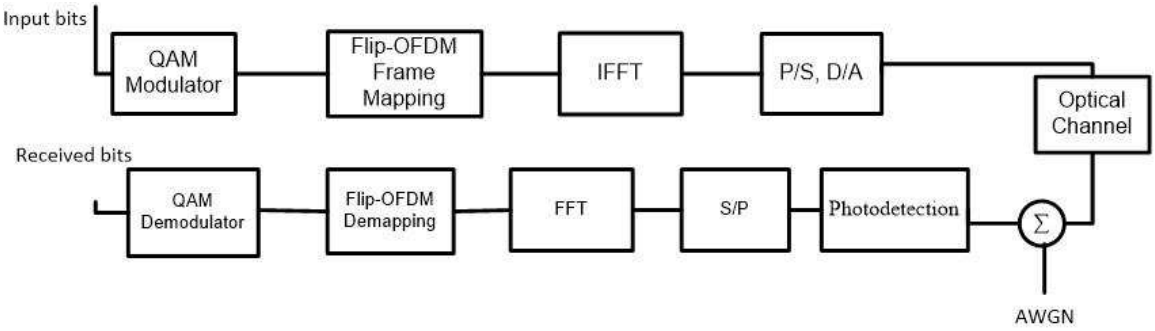

Fig. 2.20 A system block diagram of an Flip OFDM system .

A_k^m is the output of the QAM modulator of the kth subcarrier and is independent from other QAM symbols that are mapped on other sub-carriers. Hermitian symmetry is employed on each OFDM frame to ensure that the output of the IFFT block is real [9, 14–16];

$$x_n^m = A_o + \sum_{k=0}^{N/2-1} A_k exp\left(\frac{j2\pi kn}{N}\right) + A_{N/2} exp\left(j\pi k\right) + \sum_{k=N/2+1}^{N-1} A_{N-k}^* exp\left(\frac{j2\pi kn}{N}\right) \quad (2.16)$$

whereA_{N-k}^* is the conjugate symmetric QAM symbol of A_k , and A_o is the DC component. A_o and $A_{N/2}$ are set to zero to remove any DC shift or residual complex component. The output of the IFFT block is a real, bipolar time domain signal such that;

$$x(n) = x^+(n) + x^-(n) \quad (2.17)$$

where $x^+(n)$ and $x^-(n)$ are the positive and negative samples of the $x(n)$ and are defined as;

$$x^+(n) = \begin{cases} x(n), & x(n) > 0 \\ 0, & \text{otherwise} \end{cases}$$

$$x^{-}(n) = \begin{cases} x(n), & x(n) < 0 \\ 0, & \text{otherwise} \end{cases}$$

where $n = 1, 2, ..., N$.

If the sample of the output of IFFT block is positive, then it is putted as $x^{+}(n)$; if the sample is negative, its sign is flipped to positive by multiplying by negative sign and it is putted as $x^{-}(n)$.

The transmission of the positive signal $x^{+}(n)$ takes place in the first OFDM subframe, and then flipped signal $-x^{-}(n)$ is transmitted in the second subframe Figure(2.21). Cyclic prefixes of duration $\triangle$ are added to both subframes before the signals are transmitted through the dispersive optical channel.

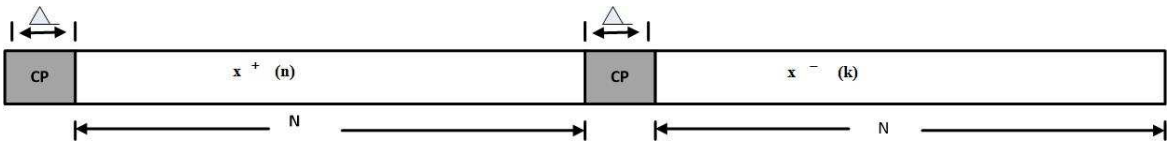

Fig. 2.21 Unipolar Flip OFDM frame .

At the receiver, both the positive and flipped negative sub-frames are used to reconstruct the bipolar OFDM frame. Firstly, the cyclic prefixes are removed from both sub-frames and the original bipolar signal is reconstructed as [30];

$$y(n) = y^{+}(n) - y^{-}(n) \tag{2.18}$$

where $y^{+}(n)$ and $y^{-}(n)$ represent the received positive and flipped negative sub-frames. FFT operations are carried out to reconstitute the bipolar signal followed by detection of the transmitted symbols.

2.4.1.3.2 Comparison of key parameters

A comparison between F-OFDM and ACO-OFDM is carried out with reference to spectral efficiency and hardware complexity [30, 31]:

a)Spectral efficiency

To obtain real bipolar time domain signals, both F-OFDM and ACO-OFDM sacrifice half of the spectrum on applying Hermitian symmetry. In the case of ACO-OFDM, only odd sub-carriers are used for information transmission and only positive time samples are

used to detect the transmitted information. Hence ACO-OFDM has one fourth of the spectral efficiency of OFDM systems employing complex signals. The spectral efficiency of F-OFDM is the same as that of ACO-OFDM as it uses twice the frame size of ACO-OFDM to transmit twice as many information symbols.

b) Complexity of Transmitter and Receiver Computational Resources
The complexity is defined as the number of IFFT/FFT operations in the transmitter and receiver. Table 2.2 shows that both ACO-OFDM and F-OFDM use the same hardware computation resources at the transmitter but the latter has a 50 % computational saving at the receiver.

Table 2.2 Comparison betweenACO-OFDM and Flip OFDM hardware complexity .

	ACO-OFDM	Flip OFDM
Transmitter	$Nlog(N)$	$Nlog(N)$
Receiver	$2Nlog(N)$	$Nlog(N)$

2.4.1.4 U-OFDM

U-OFDM has been proposed in an attempt to eliminate the 3 dB gap between the BER performance of OFDM and ACO-OFDM through the generation of unipolar signals that do not need a DC bias as in the case of DCO-OFDM.

2.4.1.4.1 System Model

Figure 2.22 shows the U-OFDM system block diagram.

U-OFDM adopts Hermitian symmetry such that;

$$A_k^m = \left(A_{N-k}^m\right)^* \tag{2.19}$$

where A_k^m represents data samples from square QAM constellation. m represents the OFDM symbol number, while $k = 0,1,2,3,.....,N-1$ denotes the subcarrier number in each OFDM frame. The subcarriers at $k = 0, N/2$ are set to zero such that;

$$A_0^m = A_{N/2}^m = 0 \tag{2.20}$$

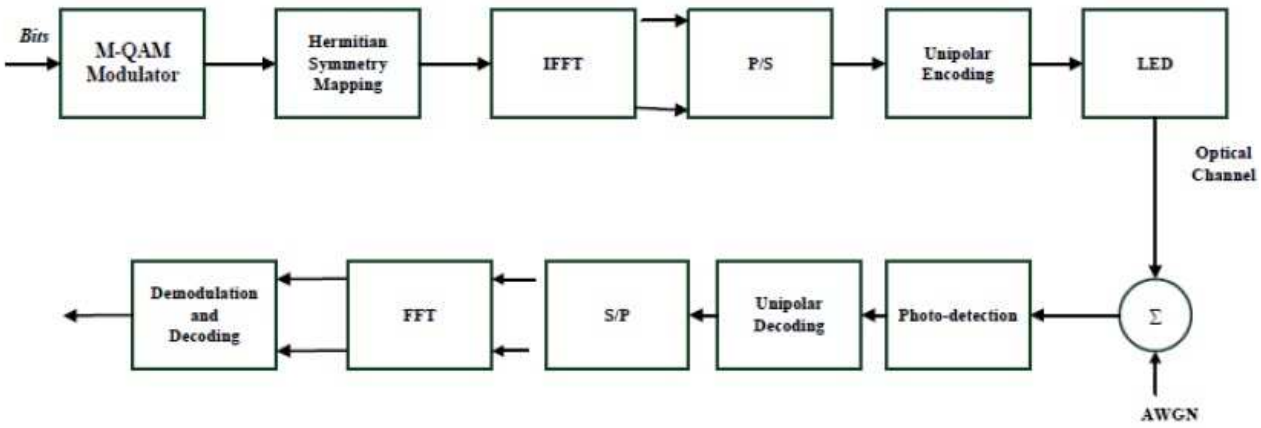

Fig. 2.22 U-OFDM block diagram.

Each OFDM frame is input to the IFFT block to transform N complex samples to N real samples. producing an output time domain signal x_n^m defined by;

$$x_n^m = \frac{1}{\sqrt{N}} \sum_{k=0}^{N-1} X_k exp\left(\frac{j2\pi kn}{N}\right) \tag{2.21}$$

where $n = 0, 1, 2, ..., N-1$. x_n^m has Gaussian distribution due to the CLT as N is sufficiently large. All x_n^m samples are real but not all are positive and thus not compatible with intensity modulation implementations (Figure 2.23).

To achieve a positive OFDM time domain signal, unipolar encoding is employed. Each time domain sample is encoded into a pair of new time samples. If the original sample is positive, then the first slot in the new sample pair with the magnitude of the original sample in the first and the second slot set to zero. If the original time domain sample is negative, the first slot in the new sample pair is set to zero, and the second slot is set with the magnitude of the original time domain sample (Figure2.24).

A rearrangement then takes place to form positive and negative blocks, illustrated in Figure 2.25. The first samples in each pair are grouped in their original order to give the positive block, and the second samples of each pair are also grouped to give the negative block. Transmission of the positive block takes place first followed by the negative block. The aim of the methodology is to ensure that frequency components of both blocks are attenuated in the same way when subjected to impairments such as ISI. A linear recombination of both blocks forms the original bipolar time domain signal.

With unipolar encoding, the OFDM length is doubled which impacts the spectral efficiency. The spectral efficiency of U-OFDM is half that of DCO-OFDM and the same as ACO-OFDM. The U-OFDM signal modulates the optical source, assumed to be ideal such

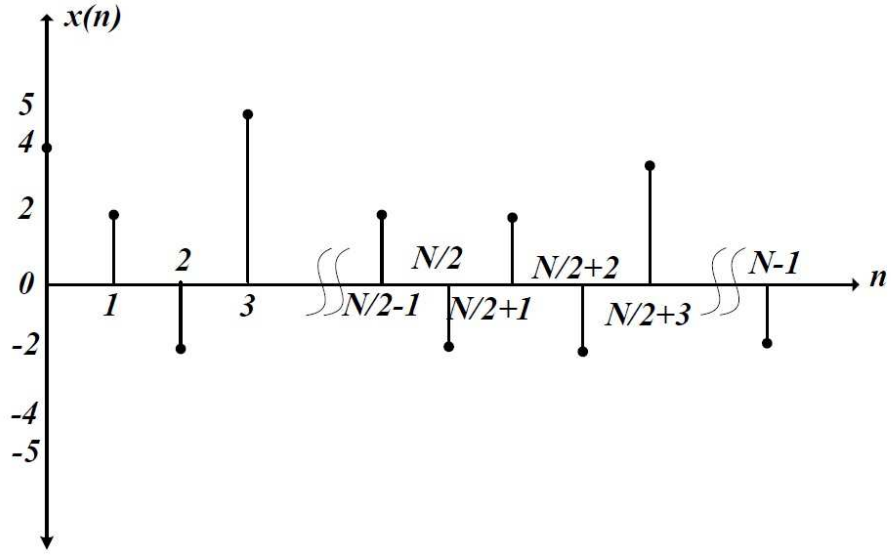

Fig. 2.23 Real OFDM time domain signal.

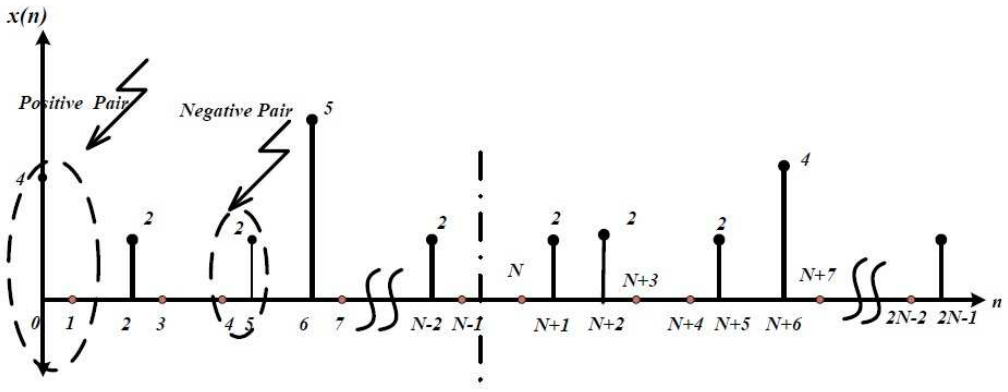

Fig. 2.24 A unipolar time domain signal.

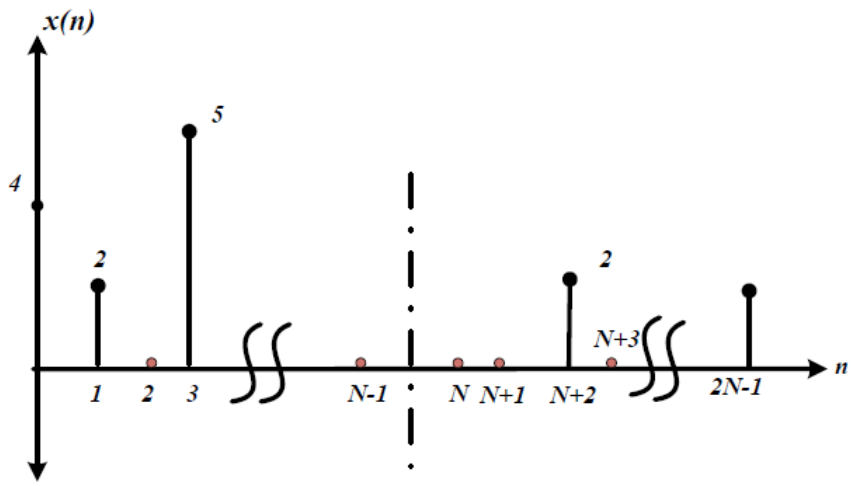

Fig. 2.25 U-OFDM time domain signal.

that a linear transformation between the input and output optical power is achieved.

There are two methods for unipolar decoding at the receiver. The first method subtracts the negative block from the positive block to obtain the original bipolar time domain signal and the resultant is input to the FFT block after which QAM demodulation takes place. This approach results in a doubling of the AWGN variance at each resulting point impacting the BER performance of U-OFDM by 3 dB to that of bipolar OFDM for the same M-QAM modulation index. U-OFDM BER performance is the same as ACO-OFDM. The second method compares the amplitude of the samples in each pair and the sample of higher amplitude is considered whilst the other is considered zero. Thus a receiver is able to detect the sign of the original sample. This method is expected to eliminate nearly half of the noise variance and hence improve performance.

2.4.1.4.2 Comparison of key parameters

a)Spectral efficiency:

To obtain real, bipolar time domain signals both U-OFDM and ACO-OFDM sacrifice half of the spectrum on applying Hermitian symmetry. In the case of ACO-OFDM, only odd sub-carriers are used for transmission and only positive time samples are used to detect the transmitted information. Hence the ACO-OFDM has one fourth of the spectral efficiency

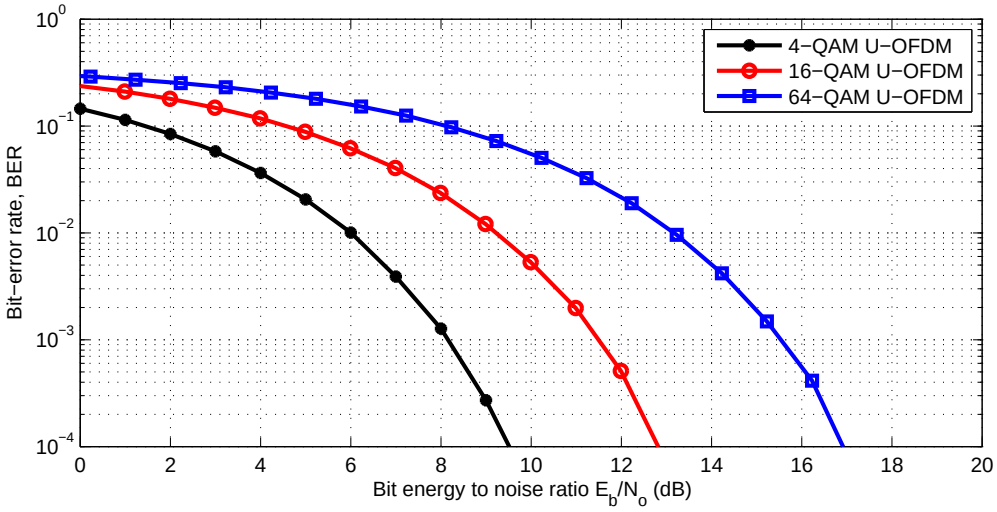

Fig. 2.26 U-OFDM BER performance vs. bit energy to noise ratio .

of OFDM systems with complex signals. The spectral efficiency of U-OFDM is the same as that of ACO-OFDM as it uses twice the frame size of ACO-OFDM to transmit twice as many information symbols.

b) BER perfromance:

Figure 2.26shows the BER performance as a function of bit Energy-to-Noise ratio of U-OFDM and a comparison between the performance of U-OFDM and ACO-OFDM is shown in Figure 2.27. U-OFDM outperforms ACO-OFDM by 3dB. The performance of U-OFDM is also compared to bipolar OFDM in Figure 2.28; the BER of Bipolar OFDM is much better than that of U-OFDM, but the gap between their performance decreases with increasing constellation size as the performance of U-OFDM is 3 dB at higher modulation orders.

2.5 Atmospheric Turbulence

Optical signals are impacted severely by atmospheric conditions such as fog and rain [3]. Photons of the propagating optical signal interact with atmospheric particles and molecules causing the absorption of photons and/or their re-radiation in different propagating directions with random phases.

Atmospheric turbulence is considered one of the major factors degrading the performance of any wireless optical communication system [3, 4, 32]. As the temperature rises, the air surrounding the earth's surface becomes warmer than the air at higher altitudes as

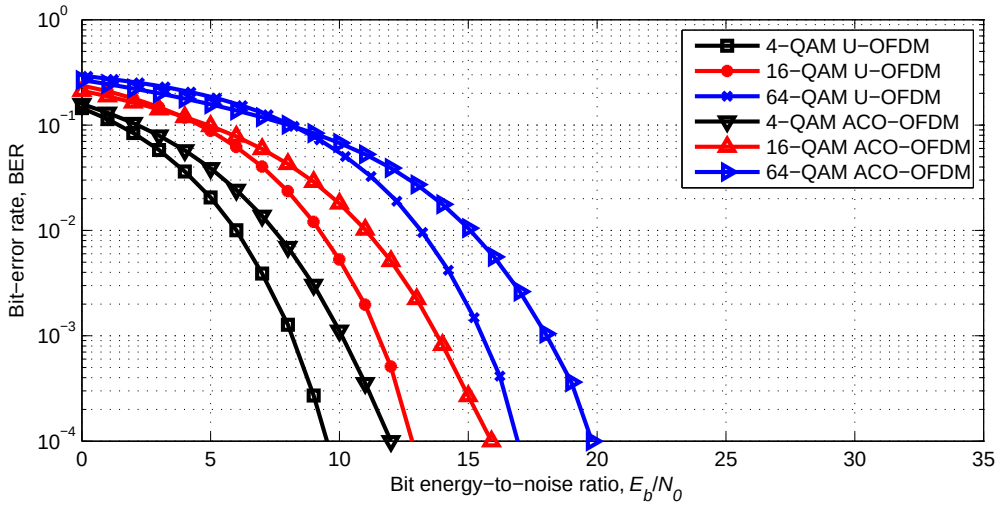

Fig. 2.27 BER performance vs. bit energy to noise ratio for ACO-OFDM and U-OFDM .

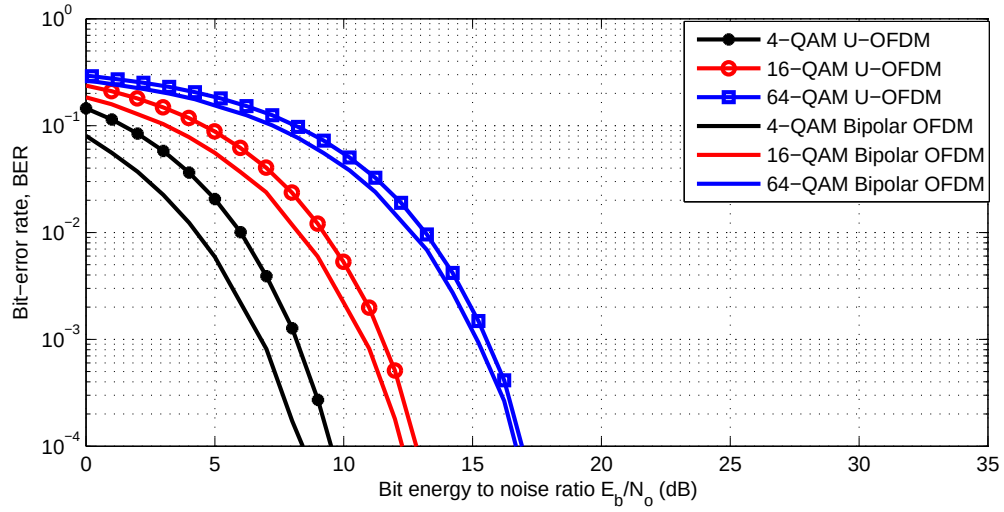

Fig. 2.28 BER performance vs. bit energy to noise ratio for Bipolar OFDM and U-OFDM .

solar radiation is absorbed. The warmer layer of air becomes less dense and rises to mix with the cooler layers inducing random temperature gradients. The resultant inhomogeneity in the air form regions of different refractive indices, referred to as discrete cells or eddies [2–4, 33]. Thus the propagating optical beam is subject to random phase and amplitude variations due to the interaction with the turbulent medium, commonly referred to as scintillation [11, 34–40]. These variations induce signal fading at the receiver resulting in some cases, severe degradation in system performance.

Atmospheric turbulence can be classified into regimes that depend on the value of the refractive index variation and degree of inhomogeneities. These regimes are also a direct function of the distance covered by the optical beam through the atmosphere and are most readily classified as weak, moderate, strong and saturated [4, 41]. Different models have been proposed to represent the statistics of these irradiance fluctuations for the different atmospheric turbulence regimes. The most well reported models are the log-normal distribution [2, 4], gamma-gamma [4] and negative exponential [4].

The random variations in refractive indices create turbulence eddies of different sizes. The smallest and the largest eddies are known as inner scale l_0 and and outer scale L_0 of the turbulence respectively; l_0 and L_0 are of the order of millimeter and several meters respectively [4]. These eddies act as lenses that cause beam spreading, wandering and scintillation. The coherence time of the atmospheric turbulence τ_o is of the order of millisecond, considered large compared to data symbol duration; thus the turbulent atmospheric channel can be treated as a slow fading channel [4].

An important parameter for describing the level of fluctuations is the index of refraction structure parameter C_n^2 which is a function of the wavelength, atmospheric altitude, and temperature. The variation in altitude results in a variation in the value of the index of refraction structure parameter, but for horizontal propagation the value of C_n^2 is usually constant. In the case of a near ground level link, C_n^2 is taken to be $1.7 * 10^{-14} m^{-2/3}$ and $8.5 * 10^{-15} m^{-2/3}$ during daytime and at night respectively [4];

$$10^{-17} \leq C_n^2 \leq 10^{-12} \tag{2.22}$$

The most relevant approaches to modelling atmospheric turbulence are presented and discussed.

2.5.1 Log-normal Model

One of the distributions proposed to describe irradiance fluctuation owing to atmospheric turbulence, is the log-normal model (Figure 2.29) the probability density function (pdf) of

which is [2, 4];

$$p(I) = \frac{1}{2\pi\sigma_l^2}\frac{1}{I}exp\left(-\frac{(ln(I/I_o) - E[l])^2}{2\sigma_l^2}\right), I \geq 0 \tag{2.23}$$

where I is the irridiance intensity in the turbulent medium, I_o is the irridiance intensity in the absence of turbulence and σ_l^2 is the log irridiance variance. In the case of horizontal propagation through a turbulent channel, as is the case in most terrestrial applications, the value of C_n^2 is kept constant and thus σ_l^2 in case of plane wave is [4, 42] ;

$$\sigma_l^2 = 1.23C_n^2k^{7/6}L_p^{11/6} \tag{2.24}$$

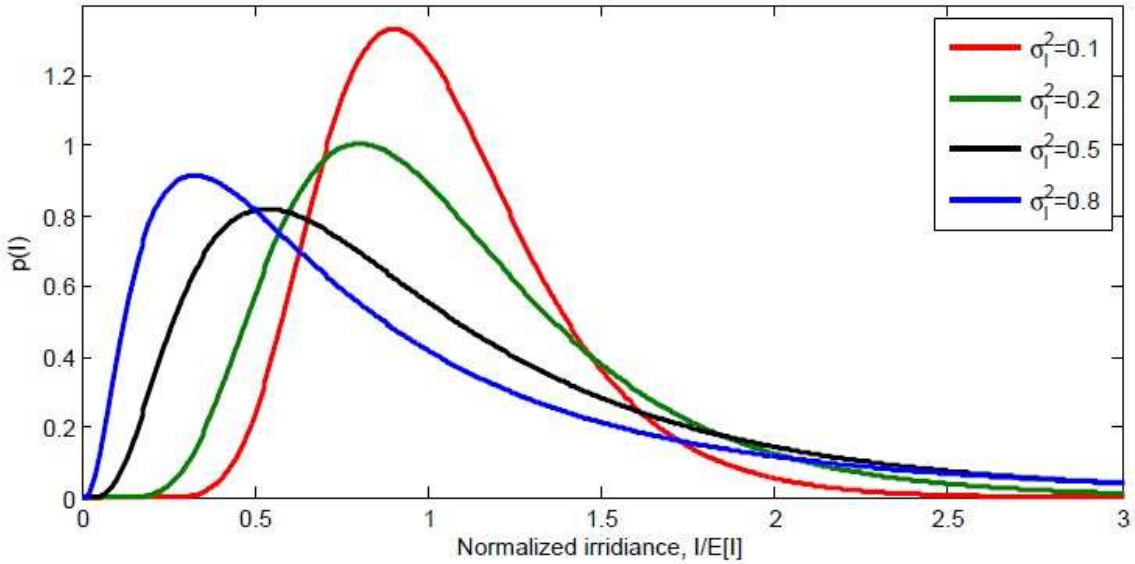

Fig. 2.29 Log-normal pdf for a range of log irridiance variance σ_l^2 .

where $k = 2\pi/\lambda$ is the wave number, and L_p is the link length. $\sigma_l^2 = 4\sigma_x^2$ where σ_x^2 is the Rytov variance, the key parameter for determining turbulence strength.

For weak turbulence, the Rytov variance increases with increasing C_n^2 and/or path length [2, 4]. As the strength of turbulence increases, the eddies create multiple scattering mechanisms not treated by the Rytov approximation solely. The Scintillation Index (SI) [2, 4] increases linearly with the Rytov parameter in weak turbulence conditions and continues to increase to a maximum value greater than unity. The regime in which the (SI) is at a maximum is characteristic of the highest strength of inhomogeneity or random focusing;

$$SI = exp\left(\sigma_l^2\right) - 1 \tag{2.25}$$

Beyond the maximum, the *SI* starts to decrease approaching unity due to self-interference owing to multiple scattering and as the Rytov variance increases. Log-normal statistics produce significant deviations with respect to experimental results as the strength of turbulence increases as multiple scattering effects are not taken into consideration; thus the log-normal distribution is most valid in weak turbulence conditions.

2.5.2 Gamma-Gamma Model

In the Gamma-Gamma model, the turbulent atmosphere is assumed to comprise both small scale (scattering) and large scale (refraction) mechanisms. In the former, scattering is due to eddies the size of which is smaller than the Fresnel Zone $R_F = (L_p/k)^{1/2}$ or the coherence length (radius) ρ_o whichever is smaller. In the latter, refraction takes place due to eddies the size of which size are greater than the Fresnel Zone or the scattering disk $\frac{L}{k\rho_o}$ whichever is greater. Small scale eddies are assumed to be modulated by the large scale eddies [4]. Therefore, the normalized received irradiance I is defined as the product of two statistically independent random processes I_x and I_y.

$$I = I_x.I_y \tag{2.26}$$

where I_x and I_y are due to large scale and small scale eddies respectively. Both classes of eddies follow a gamma distribution as [4, 43–46]:

$$p(I_x) = \frac{\alpha\,(\alpha I_x)^{\alpha-1}}{\Gamma(\alpha)} exp\,(-\alpha I_x)\,, \quad I_x > 0, \alpha > 0 \tag{2.27}$$

$$p(I_y) = \frac{\beta\,(\beta I_x)^{\beta-1}}{\Gamma(\beta)} exp\,(-\beta I_y)\,, \quad I_y > 0, \beta > 0 \tag{2.28}$$

where α and β represent the effective number of large and small scale eddies in the scattering fluctuation pdf and $\Gamma(...)$ is the gamma function.

By changing variables $I_y = I/I_x$, the conditional pdf is given by;

$$p(I/I_x) = \frac{\beta\,(\beta I/I_x)^{\beta-1}}{I_x\Gamma(\beta)} exp\left(\frac{-\beta I}{I_x}\right), \quad I > 0 \tag{2.29}$$

I_x is the conditional mean of I. To obtain the uncoditional irridiance distribution, the conditional probability $p(I/I_x)$ is averaged over the statistical distribution of I_x to obtain the

gamma-gamma irridiance distribution function Figure(2.30).

$$p(I) = \int_0^\infty p(I/I_x)p(I_x)dI_x \tag{2.30}$$

$$p(I) = \frac{2(\alpha\beta)^{(\alpha+\beta)/2}}{\Gamma(\alpha)\Gamma(\beta)} I^{(\alpha+\beta/2)-1} K_{\alpha-\beta}(2\sqrt{\alpha\beta I}), \quad I > 0 \tag{2.31}$$

$K_n(...)$ is the modified bessel function of the second kind of order n , and $\Gamma(...)$ represents the gamma function. In case of plane wave, the α and β are related as;

$$\alpha = \left[exp\left(\frac{0.49\sigma_l^2}{\left(1+1.11\sigma_l^{12/5}\right)^{7/6}} \right) - 1 \right]^{-1} \tag{2.32}$$

$$\beta = \left[exp\left(\frac{0.51\sigma_l^2}{\left(1+0.69\sigma_l^{12/5}\right)^{5/6}} \right) - 1 \right]^{-1} \tag{2.33}$$

where σ_l^2 is the rytov variance given by Equation 2.24.

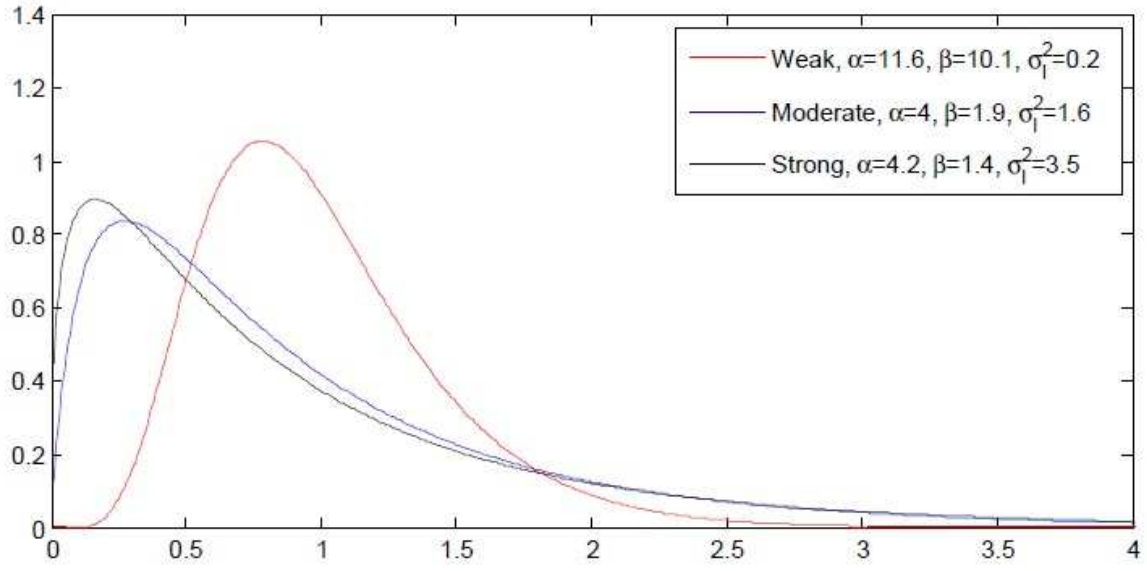

Fig. 2.30 Gamma-gamma pdf for three different turbulence regimes, namely weak, moderate, and strong .

The *SI* is thus given by;

$$SI = \alpha^{-1} + \beta^{-1} + (\alpha\beta)^{-1} \tag{2.34}$$

Substituting Equation 2.32 and Equation2.33 in Equation 2.34 gives;

$$SI = exp\left[\frac{0.49\sigma_l^2}{\left(1+1.11\sigma_l^{12/5}\right)^{7/6}} + \frac{0.51\sigma_l^2}{\left(1+0.69\sigma_l^{12/5}\right)^{5/6}}\right] - 1 \tag{2.35}$$

All turbulence scenarios from weak to strong can be expressed by the gamma-gamma turbulence model [47–50]. The value of the *SI* increases with increasing Rytov parameter reaching a maximum value greater than 1 and then approaches unity as the turbulence-induced fading approaches the saturation regime (Figure2.31).

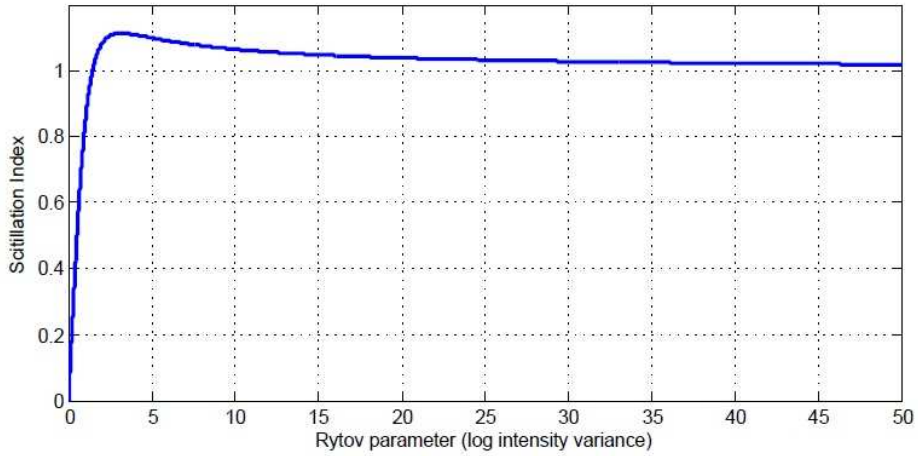

Fig. 2.31 SI against log intensity variance for $C_n^2 = 10^{-15} m^{-2/3}$ and $\lambda = 850nm$.

In weak turbulence, $\alpha \gg 1$ and $\beta \gg 1$ which means that the effective number of small and large eddies are large. As fluctuations increase ($\sigma_l^2 > 0.2$) and approach the focusing regime, the values of α and β decrease substantially; approaching strong turbulence, the value of $\beta \to 1$. While the effective number of discrete refractive scatterers α starts to increase again with increasing turbulence, the intensity becomes unbounded in the saturation regime (Figure2.32).

2.6 Capacity for O-OFDM

The channel capacity is one of the most important parameters determining system viability. The limits on capacity provide an indication of maximum data rates that can be achieved at

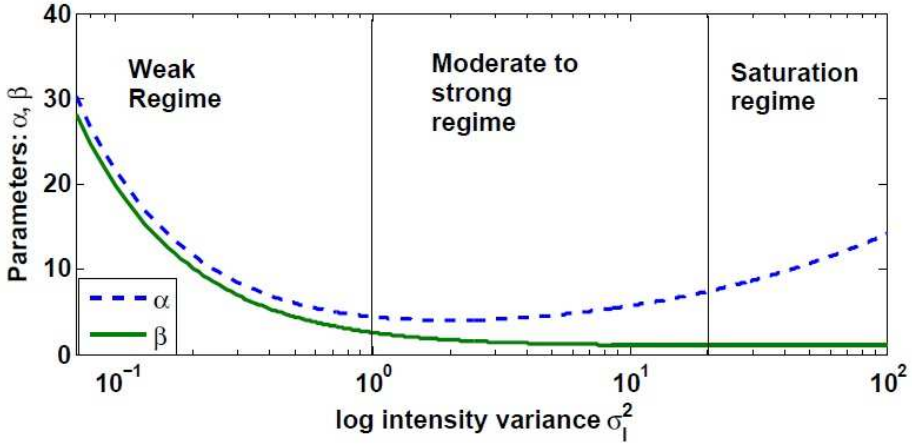

Fig. 2.32 Values of α and β under different turbulence regimes: weak, moderate to strong and saturation .

the appropriate BER. In 1940s, Shannon developed a mathematical framework relating the mutual information between the input and output of a communications channel, defining capacity as the maximum mutual information over all possible input distributions [51]. Before Shannon's theory, the adopted wisdom was that the performance of a communication system over a noisy channel resulted in compromised data rates.

The limiting factors on channel capacity are link impairments such as non-linear signal transmission, noise sources and channel characteristics. The distortion of transmitted signals is also heavily impacted by the characteristics of both the electronic and optical components in the implementation.

2.6.1 Link Impairments

The limited dynamic range of the transmitter creates non-linear distortion due to the clipping of negative signal values. Further, non-ideal optical front ends result in additional levels of distortion [52]. Pre-distortion may be employed [52] so as to restrict linear operation within a limited range constraining the transmitted power within a specific range which has an impact on attainable system performance. In addition, the average optical power is also governed by eye safety requirements [51, 52].

As the area of the receiving photodetector is significantly larger than the wavelength of the optical carrier, fast fading in the channel is not an issue as the coherence time of the channel is considered constant over the period of transmission. So slow fading in the form of path loss and log normal shadowing dominates [53].

Table 2.3 Comparison between BPSK OFDM and RF OFDM systems.

OFDM System type	E_b/N_o value at $BER = 10^{-4}$
BPSK OFDM	8.4 dB
4-QAM OFDM	5.5 dB
16-QAM OFDM	14 dB
64-QAM OFDM	24 dB

2.6.2 Capacity Optimisation

The capacity of bandlimited linear optical wireless channel subject to AWGN has been estimated under a range of constraints such as average electrical power, average optical power and peak optical power [54–57]. In [56] signal average optical power is considered, deriving an upper bound of the capacity as a function of the optical SNR using the Shannon sphere packing argument [57]. [58, 59] use a geometrical representation of signal spaces to determine the lower and upper capacity bounds under a peak optical power constraint. For OFDM systems, [60] provide an estimation of DCO-OFDM capacity under the average optical power constraint, assuming an infinite dynamic range transmitter and sufficient DC bias to ensure non-negativity. The capacity of DCO-OFDM at high electrical SNR approaches the Shannon bound, the 3 dB gap being the DC bias penalty. [61, 62] present the capacity of ACO-OFDM also assuming an infinite dynamic range transmitter under the average optical power constraint; it is shown that the capacity of ACO-OFDM is half that of Shannon due to the utilisation of half the bandwidth.

2.7 Conclusions

A brief summary of wireless optical system evolution is presented. A summary of the principles and system architectures developed for operation in the RF domain is described along with the main functional components.

An introduction to O-OFDM systems defined the main challenges with coherent and incoherent implementations together with the essential differences between O-OFDM and RF OFDM systems (Table 2.3).

A number of well reported O-OFDM designs have been introduced and their attainable system performance presented (Table compb2). The BER performance of ACO-OFDM is superior to that of DCO-OFDM at the expense of spectral efficiency. The spectral efficiency of ACO-OFDM is half that of DCO-OFDM. U-OFDM closes the 3 dB gap in performance

Table 2.4 Comparison between different O-OFDM systems.

O-OFDM System type	Spectral Efficiency	BER Performance
DCO-OFDM	The highest spectral efficiency	It is considered the worst BER performance at low modulation order, but its performance becomes better than ACO-OFDM at high modulation order.
ACO-OFDM	Its spectral effieciency is half that of DCO-OFDM	Its performance is better than DCO-OFDM by nearly 1dB at low modulation order but it degrades at higher modulation orders
Flip OFDM	The same spectral efficiency as ACO-OFDM	It has the same performance as ACO-OFDM but with lower receiver complexity
UO-OFDM	Same spectral efficiency as ACO-OFDM	It has the best BER performance and its perfromance improves at high modulation order that it approaches bipolar OFDM performance.

of ACO-OFDM but is still inferior to that of bipolar OFDM. Finally an overview on the literature of optical channel capacity was presented.

CHAPTER 3

MODIFIED ACO-OFDM (MACO-OFDM) SYSTEM MODEL AND PERFORMANCE ANALYSIS

3.1 Introduction

A modification to Asymmetrically-Clipped Optical Orthogonal Frequency Division Multiplexing (ACO-OFDM) is proposed to improve performance through the use of unipolar encoding which improves the quality of transmission through optical channels. The BER performance of the approach is estimated analytically supported by Monte Carlo simulations. Both analytical and simulation results are compared and then compared to that of the conventional ACO-OFDM system. As expected, results indicate that the proposed modification brings a slight improvement in the BER performance when compared to that of ACO-OFDM in the case of an AWGN channel. However as is detailed in Chapter 4, the approach provides a significant enhancement of performance surpassing that of ACO-OFDM in the case of a turbulent channel. Unlike U-OFDM, MACO-OFDM uses only the odd sub-carriers in the OFDM frame.

3.2 System Model and Analysis

Figure 3.1 shows the block diagram of the proposed system. In standard OFDM systems, the input bits at the transmitter are first mapped to complex symbols through a QAM modulator, where A_k^m represents the square M-QAM symbols, where m denotes the OFDM frame numbers, and k denotes the subcarrier number $k = 0, 1, 2, 3, ...N-1$. In the ACO-OFDM block, only the odd sub-carriers are employed utilising Hermitian symmetry and the outputs are input to the IFFT. Unipolar encoding is then executed and the output is converted from a parallel to a serial stream. The optical signal is transmitted through the channel after

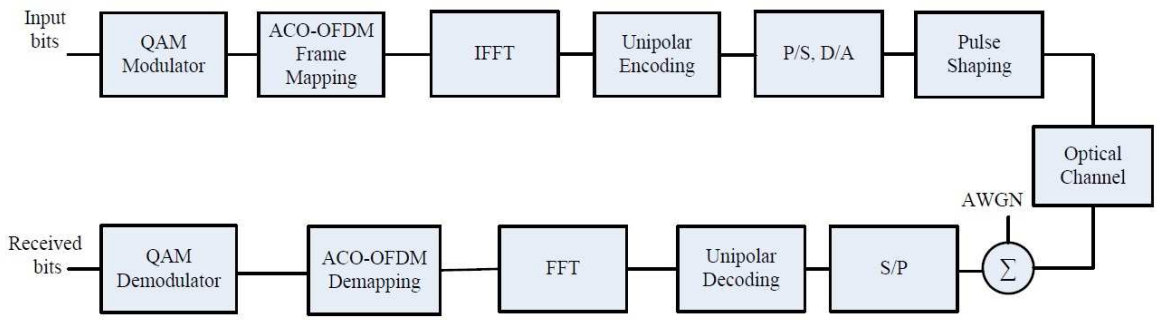

Fig. 3.1 Modified ACO-OFDM block diagram

suitable pulse shaping. At the receiver, assuming the system is subject to AWGN added after the optical to electrical conversion takes place, the signal undergoes serial-to-parallel translation. Unipolar decoding is followed by a FFT and ACO-OFDM de-mapping. Finally, the signal is QAM demodulated. A detailed mathematical model for the bit error rate BER performance is carried out in the following sections.

3.2.1 MACO-OFDM frame Mapping

In MACO-OFDM, only odd sub-carriers are used *viz*. $k = 1,3,5,7,....N-1$.The sub-carriers at $k = 0\&N/2$ are set to zero. Hermitian symmetry is then employed to ensure that the output of the IFFT block is real such that;

$$A_k^m = \left(A_{N-k}^m\right)^* \tag{3.1}$$

$$A_k^m = X_k^m + jY_k^m \tag{3.2}$$

$$A_{N-k}^m = X_k^m - jY_k^m \tag{3.3}$$

$$A_o^m = A_{N/2}^m = 0 \tag{3.4}$$

The following equations are used to determine the variance of the MACO-OFDM signal. Both X_k^m and Y_k^m are zero mean random variable (R.V.), where P is the average power per symbol such that $E\left[\left(X_k^m\right)^2\right] = E\left[\left(Y_k^m\right)^2\right] = P/2$ for $k \neq 0\&N/2$, and $E\left[X_k^m Y_k^m\right] = 0$.
From the conjugate symmetry;

$$E\left[X_k^m X_{N-k}^m\right] = \begin{cases} \frac{P}{2}, & k \neq 0 \quad \& \quad N/2 \\ 0, & \text{otherwise} \end{cases}$$

(3.5)

$$E\left[Y_k^m Y_{N-k}^m\right] = \begin{cases} \frac{-P}{2}, & k \neq 0 \quad \& \quad N/2 \\ 0, & \text{otherwise} \end{cases}$$

(3.6)

And $E\left[A_k^m\right] = 0$

$$E\left[A_k^m A_h^l\right] = \begin{cases} P, & h = N-k \quad \& \quad m = l, \quad k \neq 0 \quad \& \quad N/2 \\ 0, & \text{otherwise} \end{cases}$$

(3.7)

$$E\left[A_k^m (A_h^l)^*\right] = \begin{cases} P, & h = k \quad \& \quad m = l, \quad k \neq 0 \quad \& N/2 \\ 0, & \text{otherwise} \end{cases}$$

(3.8)

such that the MACO-OFDM frame is;

$$A_{frame}^m = [0, A_1^m, 0, A_3^m, 0, ..., A_{N/2-1}^m, 0, \left(A_{N/2-1}^m\right)^*, 0, ..., \left(A_3^m\right)^*, 0, \left(A_1^m\right)^*]$$

(3.9)

3.2.2 Inverse Fast Fourier Transform (IFFT)

A_{frame}^m is then input to the IFFT giving output x_n^m;

$$x_n^m = \frac{1}{\sqrt{N}} \sum_{k=0}^{N-1} A_k^m e^{\frac{j2\pi nk}{N}}, \qquad k = 1, 3, 5, 7, ...$$

(3.10)

The IFFT output time domain signal x_n^m is real but bipolar and is anti-symmetric around the element $N/2$ (Figure 3.2) such that;

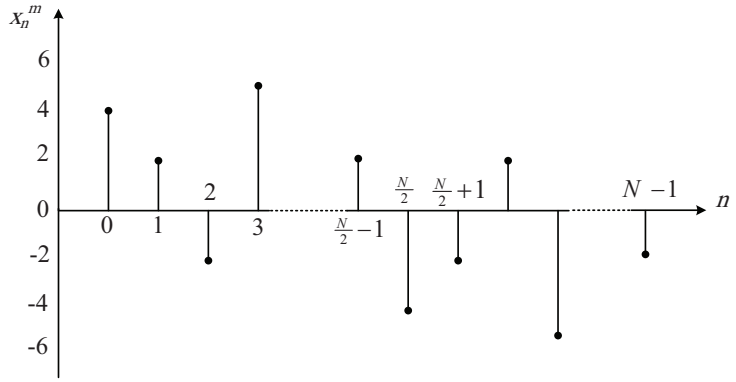

Fig. 3.2 Real time domain OFDM signal

$$x_n^m = -x_{N/2+n}^m \tag{3.11}$$

The variance of the time domain MACO-OFDM signal is;

$$\sigma_x^2 = E\left[x_n^m (x_n^m)\right] = E\left[\left[x_n^m\right]^2\right] \tag{3.12}$$

$$= \frac{1}{N}\sum_{k=0}^{N-1}\sum_{h=0}^{N-1} A_k^m A_h^m e^{\frac{j2\pi n(k+h)}{N}} \tag{3.13}$$

$$= \frac{1}{N}\sum_{k=0}^{N-1} A_k^m A_{N-k}^m e^{\frac{j2\pi n(k+(N-k))}{N}} \tag{3.14}$$

$$= \frac{1}{N}\sum_{k=0}^{N-1} A_k^m (A_k^m)^* e^{\frac{j2\pi n(k+(N-k))}{N}} \tag{3.15}$$

$$= \frac{1}{N}\sum_{k=0}^{N-1} P e^{j2\pi n} \tag{3.16}$$

$$= \frac{P}{2} \tag{3.17}$$

where $h = N-k$, and k takes only odd values.

The covariance of two samples x_n^m & x_p^m for $n \neq p$ is;

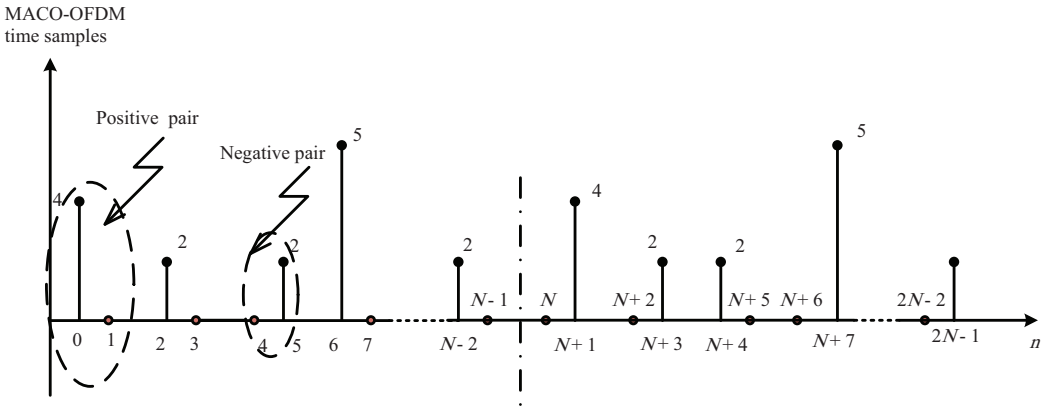

Fig. 3.3 Modified ACO-OFDM time domain signal

$$\mu_{np} = E\left[x_n^m x_p^m\right] \tag{3.18}$$

$$= \frac{1}{N}\sum_{k=0}^{N-1}\sum_{h=0}^{N-1} A_k^m A_h^m e^{\frac{j2\pi(nk+ph)}{N}} \tag{3.19}$$

$$= \frac{1}{N}\sum_{k=1}^{N-1} Pe^{\frac{j2\pi(nk+p(N-k))}{N}} \tag{3.20}$$

$$= \frac{1}{N}\sum_{k=1}^{N-1} Pe^{\frac{j2\pi(k(n-p))}{N}} \tag{3.21}$$

$$= \frac{P}{N}\sum_{k=1}^{\frac{N}{2}-1} e^{\frac{j2\pi k(n-p)}{N}} + e^{\frac{j2\pi(N-k)(n-p)}{N}} \tag{3.22}$$

$$= \frac{P}{N}\sum_{k=1}^{\frac{N}{2}-1} e^{\frac{j2\pi k(n-p)}{N}} + e^{-\frac{j2\pi k(n-p)}{N}} \tag{3.23}$$

$$= \frac{2P}{N}\sum_{k=1}^{\frac{N}{2}-1} cos(\frac{2\pi k(n-p)}{N}) \tag{3.24}$$

Therefore the correlation coefficient $\rho(n,p) = \frac{\mu_{np}}{\sigma_x^2} = 0$.

3.2.3 Unipolar Encoding & Pulse Shaping

In conventional ACO-OFDM, the bipolar real time domain signal x_n^m is clipped at zero level to ensure that the signal is positive. In the proposed system, unipolar encoding is used

instead of clipping.

Unipolar encoding represents each sample of the bipolar time domain signal by a pair of new time samples. If the time sample is positive then the first sample of the new pair is set with its amplitude, and the second sample of the new pair is set to zero; and if the original time domain sample is negative then the first sample of the new pair is set to zero and the second sample of the new pair is set with its positive amplitude (Figure 3.3).

In case of;

$$s(t) = sgn(t)x^m(n) \tag{3.25}$$

$$= \frac{sgn(t)}{\sqrt{N}} \sum_{k=0}^{N-1} A_k^m e^{\frac{j2\pi nk}{N}} \tag{3.26}$$

where

$$sgn(t) = \begin{cases} rect(\frac{t-2nT}{T}), & x(n) > 0 \\ 0, & x(n) = 0 \\ -rect(\frac{t-(2n+1)T}{T}), & x(n) < 0 \end{cases}$$

The pulse used for pulse shaping is rectangular pulse of width T and centered on the origin.It should be noted that the frame duration of s(t) equals $2NT$ and its average power σ_s^2 is given by ;

$$\sigma_s^2 = \frac{\sigma_x^2}{2} = \frac{P}{4}.$$

Furthermore, the transmission rate R_b and the average energy per bit E_b are given by;

$$R_b = \frac{Number \quad of \quad frame \quad bits}{Frame \quad duration} = \frac{N/4.log_2M}{2NT} = \frac{log_2M}{8T}\ b/s \tag{3.27}$$

$$E_b = \frac{Frame \quad energy}{Number \quad of \quad frame \quad bits} = \frac{\sigma_x^2 NT}{N/4.log_2M} = \frac{4\sigma_x^2 T}{log_2M} = \frac{2PT}{log_2M} = \frac{P}{4R_b} \tag{3.28}$$

It is assumed that the optical source is ideal following a linear transformation between the input and output optical power and that the signal transmitted through the optical channel is subject to AWGN. At the receiver, the signal becomes bipolar due to the added noise in the electrical domain. The above assumptions and model are most often used in the estimation of system performance taking into consideration the degradation in the signal due to ambient infrared radiation which produces shot noise at the receiver modelled as AWGN

where $\sigma_n = \sqrt{\frac{N_o}{2}}$.

The aim of the receiver is to reconstruct the bipolar signal "x". "$s(t)$" represents the bipolar signal "x" but in a unipolar form such that each sample of "s" represents the absolute value of "x" and its position in the first or second slot; each sample pair represents original signal sign.

Sampling at $t = nT + mNT$ takes place and after the addition of AWGN, one of the two samples in each pair is at the level of AWGN whilst the other is at the value of the original sample plus AWGN viz. the former is AWGN centred on the zero and the latter is AWGN centred on $|x|$.

Decoding is executed by comparing the amplitude of the two samples of each pair to determine the sign of the original bipolar sample. If the amplitude of the original sample is higher than its pair, the position is identified and so the sign is positive; the opposite is true for a negative sign. The transformation for each value of s is not deterministic since at each instant, it is dependent on the pair relationship and two other RVs. Further, although the transformation is non-linear, a comparison of the pair yields either a correct or an incorrect result. The procedure is random and depends on the level of AWGN at the two slots of each pair. So, the value of s is estimated as an average.

3.2.4 Correct Detection

Therefore, on the average "s" turns into $m_{correct}(x)$ when active sample and its sign are determined correctly. The active sample of each pair follows a Gaussian RV centred on "$|x|$" whilst the inactive sample follows a Gaussian RV centred on "0". So for correct detection, the value of the active sample subject to AWGN has to be greater than the value in the second slot of the pair giving an average value of s [29];

$$m_{correct}(x) = \frac{\int_{-\infty}^{\infty} \frac{sgn(x)z}{\sigma_n} \phi\left(\frac{z-|x|}{\sigma_n}\right)\left(1-Q\left(\frac{z}{\sigma_n}\right)\right) dz}{\int_{-\infty}^{\infty} \frac{1}{\sigma_n} \phi\left(\frac{z-|x|}{\sigma_n}\right)\left(1-Q\left(\frac{z}{\sigma_n}\right)\right) dz} \tag{3.29}$$

where $\phi(z) = \frac{1}{\sqrt{2\pi}} e^{-\left(\frac{z^2}{2}\right)}$ & $Q(z) = \frac{1}{\sqrt{2\pi}} \int_z^{\infty} e^{-\left(\frac{y^2}{2}\right)} dy$

the first part of Eq.(3.29) $\phi\left(\frac{z-|x|}{\sigma_n}\right) \equiv$ is the probability that the correct sample and has the value of z at the receiver ; the second part $1-Q\left(\frac{z}{\sigma_n}\right) \equiv$ is the probability that the value of the active sample (correct sample) is greater than the inactive sample of the pair and;

$$sgn(x) = \begin{cases} 1, & |x| is \quad in \quad the \quad first \quad slot \\ 0, & x = 0 \\ -1, & |x| is \quad in \quad the \quad second \quad slot \end{cases}$$

Substituting $sgn(x)$ in Eq. (3.29) gives;

$$m_{correct}(x) = \frac{\int_{-\infty}^{\infty} \frac{sgn(x)z}{\sigma_n}\phi\left(\frac{z-|x|}{\sigma_n}\right)dz - \int_{-\infty}^{\infty} \frac{sgn(x)z}{\sigma_n}\phi\left(\frac{z-|x|}{\sigma_n}\right)Q\left(\frac{z}{\sigma_n}\right)dz}{\int_{-\infty}^{\infty} \frac{1}{\sigma_n}\phi\left(\frac{z-|x|}{\sigma_n}\right)\left(1-Q\left(\frac{z}{\sigma_n}\right)\right)dz} \tag{3.30}$$

$$= \frac{sgn(x)\int_{-\infty}^{\infty} \frac{z}{\sqrt{2\pi}\sigma_n} e^{-\frac{(z-|x|)^2}{2\sigma_n^2}} dz - sgn(x)\int_{-\infty}^{\infty} \frac{z}{\sqrt{2\pi}\sigma_n} e^{-\frac{(z-|x|)^2}{2\sigma_n^2}} Q\left(\frac{z}{\sigma_n}\right)dz}{\int_{-\infty}^{\infty} \frac{1}{\sigma_n}\phi\left(\frac{z-|x|}{\sigma_n}\right)\left(1-Q\left(\frac{z}{\sigma_n}\right)\right)dz} \tag{3.31}$$

$$= \frac{sgn(x)|x| - sgn(x)\int_{-\infty}^{\infty} \frac{z}{\sqrt{2\pi}\sigma_n} e^{-\frac{(z-|x|)^2}{2\sigma_n^2}} Q\left(\frac{z}{\sigma_n}\right)dz}{\int_{-\infty}^{\infty} \frac{1}{\sigma_n}\phi\left(\frac{z-|x|}{\sigma_n}\right)\left(1-Q\left(\frac{z}{\sigma_n}\right)\right)dz} \tag{3.32}$$

$$= \frac{x - sgn(x)\int_{-\infty}^{\infty} \frac{z}{\sqrt{2\pi}\sigma_n} e^{-\frac{(z-|x|)^2}{2\sigma_n^2}} Q\left(\frac{z}{\sigma_n}\right)dz}{\int_{-\infty}^{\infty} \frac{1}{\sigma_n}\phi\left(\frac{z-|x|}{\sigma_n}\right)\left(1-Q\left(\frac{z}{\sigma_n}\right)\right)dz} \tag{3.33}$$

and the variance for correctly detected sample is [29];

$$v_{correct}(x) = \frac{\int_{-\infty}^{\infty} \frac{z^2}{\sigma_n} \phi\left(\frac{z-|x|}{\sigma_n}\right) Q\left(\frac{z}{\sigma_n}\right) dz}{\int_{-\infty}^{\infty} \frac{1}{\sigma_n} \phi\left(\frac{z-|x|}{\sigma_n}\right) \left(1 - Q\left(\frac{z}{\sigma_n}\right)\right) dz} - m_{correct}^2(x) \tag{3.34}$$

3.2.5 Erroneous Detection

Similarly for erroneous detection, the value of the active sample subject to AWGN has to be smaller than the value in the second slot of the pair. So the average value of s becomes [29];

$$m_{wrong}(x) = \frac{\int_{-\infty}^{\infty} \frac{sgn(x)z}{\sigma_n} \phi\left(\frac{z}{\sigma_n}\right) \left(1 - Q\left(\frac{z-|x|}{\sigma_n}\right)\right) dz}{\int_{-\infty}^{\infty} \frac{1}{\sigma_n} \phi\left(\frac{z}{\sigma_n}\right) \left(1 - Q\left(\frac{z-|x|}{\sigma_n}\right)\right) dz} \tag{3.35}$$

$$= \frac{\int_{-\infty}^{\infty} \frac{sgn(x)z}{\sigma_n} \phi\left(\frac{z}{\sigma_n}\right) dz - \int_{-\infty}^{\infty} \frac{sgn(x)z}{\sigma_n} \phi\left(\frac{z}{\sigma_n}\right) Q\left(\frac{z-|x|}{\sigma_n}\right) dz}{\int_{-\infty}^{\infty} \frac{1}{\sigma_n} \phi\left(\frac{z}{\sigma_n}\right) \left(1 - Q\left(\frac{z-|x|}{\sigma_n}\right)\right) dz} \tag{3.36}$$

$$= \frac{sgn(x) \int_{-\infty}^{\infty} \frac{z}{\sqrt{2\pi}\sigma_n} e^{-\left(\frac{z^2}{2\sigma_n^2}\right)} dz - \int_{-\infty}^{\infty} \frac{sgn(x)z}{\sigma_n} \phi\left(\frac{z}{\sigma_n}\right) Q\left(\frac{z-|x|}{\sigma_n}\right) dz}{\int_{-\infty}^{\infty} \frac{1}{\sigma_n} \phi\left(\frac{z}{\sigma_n}\right) \left(1 - Q\left(\frac{z-|x|}{\sigma_n}\right)\right) dz} \tag{3.37}$$

$$= \frac{\int_{-\infty}^{\infty} \frac{-z\, sgn(x)}{\sigma_n} \phi\left(\frac{z}{\sigma_n}\right) Q\left(\frac{z-|x|}{\sigma_n}\right) dz}{\int_{-\infty}^{\infty} \frac{1}{\sigma_n} \phi\left(\frac{z}{\sigma_n}\right) \left(1 - Q\left(\frac{z-|x|}{\sigma_n}\right)\right) dz} \tag{3.38}$$

The variance of wrongly detected sample $v_{wrong}(x)$ [29];

$$v_{wrong}(x) = \frac{\int_{-\infty}^{\infty} \frac{z^2}{\sigma_n} \phi\left(\frac{z}{\sigma_n}\right) \left(1 - Q\left(\frac{z-|x|}{\sigma_n}\right)\right) dz}{\int_{-\infty}^{\infty} \frac{1}{\sigma_n} \phi\left(\frac{z}{\sigma_n}\right) \left(1 - Q\left(\frac{z-|x|}{\sigma_n}\right)\right) dz} - m_{wrong}^2(x) \tag{3.39}$$

3.2.6 Non-Linear Transformation

The transformation executed is not linear and also not deterministic. The Bussgang Theorem provides a robust approach to treating the non-linear transformation of Gaussian RVs [63, 64]. The bipolar OFDM time domain signal can be approximated to a Gaussian RV if the number of carriers is sufficient (more than 64 carriers [17]) according to the CLT. The Bussgang Theorem states that if x is a Gaussian RV, then any transform $f(x)$ can be expressed as;

$$f(x) = cx + n \tag{3.40}$$

where $x\&n$ are uncorrelated such that $E[xn] = 0, \& c = constant$ given by;

$$c = \frac{E[xf(x)]}{\sigma_x^2} \tag{3.41}$$

For the cases of correct and erroneous detection, x turns into $f_{correct}(x)$ & $f_{wrong}(x)$ respectively such that the Bussgang Theorem can be rewritten as;

$$m_{correct}(x) = c_{correct}x + n_{correct} \tag{3.42}$$

$$m_{wrong}(x) = c_{wrong}x + n_{wrong} \tag{3.43}$$

3.2.6.1 Correct Detection

$c_{correct}$ can be expressed as [29];

$$c_{correct} = \frac{E[xm_{correct}(x)]}{\sigma_x^2} \tag{3.44}$$

$$= \frac{\int_{-\infty}^{\infty} \frac{xm_{correct}(x)}{\sigma_x} \phi\left(\frac{x}{\sigma_x}\right) dx}{\sigma_x^2} \tag{3.45}$$

The variance of the noise due to the non-linear transformation is [29];

$$\sigma_{n_{correct}}^2 = \int_{-\infty}^{\infty} \frac{m_{correct}^2(x)}{\sigma_x} \phi\left(\frac{x}{\sigma_x}\right) dx - c_{correct}^2 \sigma_x^2 \tag{3.46}$$

3.2.6.2 Erroneous Detection

In case of an erroneous detection, the gain and the variance of the noise part are expressed as [29];

$$c_{wrong} = \frac{\int_{-\infty}^{\infty} \frac{x m_{wrong}(x)}{\sigma_x} \phi\left(\frac{x}{\sigma_x}\right) dx}{\sigma_x^2} \tag{3.47}$$

$$\sigma^2_{n_{wrong}} = \int_{-\infty}^{\infty} \frac{m^2_{wrong}(x)}{\sigma_x} \phi\left(\frac{x}{\sigma_x}\right) dx - c^2_{wrong}\sigma_x^2 \tag{3.48}$$

3.2.7 BER Estimation

Each sample can be approximated as an independent and identically distributed (IID) RV. Furthermore, AWGN can also be treated as an IID RV. All these random non-linear transformations are equally likely and independently occurring at each time domain sample. Thus, the FFT, which is a linear operation, combines all noise components and transforms them into AWGN, preserving their variance in the frequency domain. In the case of each sample, all random processes are identical with equivalent probabilities; therefore for a whole frame, all processes occur at different rates according to their equivalent probabilities.

Therefore, noise components are calculated on the average of different values of x for both correct and erroneous detection respectively [29];

$$\bar{v}_{correct} = \int_{-\infty}^{\infty} \frac{v_{correct(x)}}{\sigma_x} \phi\left(\frac{x}{\sigma_x}\right) dx \tag{3.49}$$

$$\bar{v}_{wrong} = \int_{-\infty}^{\infty} \frac{v_{wrong(x)}}{\sigma_x} \phi\left(\frac{x}{\sigma_x}\right) dx \tag{3.50}$$

Since all processes are governed by different probabilities, the probability of correct detection and that of erroneous detection can be calculated respectively as;

$$P_{correct} = \int_{-\infty}^{\infty} \frac{2}{\sigma_x} \phi\left(\frac{x}{\sigma_x}\right) \left(1 - Q\left(\frac{x}{\sqrt{2}\sigma_n}\right)\right) dx \tag{3.51}$$

$$P_{wrong} = 1 - P_{correct} \tag{3.52}$$

The average gain factor $g_{average}$ is then calculated as [29];

$$g_{average} = P_{correct} c_{correct} + P_{wrong} c_{wrong} \tag{3.53}$$

and the average noise variance can be expressed as;

$$N_{average} = P_{correct} \left(\overline{v_{correct}} + \sigma^2_{n_{correct}} \right) + P_{wrong} \left(\overline{v_{wrong}} + \sigma^2_{n_{wrong}} \right) \tag{3.54}$$

Therefore the Signal-to-Noise-ratio (SNR) is given by [29];

$$SNR = \frac{g^2_{average} E_b}{N_{average}} \tag{3.55}$$

where E_b is the average bit energy such that the bit error rate (BER) is;

$$BER = \frac{\sqrt{M} - 1}{\sqrt{M} r} Q \left(\sqrt{\frac{3}{M-1} SNR} \right) \tag{3.56}$$

where r is the number of bits $r = log_2 \sqrt{M}$

3.3 Results

Monte Carlo simulations using MATLAB to estimate the average BER performance for 4-QAM, 16-QAM and 64-QAM are generated in order to validate the theoretical results. All BER theoretical performance results for the range of different modulation orders are be compared to results obtained through simulation.

All simulations are conducted for a 512 point IFFT/FFT MACO-OFDM system, repeated for 10000 iterations to yield an estimate of the average BER. As no fading is assumed in the IM/DD implementation, the evaluation of the performance of MACO-OFDM subject to AWGN can be considered a sufficient preliminary model that treats the performance of

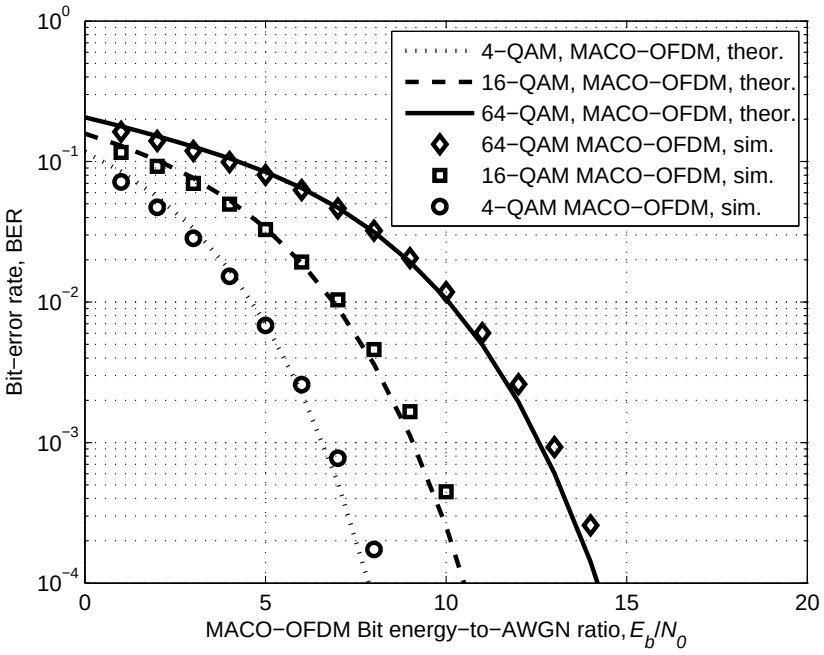

Fig. 3.4 A comparison of the BER performance of MACO-OFDM between theoretical obtained results and Monte Carlo simulations.

the proposed optical wireless technique. Figure 3.4 shows a comparison of results obtained through the theoretical model and Monte Carlo simulations, showing good agreement. The BER in case of 4-QAM, 16-QAM and 64-QAM reaches 10^{-4} at a bit Energy-to-Noise ratio of 7.5 dB, 10.5 dB, and 14.2 dB respectively.

In addition, the use of unipolar encoding/decoding results in a reduction in the required power for MACO-OFDM compared to conventional ACO-OFDM. Figure 3.5 compares the BER performance of conventional ACO-OFDM and the proposed MACO-OFDM. As MACO-OFDM occupies half the spectral efficiency of conventional ACO-OFDM, 4-QAM ACO-OFDM is compared to 16-QAM MACO-OFDM and 8-QAM ACO-OFDM is compared to 64-QAM MACO-OFDM. In summary, in the first case, the performance of the modified system compared with ACO-OFDM is better by 1 dB; in the second case, the BER of MACO-OFDM is is nearly the same when compared to that of ACO-OFDM.

Figure 3.6 shows the normalised optical power as a function of the normalised bandwidth for both ACO-OFDM and MACO-OFDM. The normalised bandwidth for ACO-OFDM is $2(1+2/N)log_2M$ [22] but with unipolar encoding, the length of the OFDM frame is doubled causing the spectral efficiency to be halved to that of ACO-OFDM [29]]; therefore, the normalised bandwidth in the case of modified ACO-OFDM is $4(1+2/N)log_2M$. MACO-OFDM using 16-QAM has the same normalised bandwidth as 4-QAM ACO-OFDM

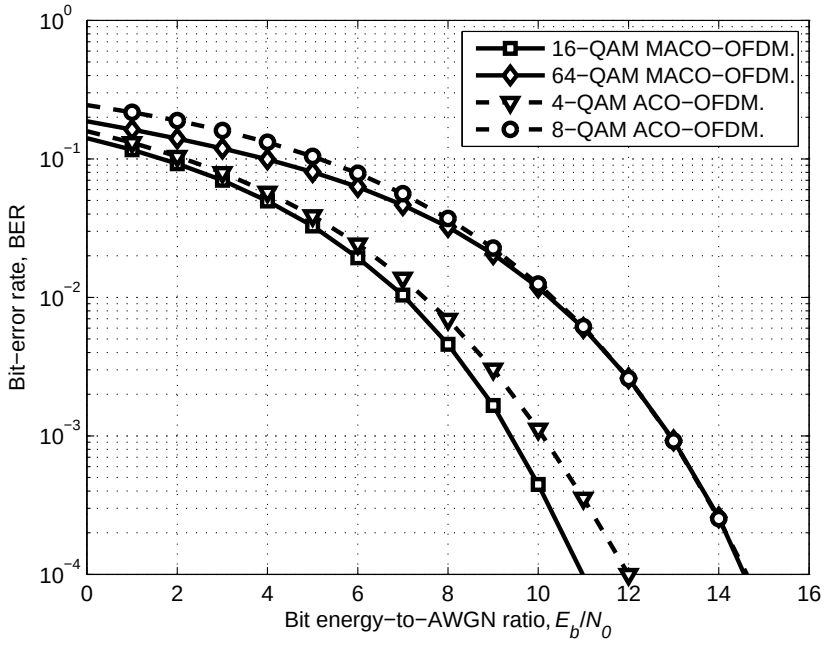

Fig. 3.5 BER comparison between MACO-OFDM and ACO-OFDM.

but requires $\backsim$ 1 dB less power. 4-QAM MACO-OFDM requires the least optical power but exhibits the worst bandwidth efficiency.

3.4 Simulations Methodology

In order to provide a meaningful estimation of system performance and in support of the analytical framework developed, a series of simulations were undertaken.

A number of simulation approaches are commonplace but here, Monte Carlo is adopted since it has been proven to be the most efficient and commonly used for the evaluation of communication systems [23–27]. The methodology provides the behaviour of each system component taking into account all possible operational scenarios. Monte Carlo simulations are characterised by a long simulation time to convergence compared to analytical methods owing to the large number of operational scenarios considered in the system evaluation. Thus a combination of Monte Carlo simulation with Matlab software is used in the performance evaluation.

Monte Carlo simulations using MATLAB were carried out for MACO-OFDM to obtain the BER curves. Figure 3.7 shows a flow chart that explains the steps carried out through the simulations.

Random bits are generated and inputted to the QAM modulator. The M-QAM symbols

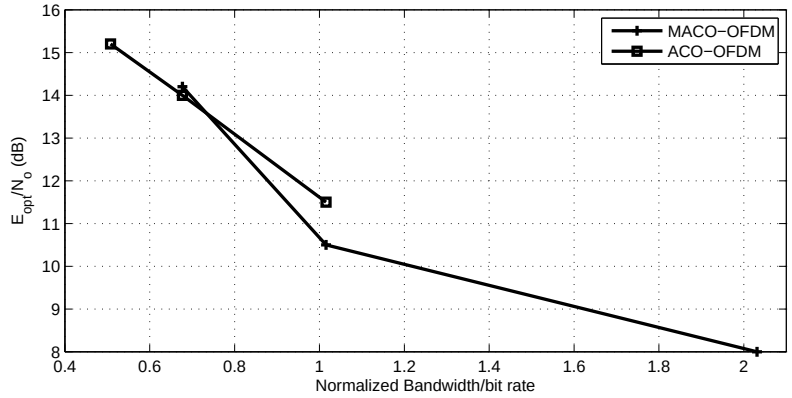

Fig. 3.6 Eb_{opt}/N_o for $BER = 10^{-4}$ and normalized optical power versus normalized bandwidth for ACO-OFDM and modified ACO-OFDM.

are mapped on the first half of the odd sub-carriers only of the OFDM frame and the even sub-carriers are set to zero. Hermitian symmetry is applied on the odd sub-carriers of the OFDM frame. The size of the OFDM frame is set to $N = 512$. The OFDM frame is then fed to the IFFT and unipolar encoding is applied to the output of the block. A Cyclic Prefix is added to the beginning of each MACO-OFDM frame which is transmitted through AWGN channel. At the receiver, the Cyclic Prefix is removed followed by decoding. Averaging process takes place taking advantage of the existing anti-symmetry. FFT and QAM demodulation are carried out after averaging and the BER is calculated. Simulations are initiated with different seed numbers and the characteristic converges to stable estimates after 10000 iterations. Different number of iterations were tested since the number of iterations varies on a case by case basis; the simulation process is repeated for 10000 iterations at different seeds provides a stable, accurate estimation of the average value for the BER at varying Signal-to-Noise Ratios (SNRs).

3.5 Conclusions

The BER performance of the proposed MACO-OFDM technique is simulated and analytically derived and both results are in good agreement.

As MACO-OFDM spectral efficiency is half that of ACO-OFDM, for a meaningful comparison of BER performance, 16-QAM MACO-OFDM is compared to 4-QAM ACO-OFDM and 64-QAM MACO-OFDM is compared to 8-QAM ACO-OFDM. Compared to ACO-OFDM, results reveal that the improvement in the performance of ACO-OFDM scheme is 1.5 dB in case of 4-QAM; the improvement decreases with increasing constellation size (Table 3.1).

Table 3.1 Comparison between MACO-OFDM and ACO-OFDM.

	$E_b/N_o\,(dB)\,atBER = 10^{-4}$
16-QAM MACO-OFDM	10.5
4-QAM ACO-OFDM	12
64-QAM MACO-OFDM	14.2
8-QAM ACO-OFDM	14.5

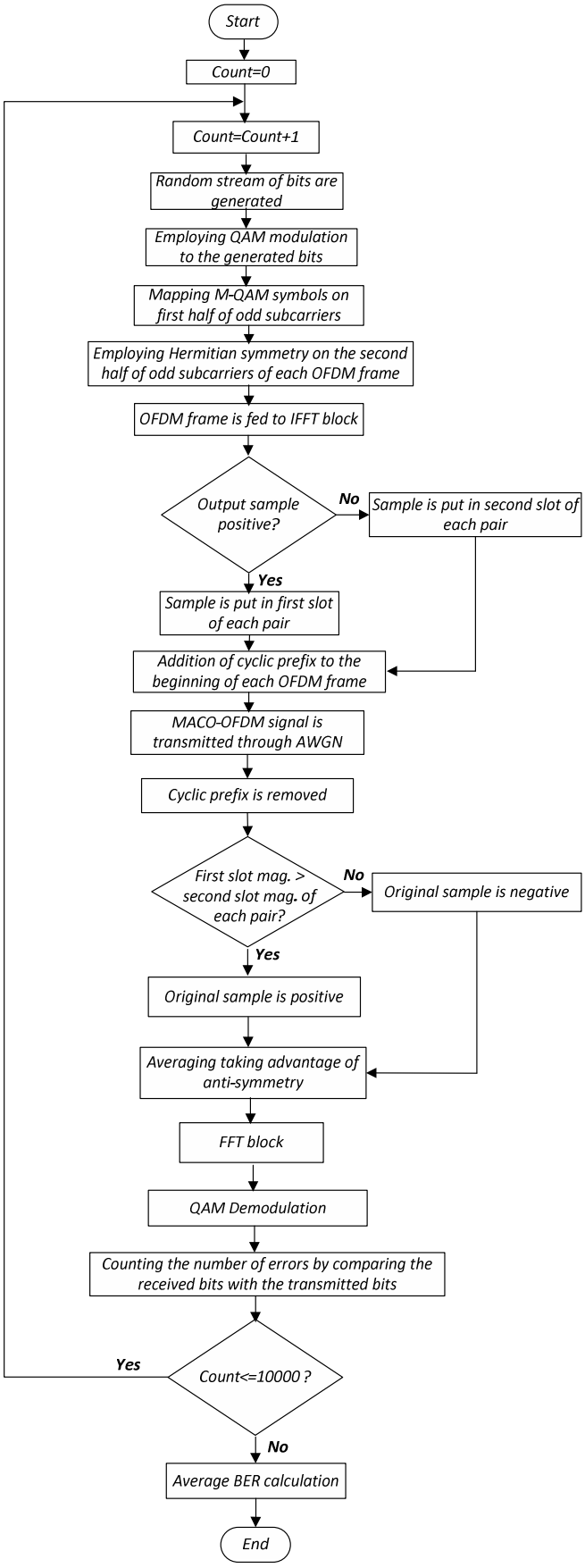

Fig. 3.7 Simulation Methodology

CHAPTER 4

MODIFIED ACO-OFDM PERFORMANCE IN OUTDOOR

4.1 Introduction

All wireless communications utilise the atmosphere as the transmission medium, a channel the characteristics of which are complex, dynamic and random with its impact on system performance is best captured statistically [4]. In the case of an optical beam, losses and turbulence induced amplitude and phase fluctuations are two of the most severe impairments. A number of models have been proposed to describe the nature of the atmospheric channel statistically [3] as explained in chapter 2. This chapter is investigating the performance of both MACO-OFDM and conventional ACO-OFDM in atmospheric turbulence channel. A comparison between their BER performance is carried out.

4.2 O-OFDM Systems Performance in Atmospheric Turbulence

The negative exponential distribution is the most suitable for the saturation regime [4] whilst the Gamma-Gamma distribution is suitable for a wide range from weak to strong turbulence [4]. So, the Gamma-Gamma model is adopted to represent atmospheric turbulence in the estimation of system performance; a comparison of the performance of both ACO-OFDM and MACO-OFDM systems is carried out.

4.2.1 Weak Atmospheric Turbulence

In case of weak atmospheric turbulence the value of both α and β are $\gg 1$. The $SI < 0.2$.

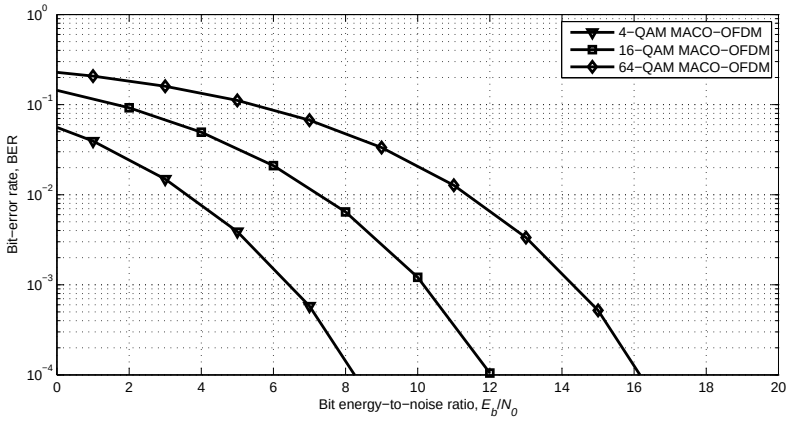

Fig. 4.1 BER performance for Mod. ACO-OFDM in case of weak atmospheric turbulence.

4.2.1.1 MACO-OFDM Performance

The BER performance of MACO-OFDM as a function of SNR for 4-QAM, 16-QAM and 64-QAM is shown in Figure 4.1

The BER performance degrades due to atmospheric turbulence when compared to its performance in the case of an ideal channel. The degradation in performance is small 2 dB for weak turbulence with $SI = 0.11, \alpha = 18.25$ and $\beta = 16.58$.

4.2.1.2 ACO-OFDM Performance

At the same channel condition as above, the BER performance of ACO-OFDM as a function of SNR for 4-QAM, 16-QAM and 64-QAM is shown in Figure 4.2. The BER degrades with respect to the performance in the case of an AWGN channel; the BER degrades by 0.5 dB, 1 dB and 1 dB for 4-QAM, 16-QAM, 64-QAM respectively.

4.2.2 Moderate to Strong Atmospheric Turbulence

For moderate to strong atmospheric turbulence, the value of $SI > 0.2$ and reaches 1.2 before entering saturation (Figure 2.31) .

4.2.2.1 MACO-OFDM Performance

As the strength of turbulence increases, the BER performance degrades (Figure 4.3,$SI = 0.7, \alpha = 4.39, and \beta = 2.56$). The performance of the system degrades by 19 dB compared to its performance in weak turbulence. For $SI = 0.98, \alpha = 3.993, and \beta = 1.7$, the strength

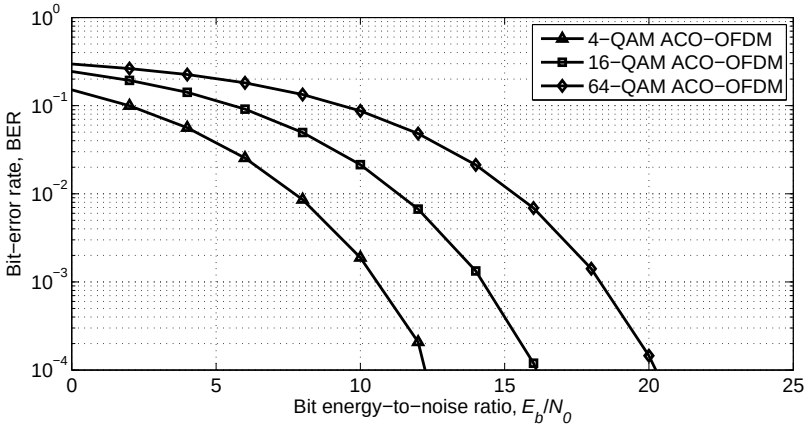

Fig. 4.2 BER performance for ACO-OFDM in case of weak atmospheric turbulence.

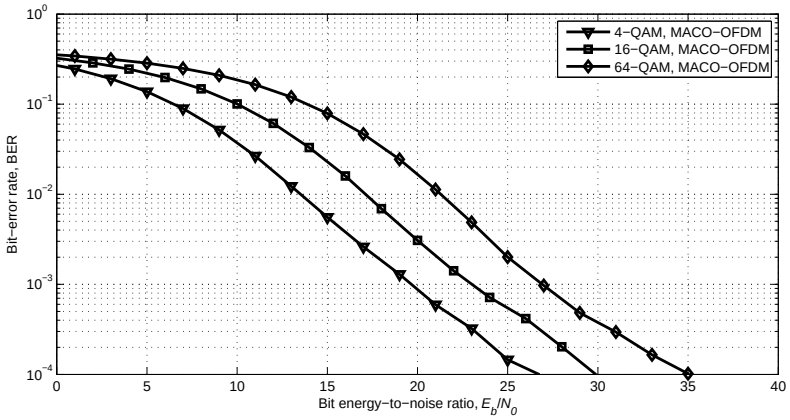

Fig. 4.3 BER performance for Mod. ACO-OFDM in case of moderate atmospheric turbulence.

of turbulence increases and the performance degrades further by 37 dB compared to the case of strong turbulence (Figure 4.4).

4.2.2.2 ACO-OFDM Performance

Figure 4.5 shows the BER performance of ACO-OFDM for $SI = 0.7$. As expected the performance deteriorates by 20 dB compared to the cases of an AWGN channel and weak turbulence. Similarly, ACO-OFDM performance is investigated for $SI = 0.98$ highlighting further degradation (Figure 4.6). It is clear that system performance degrades with increases in the strength of atmospheric turbulence.

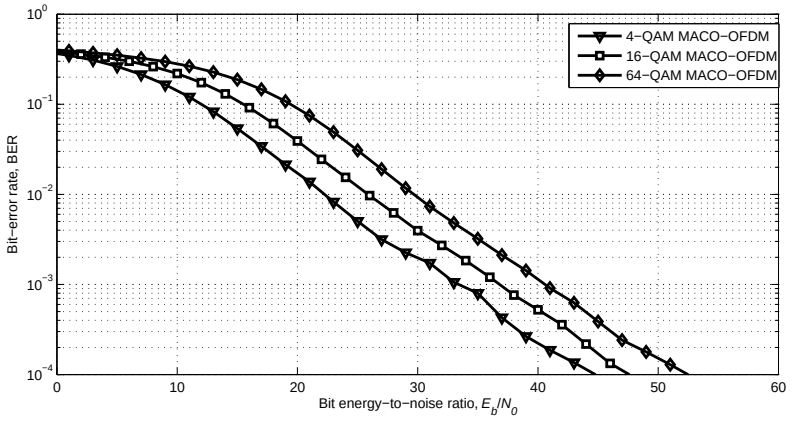

Fig. 4.4 BER performance for Mod. ACO-OFDM in case of strong atmospheric turbulence.

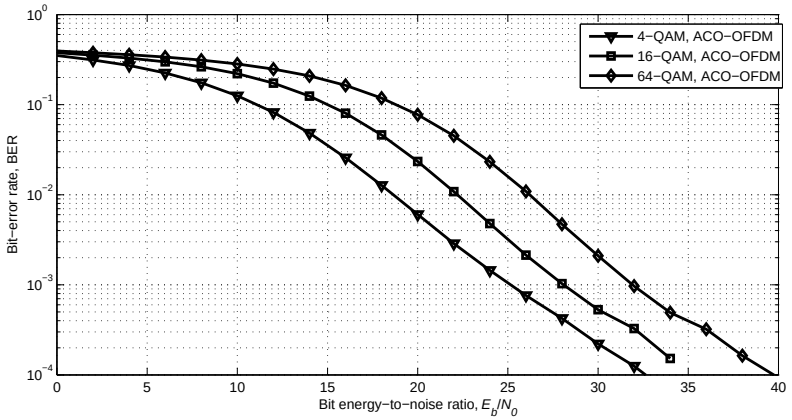

Fig. 4.5 BER performance for ACO-OFDM in case of moderate atmospheric turbulence.

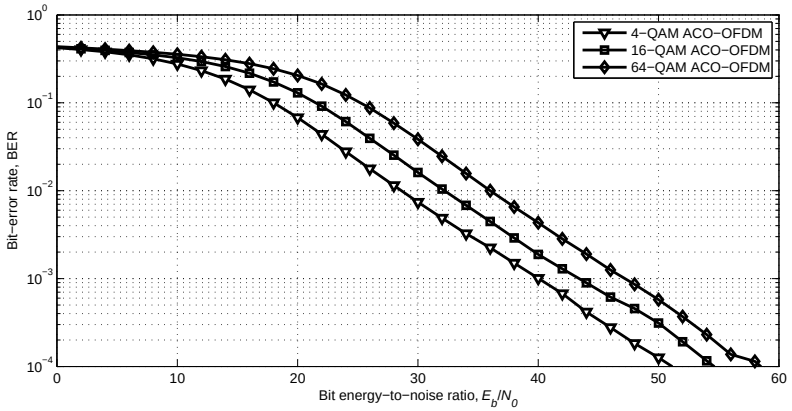

Fig. 4.6 BER performance for ACO-OFDM in case of strong atmospheric turbulence.

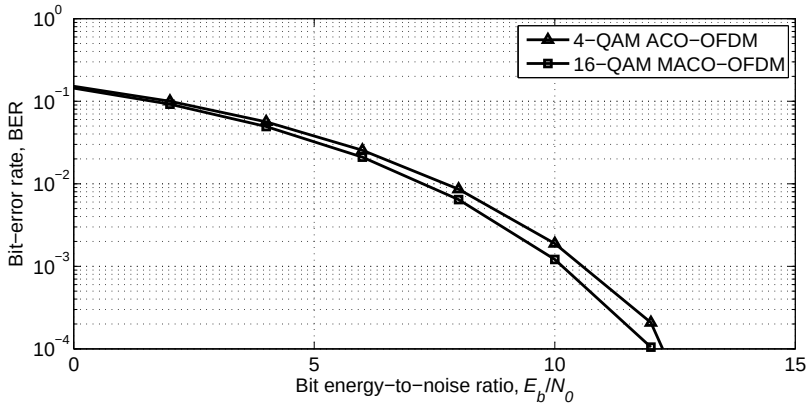

Fig. 4.7 A comparison between BER performance of ACO-OFDM and Mod. ACO-OFDM in case of weak atmospheric turbulence.

4.3 ACO-OFDM and MACO-OFDM System Performance Comparison

4.3.1 Weak Atmospheric Turbulence

A comparison between the BER performance of ACO-OFDM and MACO-OFDM is presented in Figure 4.7. Since the spectral efficiency of MACO-OFDM is half that of ACO-OFDM, for a fair comparison, the performance of 4QAM ACO-OFDM is compared to the performance of 16QAM MACO-OFDM. Under weak atmospheric turbulence, the BER performance of MACO-OFDM is better than that of ACO-OFDM by 0.5 dB, directly attributable to the use of unipolar encoding.

4.3.2 Moderate to Strong Atmospheric Turbulence

The difference in BER performance between MACO-OFDM and ACO-OFDM increases with increasing levels of turbulence (Figure 4.8, $SI = 0.7$) and (Figure 4.9, $SI = 0.98$).

4.4 Conclusions

The Log-normal distribution is used to represent only weak atmospheric turbulence; Gamma-gamma distribution is used to represent all atmospheric turbulence regimes as summarised in Table 4.1.

The BER performance of ACO-OFDM and MACO-OFDM is estimated under different atmospheric turbulence regimes and summarised in Table 4.2 and 4.3.

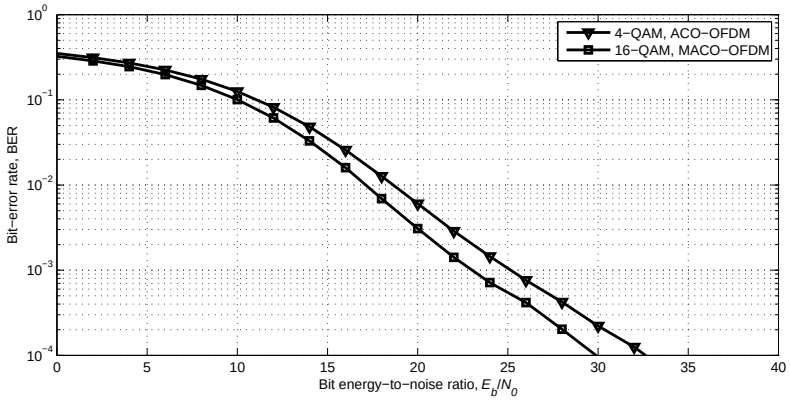

Fig. 4.8 A comparison between BER performance of ACO-OFDM and Mod. ACO-OFDM in case of moderate atmospheric turbulence.

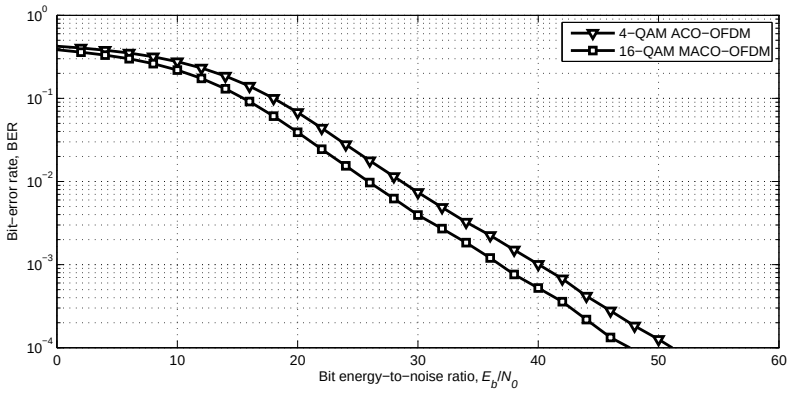

Fig. 4.9 A comparison between BER performance of ACO-OFDM and Mod. ACO-OFDM in case of strong atmospheric turbulence.

The BER performance of MACO-OFDM in the case of weak atmospheric turbulence is better by 0.5 dB than that of ACO-OFDM; however the improvement in performance increases as the strength of turbulence increases.

Table 4.1 Comparison of different atmospheric turbulence models.

	Model Availability	Model non-Availability
Lognormal Distribution	It is perfectly used to model the weak atmospheric turbulence for S.I.<0.2	It can not be used to model beyond weak atmospheric turbulence.
Gamma-Gamma Distribution	It is used to model wide range of atmospheric turbulence regimes from weak to strong S.I.<1.2	Can not be used to model saturation regime S.I.>1.2
Negative Exponential distribution	It is used to model saturation regime	Can not be used in any other atmospheric turbulence regime

Table 4.2 Comparison between BER performance for MACO-OFDM in weak, moderate and strong atmospheric turbulence.

	Weak Atmosperic Turbulence	Moderate Atmosperic Turbulence	Strong Atmosperic Turbulence
4-QAM	8.5 dB	25 dB	46 dB
16-QAM	12 dB	30 dB	59.5 dB
64-QAM	16.2	35 dB	52.5 dB

Table 4.3 Comparison between BER performance for ACO-OFDM in weak, moderate and strong atmospheric turbulence.

	Weak Atmosperic Turbulence	Moderate Atmosperic Turbulence	Strong Atmosperic Turbulence
4-QAM	12.5 dB	34 dB	51.5 dB
16-QAM	16 dB	35 dB	54.5 dB
64-QAM	20.5 dB	39.5 dB	59 dB

CHAPTER 5

MIMO MODIFIED ACO-OFDM PERFORMANCE IN OUTDOOR

5.1 Introduction

The use of Single Input Multiple Output (SIMO) diversity techniques is investigated to mitigate the impact of atmospheric turbulence on O-OFDM system performance. Multiple Input Multiple Output (MIMO) strategies have proven to be effective in improving the performance of a number of broadband wireless communications systems; it is in current use in 4G wireless networks [65]. Here the investigation is confined to the use of single laser sources at the transmitter and multiple photodetectors at the receiver.

5.2 Diversity Techniques

Space Time Processing (STP) is a class of signal processing performed on systems comprising several transmitting or receiving elements, whose signals are processed adaptively in order to exploit the multiple dimensions offered by the wireless optical channel in both the spatial (space) and temporal (time) dimensions [66]. STP techniques can be applied either at the transmitter, receiver, or both. Figure 5.1 illustrates different link structures depending on the number of antennas used in receiving or transmitting modes. Depending on the number of transmitting laser sources, the channel is classified as single input (SI) or multiple input (MI) and according to the number of receiving apertures, the channel is classified as single output (SO) or multiple output (MO) [51, 67–71].

For a communication link with N receiving apertures and M transmitting laser sources, the channel can be described by an NM matrix $H(\tau,t)$ where τ is the channel delay. The element $h_{ij}(\tau,t)$ of the matrix denotes the impulse response from transmit laser source j to receive photodetector i. The channel matrix can be written as;

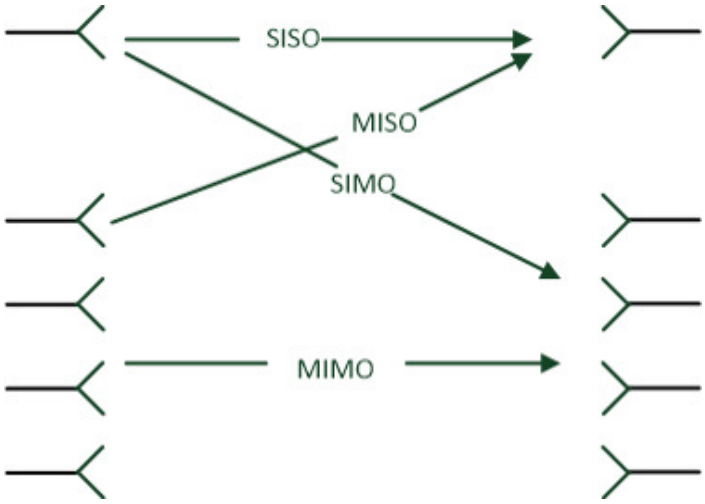

Fig. 5.1 Link structure .

$$H = \begin{bmatrix} h_{11} & h_{12} & .... & .... & h_{1M} \\ h_{21} & h_{22} & .... & .... & h_{2M} \\ .... & .... & .... & .... & .... \\ h_{N1} & h_{N2} & .... & .... & h_{NM} \end{bmatrix} \tag{5.1}$$

As the laser beam is subjected to atmospheric turbulence, different diversity techniques such as Equal Gain Combining (*EGC*) [72], Selection Combining (*SC*), and Maximal Ratio Combining (*MRC*) have been employed to mitigate the effect of turbulence [73]. Both EGC and MRC provide similar system performance but EGC exhibits < 1 dB power penalty, the cost for the reduced complexity of using equal gains. In the research, MRC is used to mitigate the impact on system performance of atmospheric turbulence.

5.2.1 Selection Combining (SC)

When SC is employed, the combiner selects the receiving aperture with the highest Signal-to-Noise Ratio (SNR). Since only one branch is used at a time, SC often requires just one receiver switched to the active aperture branch. The path output from the combiner has an SNR equal to the maximum SNR of all the branches. Since only one branch output is used, co-phasing of multiple branches is not required [51, 73].

5.2.2 Equal Gain Combining (EGC)

EGC co-phases the signals on each branch and then combines them with equal weighting, $\alpha_i = e^{\theta_i}$, where α_i is the i^{th} branch weight and θ_i is i^{th} path phase. The equalization takes place by removing the channel phase from the received symbol [51].The performance of EGC is close to that of MRC, typically exhibiting less than 1 dB power penalty, a penalty for the reduced complexity of using equal gains.

5.2.3 Maximal Ratio Combining (MRC)

MRC is based on the addition of signals from each channel. The gain of each channel is made proportional to the Root Mean Square (RMS) signal level and inversely proportional to the noise signal level. Different proportionality constants are used for each channel. The goal is to choose α_i, where α_i is the ith branch weight, that maximises the average SNR per branch. Branches with high SNR are weighted more than branches with low SNR. MRC is considered the best or optimum combiner for independent AWGN channels [51, 73]. However, MRC also requires knowledge of the time-varying SNR on each branch, which can be very difficult to measure.

5.3 System Model and Results

A Single Input (laser source), Multiple Outputs (photodetectors) (SIMO) geometry is chosen in the goal of increasing the robustness to atmospheric turbulence of both ACO-OFDM and MACO-OFDM systems (Figure 5.2). The geometry, classified as receive diversity is usually employed to combat fading, is considered relatively easy to implement although it does have a disadvantage in that further processing is required in the receiver [51, 73]. With MRC, branches of higher SNR are weighted higher and then added together. The estimation of the BER for O-OFDM is carried out following the same principles.

Single laser source and multiple photodetectors ($SIMO$) system is applied in our work for both ACO-OFDM and Mod. ACO-OFDM systems as shown in fig. 5.2.

5.3.1 SIMO ACO-OFDM Performance in Atmospheric Turbulent Channel

The BER performance is investigated for ACO-OFDM employing MRC diversity at the receiver for weak, moderate and strong atmospheric turbulence. The performance is evaluated for an increasing number of photodetectors viz. $nRx = 1, 2, and 4$.

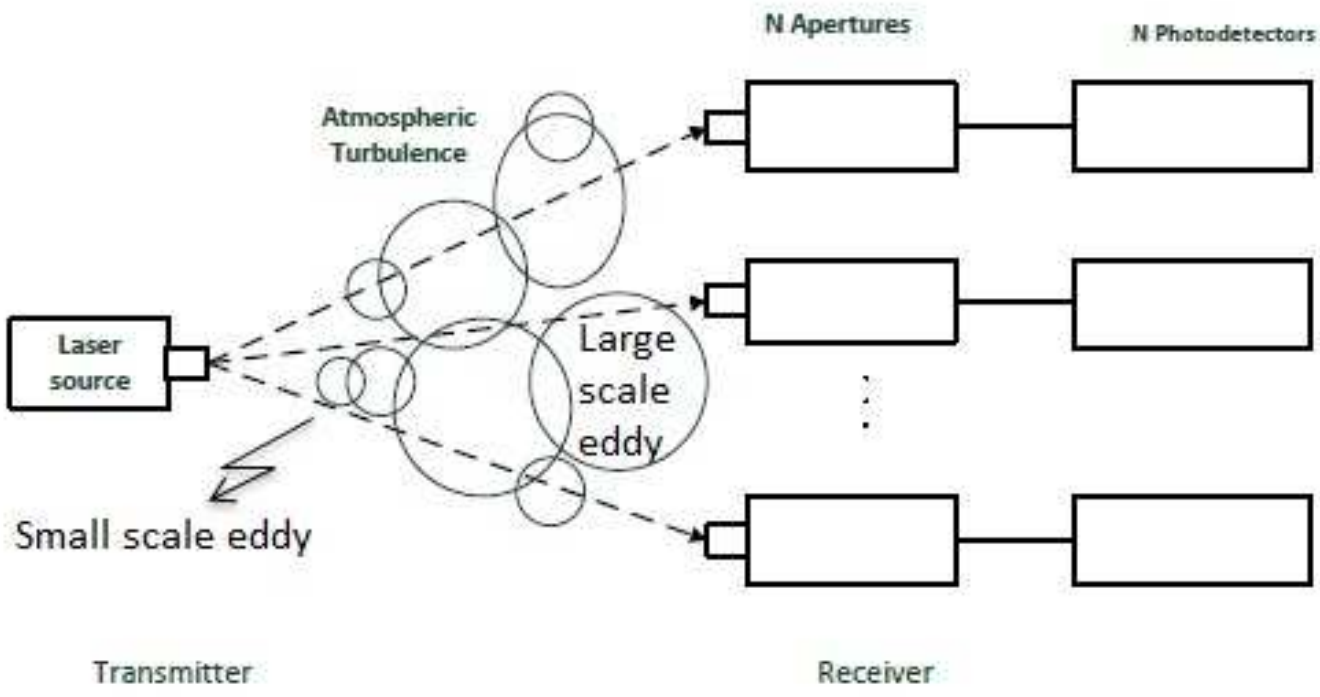

Fig. 5.2 Block diagram of *SIMO* system .

5.3.1.1 Weak Turbulence

The BER performance for 4-QAM, 16-QAM, and 64-QAM ACO-OFDM is estimated at $SI = 0.11$, $\alpha = 18.2530$ and $\beta = 16.5793$ and the results are shown in Figure 5.3, Figure 5.4, and Figure 5.5 respectively.

As expected the BER improves as the number of receiving apertures increases;

- For 4-QAM ACO-OFDM, the BER performance improves by 4 dB when the number of receiver increases to 2 and by 3.5 dB when the number of receivers increases to 4.
- For 16-QAM ACO-OFDM, the BER performance improves by 4 dB and 3.5 dB as the number of receiving apertures increases to 2 and 4 respectively.
- For 64-QAM ACO-OFDM, an improvement in BER performance of 4 dB and 3 dB is achieved as the number of receiving apertures increases to 2 and 4 respectively

5.3.1.2 Moderate Turbulence

The BER performance for 4-QAM, 16-QAM, and 64-QAM SIMO ACO-OFDM is evaluated at an increased strength of turbulence (SI=0.7 , $\alpha = 4.3939$ and $\beta = 2.5636$) and the

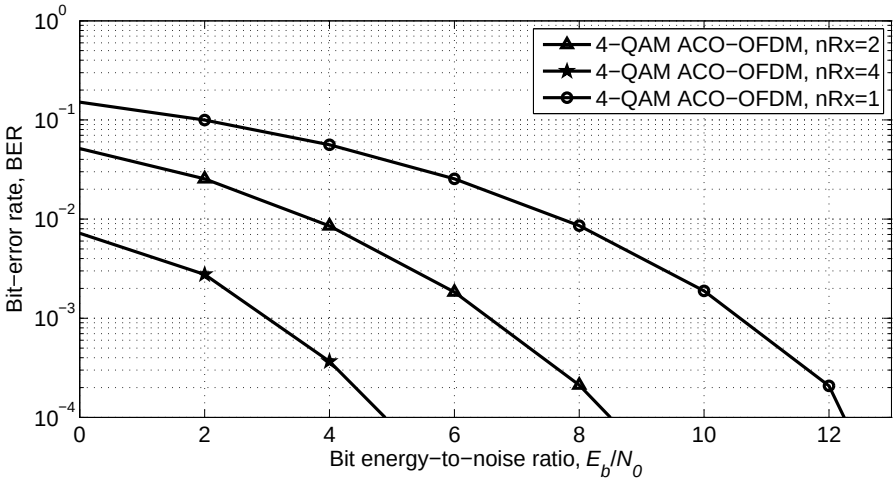

Fig. 5.3 BER performance for 4-QAM SIMO ACO-OFDM in case of weak atmospheric turbulence.

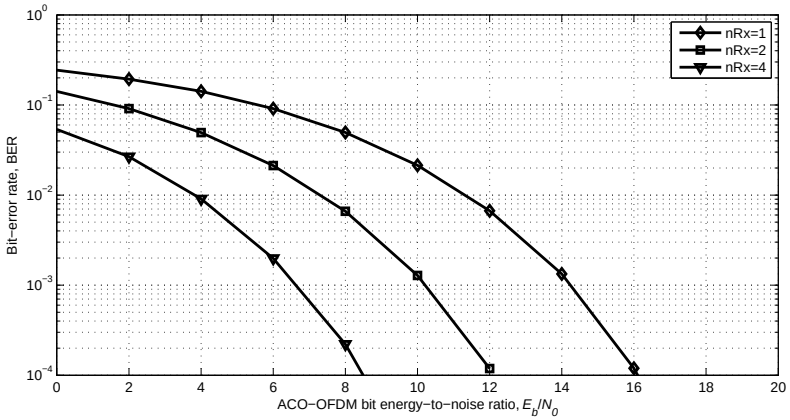

Fig. 5.4 BER performance for 16-QAM SIMO ACO-OFDM in case of weak atmospheric turbulence.

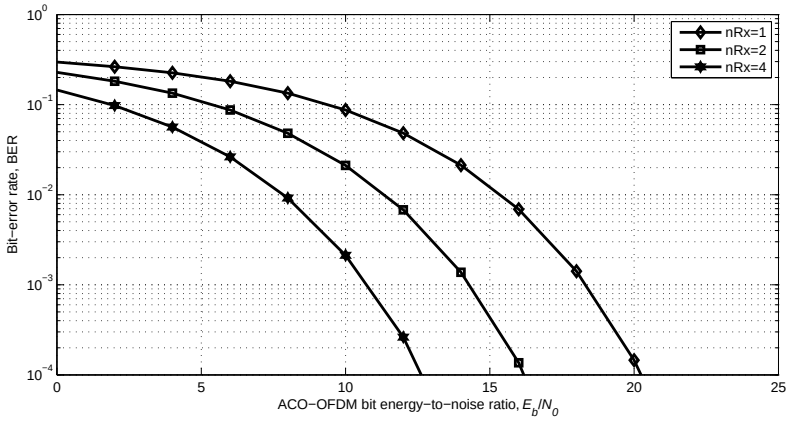

Fig. 5.5 BER performance for 64-QAM SIMO ACO-OFDM in case of weak atmospheric turbulence.

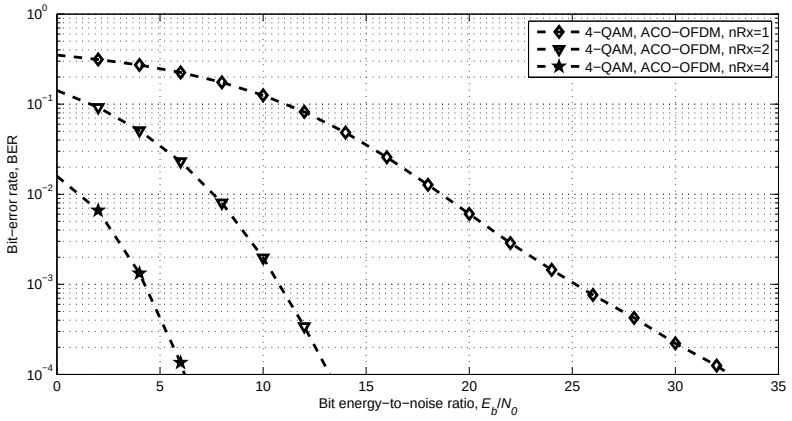

Fig. 5.6 BER performance for 4-QAM SIMO ACO-OFDM in case of moderate atmospheric turbulence.

results are shown in Figure 5.6 , Figure 5.7 and Figure 5.8.

The BER performance improves with increasing number of receiving apertures;

- the BER performance for 4-QAM improves by 19.5dB as the number of receiving apertures doubles to 2; an increase of 7 dB is achieved when nRx=4.
- for 16-QAM, an improvement in performance of 18.5 dB and 7 dB is obtained when nRx=2 and 4 respectively.
- for 64-QAM, the improvement of nearly 19.5 dB and 6 dB is achieved increasing nRx to 2 and 4 respectively.

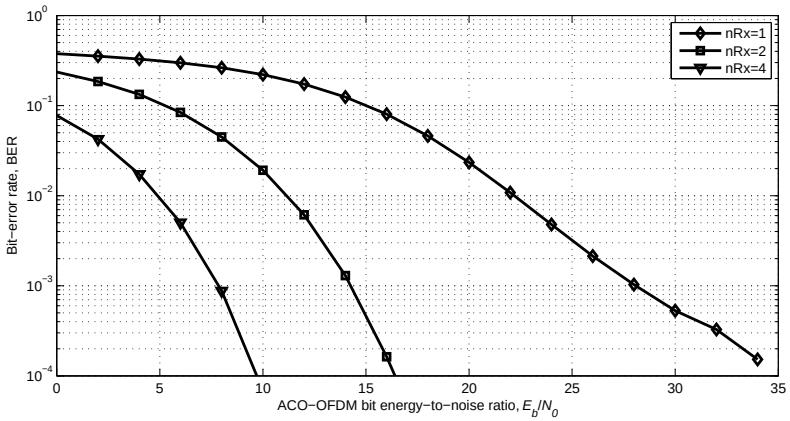

Fig. 5.7 BER performance for 16-QAM SIMO ACO-OFDM in case of moderate atmospheric turbulence.

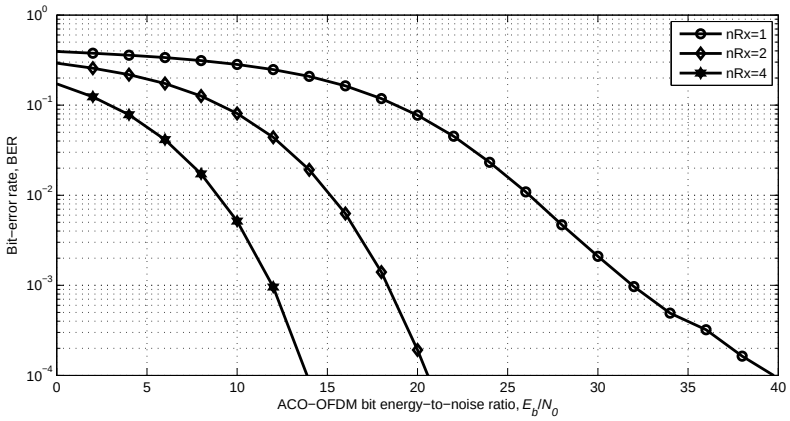

Fig. 5.8 BER performance for 64-QAM SIMO ACO-OFDM in case of moderate atmospheric turbulence.

Also, as expected, the BER performance in moderate turbulence is inferior to that in weak turbulence;

- for 4-QAM, the BER degrades by 20 dB, 5 dB and 1.6 dB for nRx=1,2,and 4
- for 16-QAM, the BER degrades by 19 dB, 4.5 dB, and 1 dB at nRx=1, 2, and 4
- for 64-QAM, the performance is worse by 19.5 d B, 4.5 dB, and 1dB at nRx=1,2, and 4.

5.3.1.3 Strong Atmospheric Turbulence

The BER performance for 4-QAM, 16-QAM, and 64-QAM SIMO ACO-OFDM is evaluated at strong atmospheric turbulence ($SI = 0.98$, $\alpha = 3.9929$, and $\beta = 1.7018$) and the results are shown in Figure 5.9, Figure 5.10and Figure 5.11. The BER for SIMO ACO-OFDM is, as expected, better than that of ACO-OFDM and improves with increasing number of receiving apertures. For 4-QAM, the performance improves by 30.5 dB and 11.5 dB when nRx increases to 2 and 4 respectively. Also, for 16-QAM, the performance improves by 32 dB and 11.5 dB for an increase of nRx to 2 and 4. In case of 64-QAM, an improvement in the performance on increasing the nRx to 2 and 4 is 33dB and 11.5dB respectively.

Checking the BER performance at $SI = 0.98$, $\alpha = 3.9929$, and $\beta = 1.7018$ is carried out as seen in the following figures for 4, 16, and 64 QAM respectively.

When comparing the BER performance in case of SIMO ACO-OFDM to that in case of ACO-OFDM, the performance improves by increasing the number of receiving apertures.

5.3.2 SIMO MACO-OFDM Performance in Atmospheric Turbulence

The BER performance is also investigated for MACO-OFDM employing the MRC diversity at the receiver for weak, moderate and strong atmospheric turbulence. The performance is evaluated for an increasing number of photodetectors viz. nRx =1, 2 and 4.

5.3.2.1 Weak Atmospheric Turbulence

The BER performance for 4-QAM, 16-QAM, and 64-QAM MACO-OFDM is estimated at $SI = 0.11$, $\alpha = 18.2530$ and $\beta = 16.5793$ and the results are shown in Figure 5.12, Figure 5.13, and Figure 5.14 respectively.

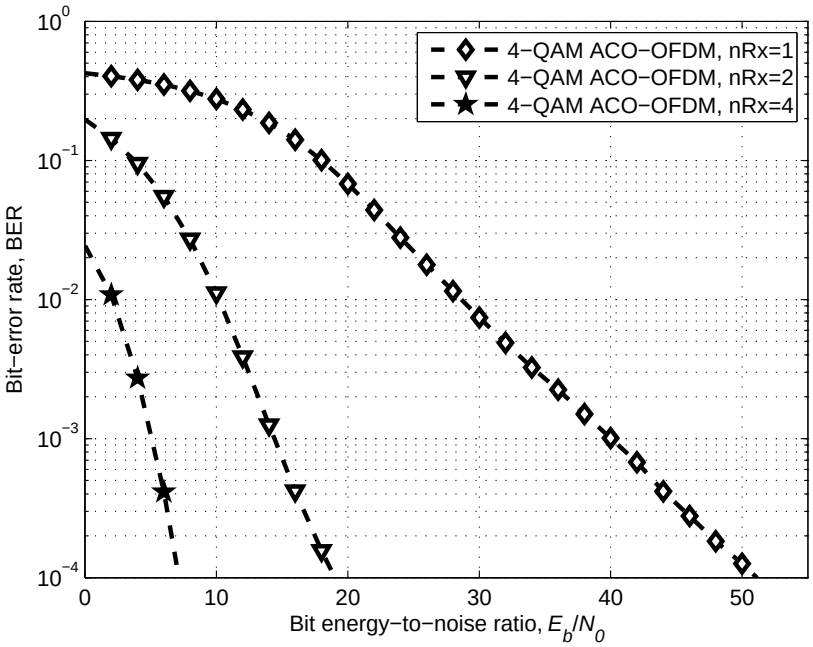

Fig. 5.9 BER performance for 4-QAM SIMO ACO-OFDM in case of strong atmospheric turbulence.

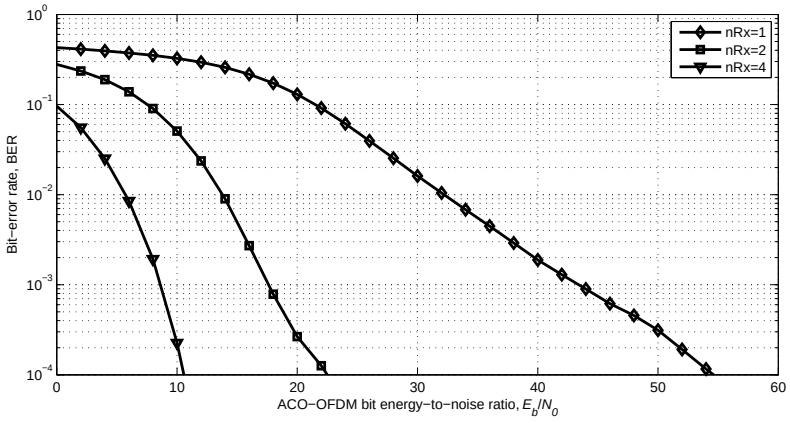

Fig. 5.10 BER performance for 16-QAM SIMO ACO-OFDM in case of strong atmospheric turbulence.

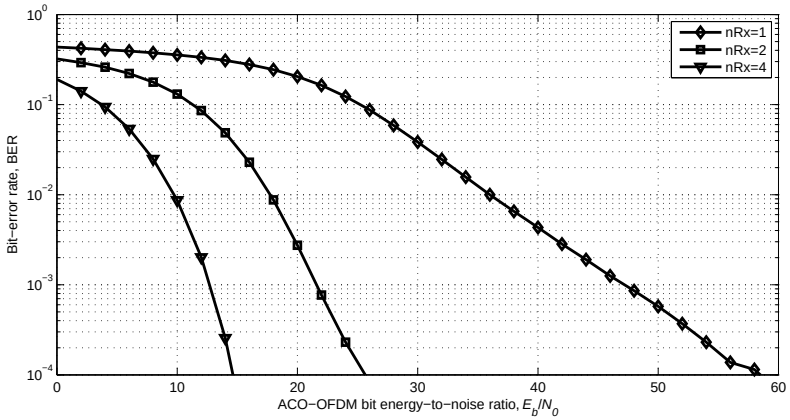

Fig. 5.11 BER performance for 64-QAM SIMO ACO-OFDM in case of strong atmospheric turbulence.

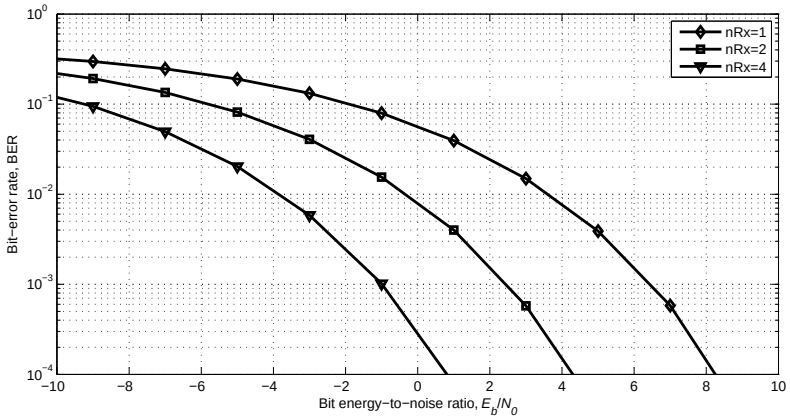

Fig. 5.12 BER performance for 4-QAM SIMO MACO-OFDM in case of weak atmospheric turbulence.

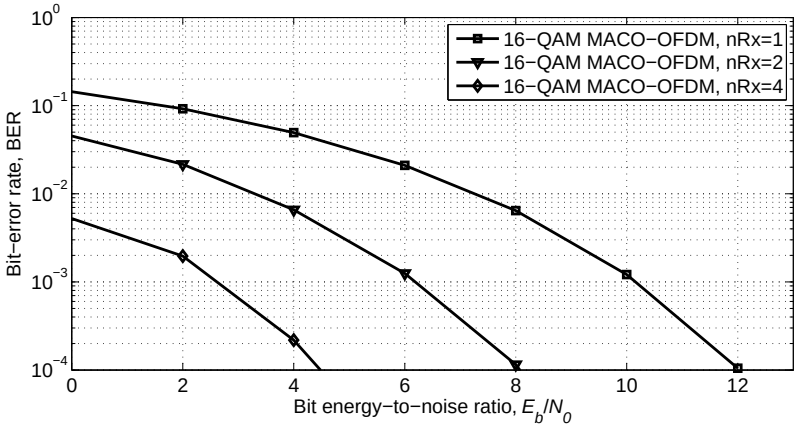

Fig. 5.13 BER performance for 16-QAM SIMO MACO-OFDM in case of weak atmospheric turbulence.

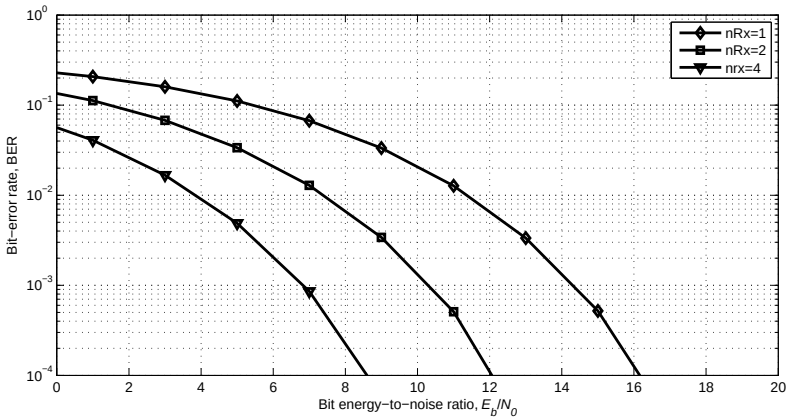

Fig. 5.14 BER performance for 64-QAM SIMO MACO-OFDM in case of weak atmospheric turbulence.

5.3.2.2 Moderate Turbulence

The BER performance for 4-QAM, 16-QAM, and 64-QAM SIMO MACO-OFDM is evaluated for moderate atmospheric turbulence (SI to 0.7 , $\alpha = 4.3939$ and $\beta = 2.5636$) and the results shown in Figure 5.15, Figure 5.16 and Figure 5.17

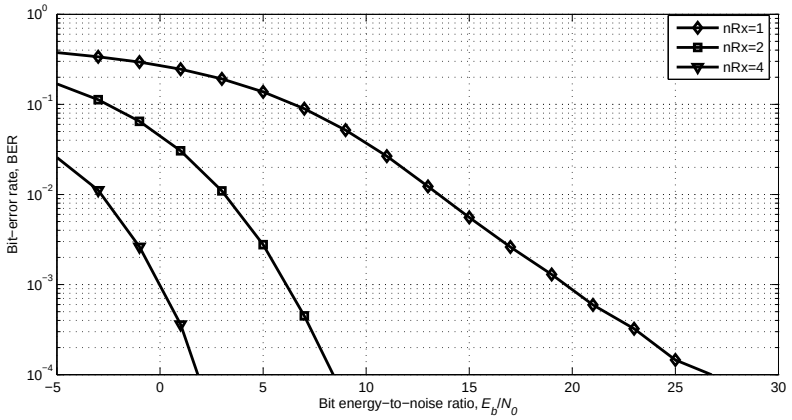

Fig. 5.15 BER performance for 4-QAM SIMO MACO-OFDM in case of moderate atmospheric turbulence.

5.3.2.3 Strong Turbulence

The BER performance for 4-QAM, 16-QAM, and 64-QAM SIMO MACO-OFDM is evaluated at strong atmospheric turbulence ($SI = 0.98$, $\alpha = 3.9929$, and $\beta = 1.7018$) and the results shown in Figure 5.18, Figure 5.19 and Figure 5.20.

5.3.3 Performance Comparison

The BER performance of both 4-QAM ACO-OFDM and 16-QAM MACO-OFDM employing MRC diversity at the receiver for weak, moderate and strong atmospheric turbulence is evaluated for an increasing number of photodetectors viz. nRx =1, 2 and 4; the results are shown in Figure 5.21, Figure 5.22 and Figure 5.23.

The BER performance of MACO-OFDM in weak turbulence better than that of ACO-OFDM by nearly 0.5 dB at nRx=1, 2, and 4 . The level of improvement between the systems is increased as the strength of turbulence evolves to moderate and strong turbulence.

As stated before, the BER performance degrades as the scintillation strength increases. A comparison between BER performance in weak and strong atmospheric turbulence is carried out in figure 5.24.

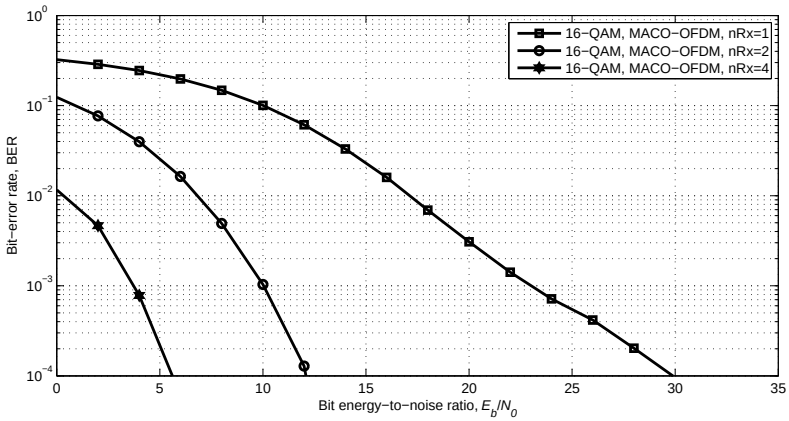

Fig. 5.16 BER performance for 16-QAM SIMO MACO-OFDM in case of moderate atmospheric turbulence.

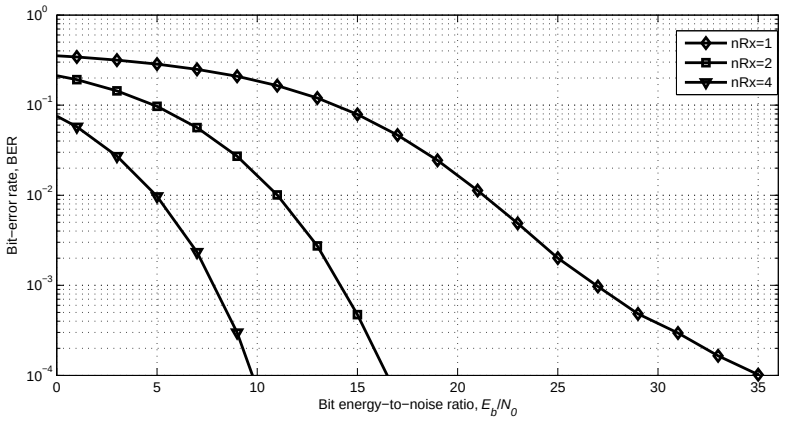

Fig. 5.17 BER performance for 64-QAM SIMO MACO-OFDM in case of moderate atmospheric turbulence.

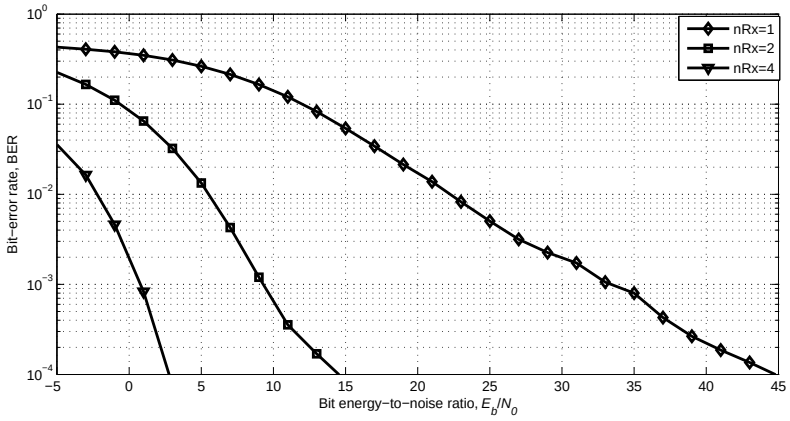

Fig. 5.18 BER performance for 4-QAM SIMO MACO-OFDM in case of strong atmospheric turbulence.

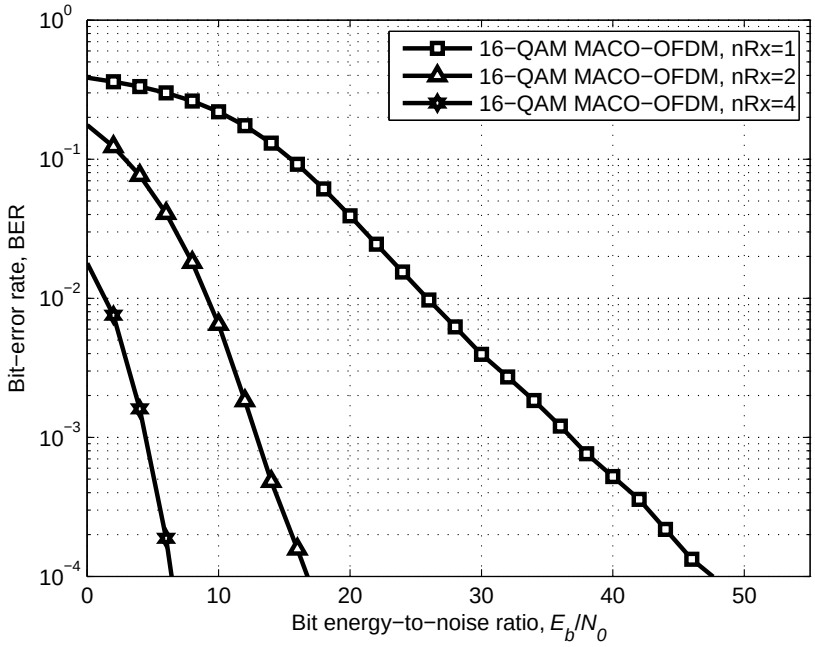

Fig. 5.19 BER performance for 16-QAM SIMO MACO-OFDM in case of strong atmospheric turbulence.

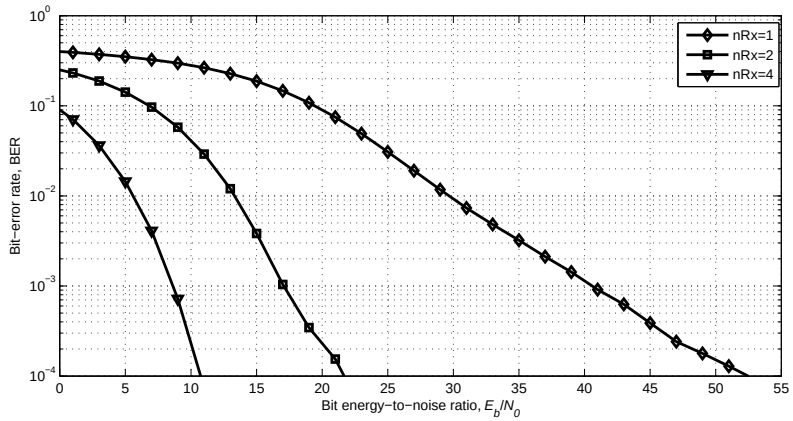

Fig. 5.20 BER performance for 64-QAM SIMO MACO-OFDM in case of strong atmospheric turbulence.

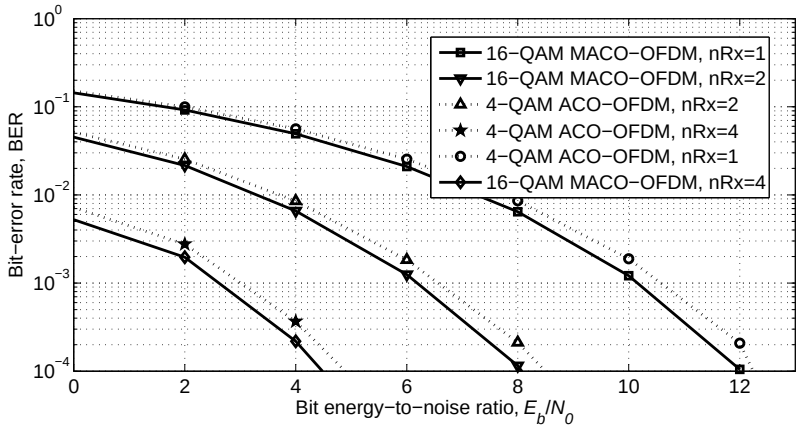

Fig. 5.21 BER performance for 16-QAM SIMO MACO-OFDM and 4-QAM SIMO ACO-OFDM in case of weak atmospheric turbulence.

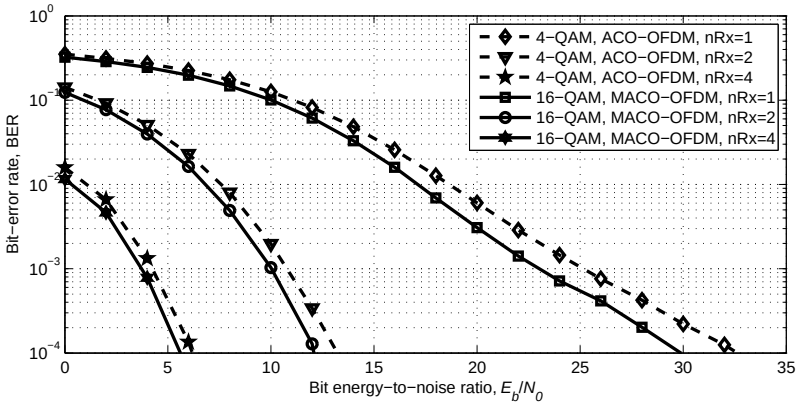

Fig. 5.22 BER performance for 16-QAM SIMO MACO-OFDM and 4-QAM SIMO ACO-OFDM in case of moderate atmospheric turbulence.

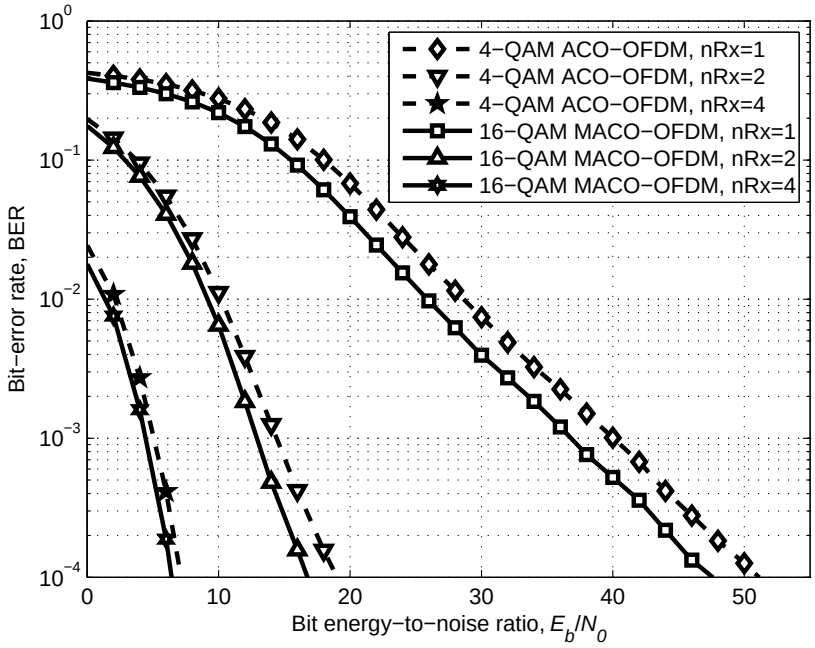

Fig. 5.23 BER performance for 16-QAM SIMO MACO-OFDM and 4-QAM SIMO ACO-OFDM in case of strong atmospheric turbulence.

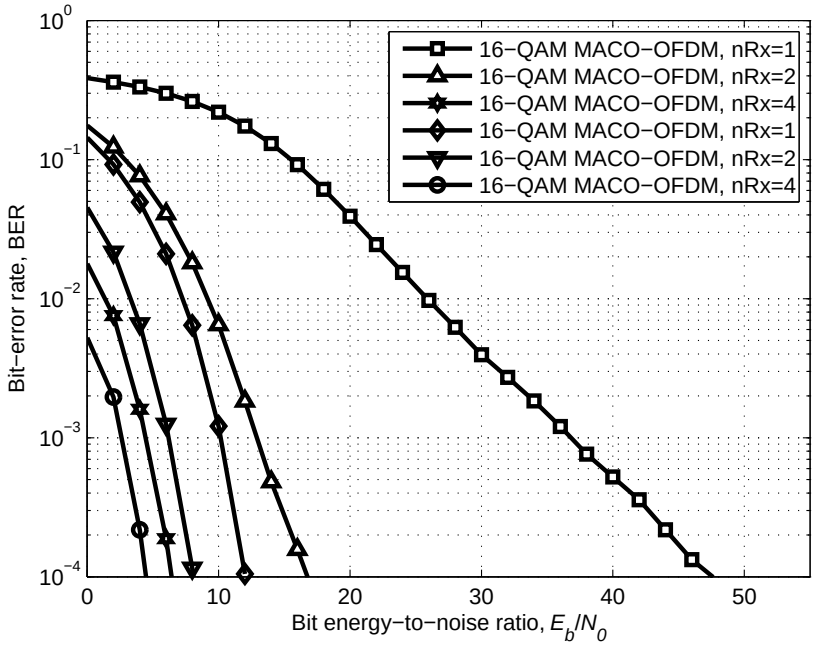

Fig. 5.24 Comparison between BER performance for 16-QAM SIMO MACO-OFDM in case of weak and strong atmospheric turbulence.

5.4 Limitation on Receiving Photodetectors

To receive uncorrelated signals, the receiving apertures should be separated from each other by a minimum distance equal to the spatial coherence length ρ_o which is of the order of centimetres for the laser sources utilised in practice [4]. The optical source is chosen of wide divergence, with the beam footprint covering the entire Field-of-View (FOV) of all the nRx photodetectors at the receiver [4]. The increase of the number of receiving photodetectors from 1 to 2 results in diversity gain of 20 dB, while when increased from 2 to 4 results in diversity gains of only 5 dB in moderate atmospheric turbulence. So it is expected that increasing the number of receiving photodetectors beyond 4 will provide a diversity gain of less than 5 dB. Also, from an implementation perspective spacing four photodetectors to ensure that the received signals are uncorrelated is far more demanding and cumbersome than spacing two photodetectors [4]; thus increasing nRx to more than 4 is much more complicated from an operational specification viewpoint for a concomitant modest increase in diversity gain.

5.5 Conclusions

Due to the nature of light, atmospheric turbulence impacts significantly on the transmission of the signal, not a limiting factor in Radio Frequency communications. This chapter addresses the mitigation of the effect of atmospheric turbulence on the transmitted light signal through the use of receiver diversity. Using MRC diversity at the receiver mitigates the impact of scintillation on system performance. As all branches are used simultaneously the signal in each branch is weighted with a gain coefficient according to its own SNR. Thus the highest achievable SNR at the receiver is selected at all times. However the gain in performance robustness is at the expense of a more complex receiver and assumes knowledge of the channel.

The BER performance for both ACO-OFDM and MACO-OFDM in tandem with MRC is estimated. As expected the performance of both systems improves with an increase in the number of receiving apertures (nRx) summarised for SIMO ACO-OFDM in Table 5.1, Table 5.2, Table 5.3 and SIMO MACO-OFDM in Table 5.4, Table 5.6 and Table 5.7.

MACO-OFDM in tandem with MRC at the receiver outperforms ACO-OFDM in weak turbulence as shown in Table 5.7. As the strength of turbulence increases, the difference in performance of MACO-OFDM and ACO-OFDM decreases as summarised in Table 5.8 and Table 5.9.

Table 5.1 Comparison between BER Performance for SIMO ACO-OFDM in Weak Atmospheric Turbulence.

$SNR\|_{BER=10^{-4}}$			
Modulation Order	nRx=1	nRx=2	nRx=4
4-QAM ACO-OFDM	12.5 dB	8.5 dB	5 dB
16-QAM ACO-OFDM	16 dB	12 dB	8.5 dB
64-QAM ACO-OFDM	20.5 dB	16.5 dB	12.5

Table 5.2 Comparison between BER Performance for SIMO ACO-OFDM in Moderate Atmospheric Turbulence.

$SNR\|_{BER=10^{-4}}$			
Modulation Order	nRx=1	nRx=2	nRx=4
4-QAM ACO-OFDM	32.5 dB	13 dB	6 dB
16-QAM ACO-OFDM	35 dB	16.5 dB	9.5 dB
64-QAM ACO-OFDM	39.5 dB	20.5 dB	14 dB

Table 5.3 Comparison between BER Performance for SIMO ACO-OFDM in Strong Atmospheric Turbulence.

$SNR\|_{BER=10^{-4}}$			
Modulation Order	nRx=1	nRx=2	nRx=4
4-QAM ACO-OFDM	50.5 dB	19.5 dB	6.5 dB
16-QAM ACO-OFDM	54.5 dB	22.5 dB	10.5 dB
64-QAM ACO-OFDM	59 dB	26 dB	14.5 dB

Table 5.4 Comparison between BER Performance for SIMO MACO-OFDM in Weak Atmospheric Turbulence.

$SNR\|_{BER=10^{-4}}$			
Modulation Order	nRx=1	nRx=2	nRx=4
4-QAM MACO-OFDM	8.5dB	4.3 dB	0.9 dB
16-QAM MACO-OFDM	12 dB	8 dB	4.5 dB
64-QAM MACO-OFDM	16.2 dB	12 dB	8.5

Table 5.5 Comparison between BER Performance for SIMO MACO-OFDM in Moderate Atmospheric Turbulence.

$SNR\|_{BER=10^{-4}}$			
Modulation Order	nRx=1	nRx=2	nRx=4
4-QAM MACO-OFDM	28 dB	8 dB	1.8 dB
16-QAM MACO-OFDM	30 dB	12.5 dB	6 dB
64-QAM MACO-OFDM	35 dB	16.5 dB	9.5 dB

Table 5.6 Comparison between BER Performance for SIMO MACO-OFDM in Strong Atmospheric Turbulence.

$SNR\|_{BER=10^{-4}}$			
Modulation Order	nRx=1	nRx=2	nRx=4
4-QAM MACO-OFDM	45 dB	14.5 dB	3 dB
16-QAM MACO-OFDM	48 dB	17 dB	6 dB
64-QAM MACO-OFDM	52.5 dB	22 dB	10.5 dB

Table 5.7 Comparison between BER Performance for SIMO MACO-OFDM and ACO-OFDM in Weak Atmospheric Turbulence.

$SNR\|_{BER=10^{-4}}$			
	nRx=1	nRx=2	nRx=4
4-QAM ACO-OFDM	12.5 dB	8.5 dB	5 dB
16-QAM MACO-OFDM	12 dB	8 dB	4.5 dB

Table 5.8 Comparison between BER Performance for SIMO MACO-OFDM and ACO-OFDM in Moderate Atmospheric Turbulence.

$SNR\|_{BER=10^{-4}}$			
	nRx=1	nRx=2	nRx=4
4-QAM ACO-OFDM	32.5 dB	13 dB	6 dB
16-QAM MACO-OFDM	30 dB	12.5 dB	6 dB

Table 5.9 Comparison between BER Performance for SIMO MACO-OFDM and ACO-OFDM in Strong Atmospheric Turbulence.

$SNR\|_{BER=10^{-4}}$			
	nRx=1	nRx=2	nRx=4
4-QAM ACO-OFDM	50.5 dB	19.5 dB	6.5 dB
16-QAM MACO-OFDM	48 dB	17 dB	6 dB

CHAPTER 6

CAPACITY OF MACO-OFDM SYSTEMS

6.1 Introduction

The capacity of MACO-OFDM is evaluated in the presence of a channel subject to AWGN and compared to that of ACO-OFDM. Furthermore, capacity is then evaluated in the presence of atmospheric turbulence $(followinga \quad Gamma-Gamma \quad channel)$ adopting a SIMO system architecture.

6.2 Shannon's Channel Capacity

Channel capacity is considered the tight upper bound on the rate at which information can be transmitted with low error probability and affected by factors such as;

- distance and the associated attenuation
- induced noise
- non-linear effects

Shannon's Channel Capacity Theorem [54] states that if the signal is transmitted at data rate (R) less than or equal to the channel capacity (C), then a coding technique that enables transmission over a noisy channel with no errors can be used given by;

$$C = B\,log_2\left(1+\frac{S}{N}\right) \tag{6.1}$$

where C is the channel capacity, B is the channel bandwidth in Hertz, S is the signal power and N is the noise power (N_oB) [54] , N_o being the single sided power spectral density of AWGN. The probability of error is nearly equal to 1 for every symbol if $R > C$.

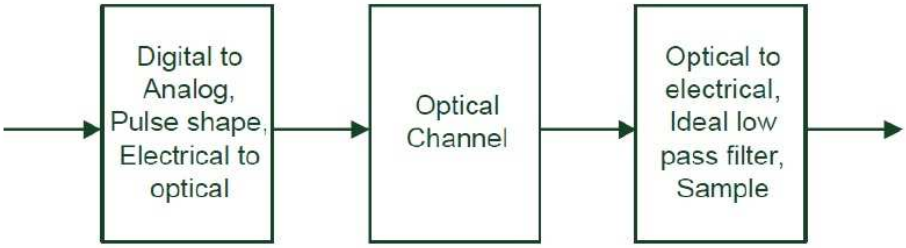

Fig. 6.1 Signal model used in capacity calculations.

6.3 O-OFDM in AWGN

As signals in IM/DD systems are unipolar, techniques used to evaluate channel capacity are different from that of bipolar systems. MACO-OFDM operates in the unipolar regime and thus is evaluated as a superposition of orthogonal basis functions over the time period so that the signal is represented by their sum which is always positive. In the case of a band-limited bipolar signal, samples are taken at the Nyquist rate and sequences of bipolar samples can be converted to a bipolar continuous signal through the use of a low pass filter [54–62]; thus samples can be represented as points in multi-dimensional space where each dimension represents its value. In the case of unipolar samples most of the sequences correspond to bipolar continuous band-limited signals.

It is assumed that the band limiting takes place at the receiver, either at the optical-to-electrical conversion step or in the electrical domain, in so doing removing the constraint that the continuous band-limited signal the samples represent must be unipolar. The use of OFDM guarantees transmission in frequency selective channels even when the channel is subject to multipath fading [61].

6.3.1 Capacity of MACO-OFDM

Figure 6.1 represents the signal model used to calculate the capacity of MACO-OFDM.

The model assumes;

$$y(m) = x(m) + n(m) \tag{6.2}$$

where $x(m)$, $y(m)$, and $n(m)$ represent the input signal, output signal and Additive

White Gaussian Noise. So the capacity can be represented as [54, 61, 62]

$$C = max\left[I\left(x,y\right)\right] \tag{6.3}$$

$I\left(x,y\right)$ is the mutual information given by;

$$I\left(x,y\right) = h\left(y\right) - h\left(n\right) \tag{6.4}$$

where $h\left(y\right)$ is the differential entropy of the output signal plus the noise, and $h\left(n\right)$ is the differential entropy of the noise such that;

$$h\left(y\right) = \int_{-\infty}^{\infty} f_y\left(y\right) log_2\left(f_y\left(y\right)\right) dy \tag{6.5}$$

$f_y\left(y\right)$ is the pdf of the output samples such that $h\left(y\right)$ depends on the pdf of the signal plus noise which means that it depends on the pdf of the signal as the noise is governed by a Gaussian distribution.

Channel capacity is deteremined according to the constraints put on maximization [62]; for the purposes of the estimation of capacity, the average power is considered as it is the most common constraint owing to eye safety and/or design considerations. Then all transmitted samples are subject to the constraint such that;

$$P_o = \int_0^{\infty} x f_x\left(x\right) dx \leqslant P_{o_{max}} \tag{6.6}$$

where P_o is the average power of the transmitted signal and $P_{o_{max}}$ is the maximum allowable mean optical power.

As detailed in Chapter 3, only odd sub-carriers are utilised to carry data while even ones are set to zero and in turn the Hermitian constraint means there are only $N/4$ independent complex inputs permitting unipolar encoding to be implemented. The size of both the IFFT and FFT is assumed to be sufficiently large to satisfy the central limit theorem (CLT).

The capacity of the system can be readily estimated by applying Shannon capacity formulation [54]. As there are $2N$ samples instead of N as is the case for ACO-OFDM, the effective bandwidth of the channel for MACO-OFDM is halved such that;

$$C_{ModACO-OFDM} = \frac{1}{2} \times \left(C_{ACO-OFDM}\right) = \frac{1}{2} \times \left(\frac{1}{4} log_2\left(1 + \frac{S}{N}\right)\right) \tag{6.7}$$

where S is the signal and N is the noise power respectively.

The estimated capacity of both MACO-OFDM and ACO-OFDM is displayed in Fig-

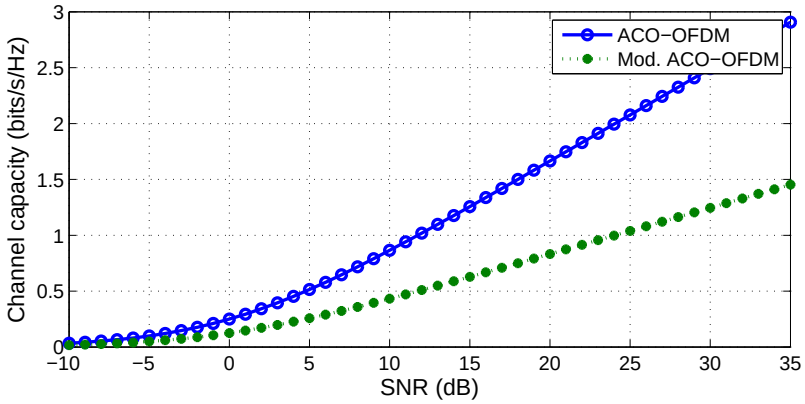

Fig. 6.2 Channel capacities for an optical channel with mean optical power constraint for ACO-OFDM and MACO-OFDM.

ure(6.2).

As expected, the capacity of ACO-OFDM is higher than that of MACO-OFDM. The capacity for a $SNR > 20$ dB is high as the distribution of the signal plus noise is nearly equal to the distribution of the signal only; however at relatively low SNRs, the effect of noise on the distribution becomes more significant. As is evident in Figure 6.2, at low SNR the capacities of both techniques are similar but as the SNR increases, the capacity of ACO-OFDM becomes significantly higher.

6.4 SIMO MACO-OFDM Capacity in Atmospheric Turbulent Channel

As stated in Chapter 5, the Gamma-Gamma distribution is used to model atmospheric turbulence as it represents all regimes from weak to strong turbulence accurately. Furthermore, as the performance of OFDM degrades in the presence of turbulence, SIMO is used to combat fading and increase the capacity of the system. Higher bandwidths, data rates and hence capacities are achieved through the use of multiple photodetectors at the receiver.

The channel capacity for MIMO OFDM is given by [74–77];

$$C = E\left[\frac{1}{N}\sum_{n=1}^{N} log_2\left(I_m + \frac{\rho}{M_t}\tilde{H}_n\tilde{H}_n^H\right)\right] \tag{6.8}$$

where N is the number of OFDM subcarriers, ρ is the averageSNR, M_t is the number of transmitting sources, m is the $min(nRx, M_t)$, nRx is the number of receiving apertures, $\tilde{H}$ is the the gamma-gamma channel coefficient matrix at subcarrier n, and H denotes the

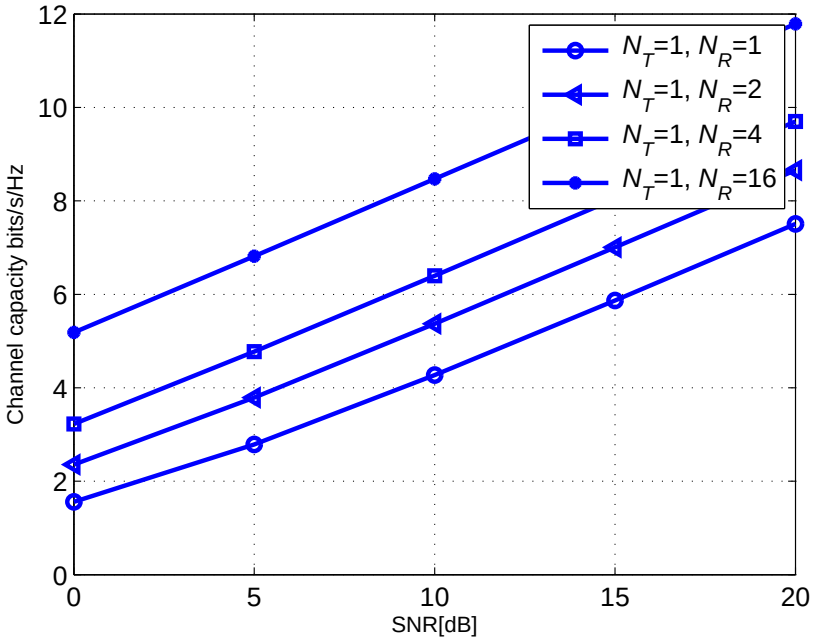

Fig. 6.3 Channel capacities for an optical channel with mean optical power constraint for MACO-OFDM in weak atmospheric turbulence.

Hermitian transpose.

In case of SIMO, $M_t = 1$ and, therefore the channel capacity takes the form [76, 78–81];

$$C = E\left[\frac{1}{N}\sum_{n=1}^{N} log_2\left(1+\rho||\tilde{H}_n||^2\right)\right] \tag{6.9}$$

The channel capacity is estimated through a MATLAB based simulation for SIMO MACO-OFDM assuming a gamma-gamma channel.

6.4.1 SIMO MACO-OFDM Capacity in Weak Atmspheric Turbulence

Channel capacity has been evaluated in weak turbulence at $SI = 0.11$ (Figure 6.3). An increase of 2 bits/s/Hz in the capacity in all orders results as the SNR increases by 5 dB.

As expected as the number of receiving photodetectors increases, the capacity increases (Figure6.4).

Table 6.1 summarises system capacity at a SNR = 20 dB as a function of the number of receivers; the capacity increases from 7.5 bits/s/Hz, 8.6 bits/s/Hz, 9.7 bits/s/Hz to 11.8 bits/s/Hz for SISO (1x1), 1x2, 1x4 and 1x16 respectively.

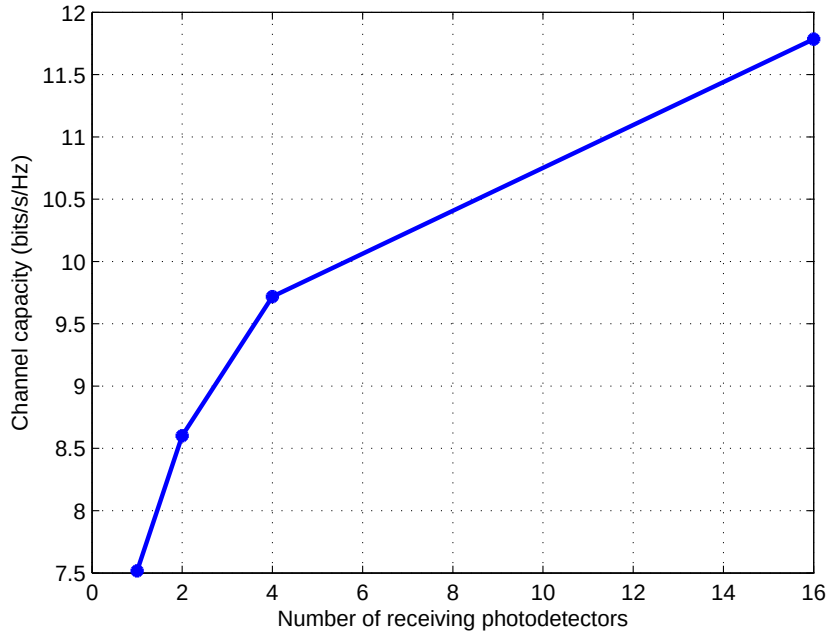

Fig. 6.4 Channel capacities vs the number of receiving photodetectors.

Table 6.1 Comparison between channel capacity values at SNR=20 dB by increasing receiving photodetector numbers in case weak atmospheric turbulence.

nRx	Channel capacity
1	7.5164
2	8.6007
4	9.7178
16	11.7842

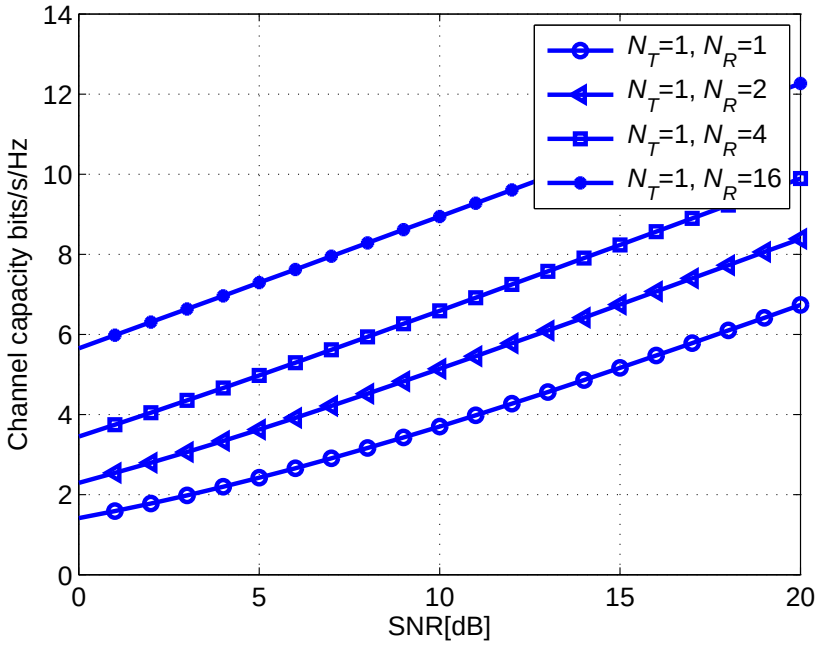

Fig. 6.5 Channel capacities for an optical channel with mean optical power constraint for MACO-OFDM in moderate atmospheric turbulence.

6.4.2 SIMO MACO-OFDM Capacity in Moderate Atmspheric Turbulence

Similarly, channel capacity is also evaluated for SIMO MACO-OFDM in moderate atmospheric turbulence, at $SI = 0.7$ (Figure 6.5). As expected, the channel capacity increases as the number of receiving photodetectors increase.

At a SNR= 20 dB, channel capacity is estimated at a range of orders $-1x1, 1x2, 1x4, and 1x16$˘ and depicted in Figure 6.6. The capacity improves as the diversity order increases.

Table 6.2 presents system capacity at a SNR = 20 dB as a function of the number of receivers; the capacity increases from 6.7 bits/s/Hz, 8.4 bits/s/Hz, 9.9 bits/s/Hz to 12 bits/s/Hz for SISO,$1x2, 1x4, and 1x16$ respectively.

6.4.3 SIMO MACO-OFDM Capacity in Strong Atmspheric Turbulence

Finally channel capacity is estimated for SIMO MACO-OFDM in strong atmospheric turbulence, at $SI = 0.98$ (Figure 6.7). Channel capacity increases as the number of receiving photodetectors increase; an increase of 2 bits/s/Hz in the capacity for all orders results from an increase in the SNR of 2 dB. Also noticeable is that the channel capacity performance is

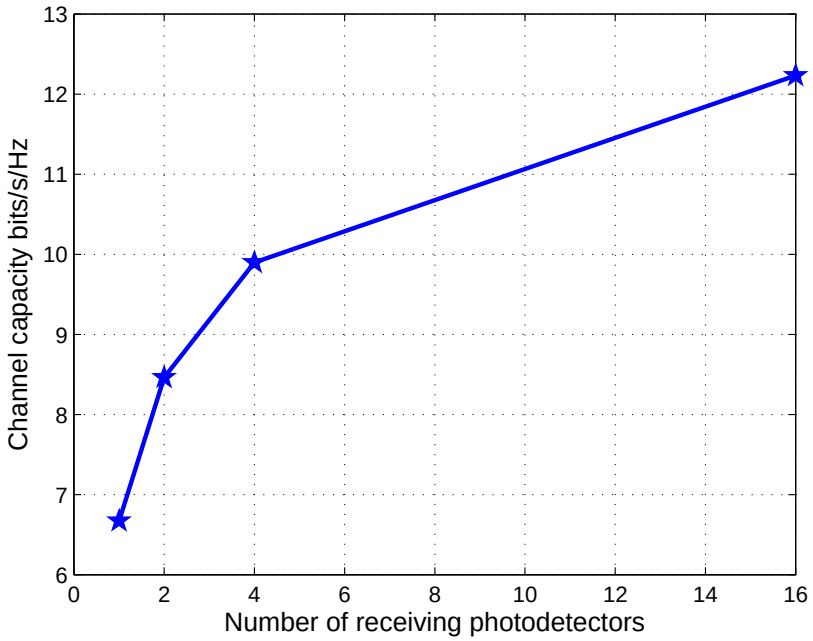

Fig. 6.6 Channel capacities vs the number of receiving photodetectors in moderate atmospheric turbulence.

nearly similar to that for moderate atmospheric turbulence as the difference in the SI value is not significant.

Figure 6.8 shows the relationship between channel capacity and the number of receiving photodetectors; the capacity improves as the diversity order increases.

Table 6.3 presents system capacity at a SNR $= 20$ dB as a function of the number of receivers; the capacity increases from 6.4 bits/s/Hz, 8.3 bits/s/Hz, 10.0 bits/s/Hz to 12 bits/s/Hz for SISO, 1x2, 1x4, and 1x16 respectively.

The relationship between channel capacity and the number of receiving photodetectors is directly proportional.

6.5 Conclusions

The chapter presents an evaluation of the channel capacity of MACO-OFDM in the case of flat fading AWGN channels. Using the channel capacity performance of ACO-OFDM as the reference, the capacity of MACO-OFDM is estimated. Table 6.4 summarises a comparison between capacity of ACO-OFDM and MACO-OFDM in AWGN.

Given the spectral efficiency of MACO-OFDM is half that of ACO-OFDM, as expected the channel capacity of MACO-OFDM is evaluated to be half that of ACO-OFDM.

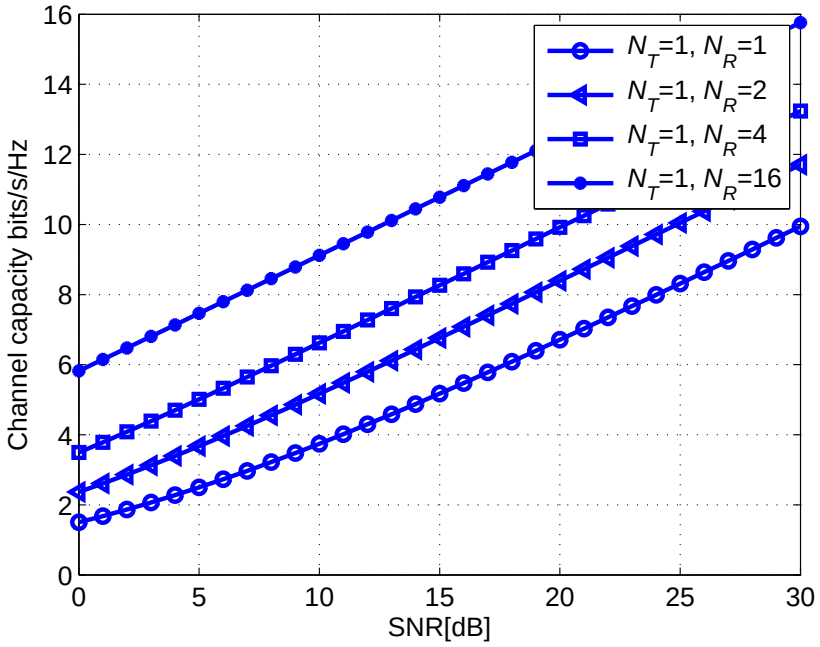

Fig. 6.7 Channel capacities for an optical channel with mean optical power constraint for MACO-OFDM in strong atmospheric turbulence.

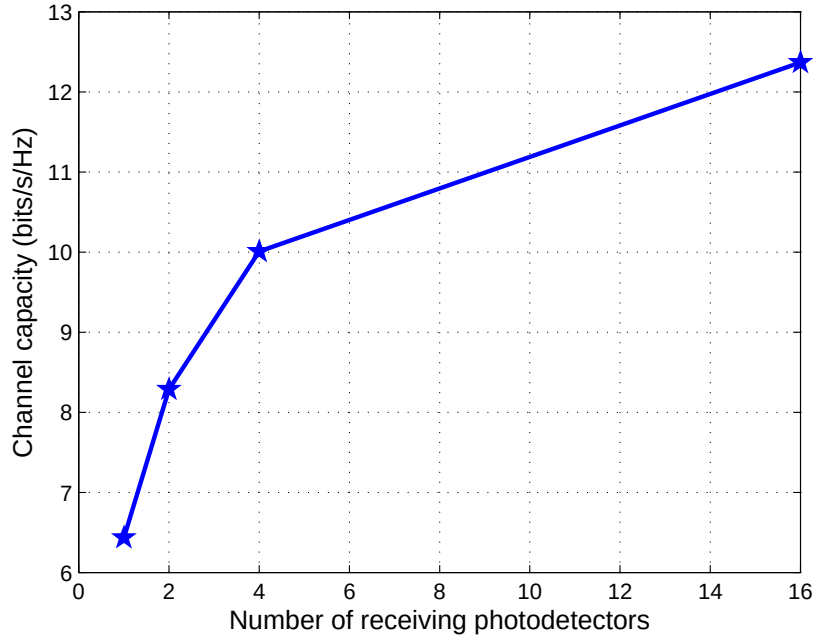

Fig. 6.8 Channel capacities vs the number of receiving photodetectors in strong atmospheric turbulence.

Table 6.2 Comparison between channel capacity values at SNR=20 dB by increasing receiving photodetector numbers in case moderate atmospheric turbulence.

nRx	Channel capacity
1	6.6216
2	8.4912
4	9.8701
16	12.2589

Table 6.3 Comparison between channel capacity values at SNR=20 dB by increasing receiving photodetector numbers in case strong atmospheric turbulence.

nRx	Channel capacity
1	6.4008
2	8.3023
4	9.8625
16	12.3929

The channel capacity of MACO-OFDM in a turbulent channel is estimated adopting a SIMO system with MRC diversity at the receiver, assuming the different turbulence regimes are best characterised by the gamma-gamma model. As the number of receiving apertures increases, the capacity values increase (Table 6.5). The capacity in weak, moderate, and strong turbulence is enhanced due to the use of SIMO. The capacity increases by nearly 1.1 bits/s/Hz when nRX increases to 2 and 4 in case of weak turbulence and by nearly 2 bits/s/Hz when nRx increases to 16. In the case of moderate atmospheric turbulence, the capacity increases by 1.79 bits/s/Hz when nRx increases to 2, by 1.4 bits/s/Hz when nRx increased to 4 and by 2.3 bits/s/Hz when nRx increased to 16. In strong turbulence, the capacity increases by 1.85 bits/s/Hz , 1.72 bits/s/Hz, and 2.36 bits/s/Hz when nRx increased to 2, 4, and 16 respectively.

Table 6.4 Comparison between channel capacity values at different SNR values for both ACO-OFDM and MACO-OFDM.

SNR	MACO-OFDM	ACO-OFDM
-10	0.0172	0.0344
0	0.1250	0.2500
10	0.4324	0.8649
20	0.8323	1.6646
30	1.2459	2.4918

Table 6.5 Comparison between channel capacity values at different atmospheric turbulence regimes .

nRx	Weak Atmospheric Turbulence	Moderate Atmospheric Turbulence	Strong Atmospheric Turbulence
1	7.5164	6.6711	6.4332
2	8.6007	8.4615	8.2867
4	9.7178	9.8979	10.0092
16	11.7842	12.2316	12.3673

CHAPTER 7

CONCLUSIONS AND FUTURE WORK

7.1 Optical OFDM (O-OFDM)

The challenges of operating in the RF spectrum have stimulated research in alternative wireless network implementations such as solutions utilising the optical band of the spectrum. Wireless optical systems consume relatively low power, operate in a license free spectrum, offer the option to create and isolate a wireless cell by direct control of the illumination and are viewed as one of the options in the suite of networking schemes under the next wireless network classification.

Orthogonal Frequency Division Multiplexing (OFDM) has been the subject of extensive research and has been successfully adopted in a range of wired and wireless communications systems. OFDM is spectrally efficient, has an inherent robustness against narrowband interference, employs a simple equalization technique compared to single-carrier systems, and is highly robust to multi-path environments.

Despite of the widespread use of OFDM in RF wireless communications, it has only recently been the subject of development in respect of optical links. The evolution of the optical implementation has been gated by developments in digital signal processing, enabling highly complex processing to be executed to manage system impairments at low cost in turn facilitating transmission at very high data rates.

Two classes of optical OFDM (O-OFDM) system implementations have been defined; coherent optical OFDM (CO-OFDM) and direct detection, non-coherent optical OFDM (DDO-OFDM). The former draws on classical coherent techniques with a laser source at the receiver to locally generate a carrier; performance is governed significantly by the coherence of the laser. In the case of DDO-OFDM, the OFDM signal is transmitted as an intensity level on the optical carrier which translates into a much simpler receiver implementation but at

the expense of more optical power and the use of guard bands between the optical carrier and the OFDM sub-carriers. In the research, the focus is on DDO-OFDM.

Operation in the incoherent domain and due to the fact that OFDM signals are complex, several techniques have been developed to convert the signal into a real and positive value that directly modulates the source for onward transmission. Any method selected has an associated set of conditions which in turn impose a level of degradation on performance. In O-OFDM implementations, Hermitian symmetry is invoked in most cases such that the OFDM signal is unipolar.

Asymmetrically-Clipped Optical OFDM (ACO-OFDM) has been proven to be more power efficient than approaches utilising a DC bias, albeit at reduced spectral efficiency. However a 3 dB penalty in BER performance between ACO-OFDM and bipolar OFDM system exists. The proposed modification to ACO-OFDM through the use of unipolar encoding is employed to decrease the gap between ACO-OFDM performance and that of bipolar OFDM. Results indicate that the proposed modification brings a slight improvement of the BER performance when compared to that of ACO-OFDM.

7.2 Atmospheric Turbulence

Wireless optical signals are impacted severely by atmospheric conditions, turbulence being one of the major factors that degrade the performance. The propagating beam is subject to random phase and amplitude variations inducing signal fading at the receiver. Atmospheric turbulence can be classified into regimes that depend on the value of the refractive index variation and a number of models have been proposed; log-normal distribution, gamma-gamma and negative exponential.

The Gamma-Gamma distribution has proven its accuracy in describing the full range of atmospheric turbulence regimes from weak to strong while the log-normal distribution can only be used to model weak atmospheric turbulence and the negative exponential is only valid to model the saturation regime. Thus the Gamma-Gamma model is employed to estimate the impact on system performance of three turbulence regimes.

7.3 Single Input Multiple Output (SIMO)

Multiple Input Multiple Output (MIMO) strategies have proven to be very effective in improving the performance of a number of broadband wireless communications systems. The use MIMO is investigated to mitigate the impact of atmospheric turbulence on O-OFDM system performance; a Single Input (laser source), Multiple Outputs (photodetec-

tors) (SIMO) geometry is chosen in the goal of increasing the robustness to atmospheric turbulence of both ACO-OFDM and MACO-OFDM systems.

7.4 Channel Capacity

Channel capacity is considered the tight upper bound on the rate at which information can be transmitted. As O-OFDM signals are unipolar, capacity is evaluated as a superposition of orthogonal basis functions over the time period so that the signal is represented by their sum. The capacity for both ACO-OFDM and MACO-OFDM systems was estimated using Shannon's formulation with and without turbulence.

7.5 System Performance Results

A detailed mathematical analysis of the BER performance for both ACO-OFDM and MACO-OFDM subject to AWGN and verified through simulations show that MACO-OFDM provides an improved BER compared to that of ACO-OFDM but at the expense of a doubling of the spectral efficiency. The average BER was estimated for 4-QAM, 16-QAM and 64-QAM modulation and the resultant improvement ranged from 1.5 dB to only 0.3 dB; as the modulation order increases, the performance of both systems becomes similar.

The performance of both systems is compared under atmospheric turbulence. Table 7.1 summarises the SNR value at BER$= 10^{-4}$ for 4-QAM ACO-OFDM and 16-QAM MACO-OFDM in the case of weak, moderate and strong atmospheric turbulence.

The performance for both systems in turbulence improves with the introduction of MIMO techniques. A SIMO geometry with an increasing the number of receiving apertures improved the BER performance of MACO-OFDM more significantly than that of ACO-OFDM, the most marked being for weak turbulence. Then the difference in performance between the two systems decreases as the strength of turbulence increases. Table 7.2 and Table 7.3 summarise the performance of both systems for nRx=2 and nRx=4 in different atmospheric turbulence regimes.

The capacity of MACO-OFDM subject to AWGN was evaluated to be quarter that of Shannon's capacity. It is noticeable that the capacity is affected by atmospheric conditions, but as the number of receiving apertures increases, the impact of turbulence decreases.

7.6 Future Work

A number of future research strands have arisen from the research;

Table 7.1 Comparison between different MACO-OFDM and ACO-OFDM systems in atmospheric turbulent channel.

O-OFDM type	Weak Atmospheric Turbulence at S.I.=0.11	Moderate Atmospheric Turbulence at S.I.=0.7	Strong Atmospheric Turbulence at S.I.=0.98
4-QAM ACO-OFDM	15dB	35dB	54dB
16-QAM MACO-OFDM	9.5dB	32.5dB	49.5dB

Table 7.2 Comparison between different MACO-OFDM and ACO-OFDM systems in atmospheric turbulent channel at nRx=2.

O-OFDM type	Weak Atmospheric Turbulence at S.I.=0.11	Moderate Atmospheric Turbulence at S.I.=0.7	Strong Atmospheric Turbulence at S.I.=0.98
4-QAM ACO-OFDM	16dB	19.5dB	28dB
16-QAM MACO-OFDM	10dB	14.8dB	20dB

Table 7.3 Comparison between different MACO-OFDM and ACO-OFDM systems in atmospheric turbulent channel at nRx=4.

O-OFDM type	Weak Atmospheric Turbulence at S.I.=0.11	Moderate Atmospheric Turbulence at S.I.=0.7	Strong Atmospheric Turbulence at S.I.=0.98
4-QAM ACO-OFDM	11.5dB	8dB	10dB
16-QAM MACO-OFDM	6.5dB	7dB	9dB

- Evaluation of the performance of both ACO-OFDM and MACO-OFDM experimentally
- Experimental Validation of MACO-OFDM performance in outdoor environments subject to atmospheric turbulence. By investigating the BER performance in different atmospheric turbulence regimes.
- Further analysis of the optimum MIMO technique to improve MACO-OFDM performance is a meaningful extension of the preliminary analysis presented on the SIMO geometry e.g. use of multiple transmitting lasers and multiple receiving apertures. Investigating the system performance of both systems as a function of the number of sources and receivers and its impact on channel capacity provides a deeper understanding of the value of MIMO for non-coherent optical OFDM systems.

REFERENCES

[1] "Free space optics." http://www.freespaceoptics.org/. Accessed: 2015-02-01.

[2] H. A. Shaban, S. D. A. E. Aziz, A. K. AboulSeoud, and M. H. Aly, "Error performance of free space optical mimo systems in weak, moderate, and severe atmospheric turbulence channels," in *Electrical and Computer Engineering (CCECE), 2011 24th Canadian Conference*, (Niagara Falls), pp. 777 – 782, May 8-11 2011.

[3] S. Hranilovic, *Wireless Optical Communication Systems*. Springer Science and Business Media, Inc., 2005.

[4] Z. Ghassemlooy, W. Popoola, and S. Rajbhandari, *Optical Wireless Communications System and Channel Modelling with MATLAB*. CRC Press, 2013.

[5] R. V. Nee and R. Prasad, *OFDM For Wireless Multimedia Communications*. Artech House, 2000.

[6] H. Schuzle and C. Luders, *Theory and Applications of OFDM and OCDMA Wideband Wireless Communications*. John Wiley, 2005.

[7] S. Glisic, *Advanced WirelessCommunications 4G Technologies*. John Wiley, 2004.

[8] U. Madhow, *Fundamentals of Digital Communications*. Cambridge University Press, 2008.

[9] J. Armstrong, "OFDM for optical communications," *J. Lightw. Technol.*, vol. 27, no. 3, pp. 189–204, 18 Feb. 2009.

[10] Y. London and D. Sadot, "Nonlinear effects mitigation in coherent optical ofdm system in presence of high peak power," *IEEE/OSA Journal on Lightwave Technology (IEEE/OSA JLT)*, vol. 29, no. 21, pp. 3275 – 3281, Sept. 2011.

[11] Y. Xiang, L. Zengji, Y. Peng, and S. Tao, "Ber performance analysis for m-ary ppm over gamma-gamma atmospheric turbulence channels," in *Wireless Communications Networking and Mobile Computing (WiCOM)*, (Chengdu), pp. 1–4, Sep. 23-25 2010.

[12] "Claude Chappe's telegraph, howpublished = http://www.wordworx.co.nz/Globaltimeline.htm." Accessed: 2014-06-06.

[13] P. David A. Johnson, *Handbook of Optical Through the Air Communications*. imagineering E-zine, 2008.

[14] I. D. William Shieh, *OFDM for Optical Communications*. Elsevier press, 2010.

[15] L. Chen, B. Krongold, and J. Evans, "Performance evaluation of optical OFDM systems with nonlinear clipping distortion," in *IEEE Int. Conf. Commun. (ICC 2009)*, (Dresden), pp. 1–5, June 14-18 2009.

[16] S. Dimitrov, S. Sinanovic, and H. Haas, "A comparison of OFDM- based modulation schemes for OWC with clipping distortion," in *2nd IEEE Workshop, GLOBECOM Workshops (GC Wkshps)*, (Houston,TX), pp. 787– 791, Dec. 5-9 2011.

[17] S. Engelberg, "The central limit theorem and low-pass filters," in *Electronics, Circuits and Systems, 2004. ICECS 2004. Proceedings of the 2004 11th IEEE International*, pp. 65–68, 2004.

[18] "Ber of bpsk ofdm in awgn." http://www.dsplog.com/2008/06/10/ofdm-bpsk-bit-error/. Accessed: 2015-02-10.

[19] "Ber of m-qam ofdm in awgn." http://www.mathworks.com/matlabcentral/fileexchange/25694-ber-of-ofdm-using-16-qam-in-awgn/content//qam_ofdm_commtoolbox.m. Accessed: 2015-02-10.

[20] W. S. Qi Yang, Abdullah Al Amin, *Impact of Nonlinearities on Fiber Optic Communications*. Springer, 2011.

[21] S. Dimitrov, S. Sinanovic, and H. Haas, "Clipping noise in OFDM- based optical wireless communication systems," *IEEE Trans. On Commun.*, vol. 60, no. 4, pp. 1072–1081, April 12 2012.

[22] J. Armstrong and B. J. C. Schmidt, "Comparison of asymmetrically clipped optical OFDM and DC-biased optical OFDM in awgn," *IEEE Commun. Letters*, vol. 12, no.5, pp. 343–345, May 16 2008.

[23] L. Chen, B. Krongold, and J. Evans, "Diversity combining for asymmetrically clipped optical OFDM in IM/DD channels," in *IEEE Global Telecommun. Conf. (GLOBECOM 2009)*, (Honolulu, HI), pp. 1–6, Nov. 30 - Dec. 4 2009.

[24] J. Armstrong and A. Lowery, "Power efficient optical OFDM," *Electronics Letters*, vol. 42, no.6, pp. 370–372, March 27 2006.

[25] S. D. Dissanayake, K. Panta, and J. Armstrong, "A novel technique to simultaneously transmit ACO-OFDM and DCO-OFDM in IM/DD systems," in *IEEE Global Telecommun. (GLOBECOM) Workshops (GC Wkshps)*, (Houston,TX), pp. 782 –786, Dec. 5-9 2011.

[26] S. K. Wilson and J. Armstrong, "Transmitter and receiver methods for improving asymmetrically- clipped optical OFDM," *Wireless Communications IEEE Trans. Commun.*, vol. 8, no.9, pp. 4561 – 4567, Oct. 13 2009.

[27] S. Dimitrov, S. Sinanovic, and H. Haas, "Double-sided signal clipping in ACO-OFDM wireless communication systems," in *IEEE Int. Conf. Commun. (ICC 2009)*, (Kyoto), pp. 1–5, June 5-9 2009.

[28] J. Armstrong, B. J. Schmidt, D. Karla, H. A. Suraweera, and A. J. Lowery, "Performance of asymmetrically clipped optical OFDM in AWGN for an intensity modulated direct detection system," in *IEEE Global Telecommun. Conf. (GLOBECOM)*, (San Francisco, CA), pp. 1–5, Nov. 27 - Dec.1 2006.

[29] D. Tsonev, S. Sinanovic, and H. Haas, "Novel unipolar orthogonal frequency division multiplexing (U-OFDM) for optical wireless," in *Vehicular Technology Conference (VTC Spring)*, (Yokohama), pp. 1–5, May 6-9 2012.

[30] N. Fernando, Y. Hong, and E. Viterbo, "Flip-OFDM for optical wireless communications," in *Information Theory Workshop (ITW)*, (Paraty), pp. 5–9, Oct. 16-20 2011.

[31] N. Fernando, Y. Hong, and E. Viterbo, "Flip-ofdm for unipolar communication systems," *IEEE Transactions on Communications*, vol. 60, no.12, pp. 3726– 3733, Dec. 2012.

[32] B. T. Vu, N. T. Dang, T. C. Thang, and A. T. Pham, "Bit error rate analysis of rectangular qam/fso systems using an apd receiver over atmospheric turbulence channels," *J. OPT. COMMUN. NETW*, vol. 5, no.5, pp. 437–446, May 2013.

[33] M. Mofidi and A. Chaman-motlagh, "Error and channel capacity analysis of simo and miso free-space optical communications," in *20th Iranian Conferance on Electrical Engineering, (ICEE2012)*, (Tehran, Iran), pp. 1414–1418, May 15-17 2012.

[34] H. E. Nistazakis, A. N. Stassinakis, H. G. Sandalidis, and G. S. Tombras, "Qam and psk ofdm rofso over m-turbulence induced fading channels," *IEEE Photonics Journal*, vol. 7, no.1, Feb. 2015.

[35] J.-B. Wang, M. Sheng, X. Song, Y. Jiao, and M. Chen, "Comments on 'ber performance of fso links over strong atmospheric turbulence channels with pointing errors," *IEEE Commun. Letters*, vol. 16, no.1, pp. 22 – 23, Jan. 2012.

[36] P. Liu, X. Wu, K. Wakamori, T. D. Pham, M. S. Alam, and M. Matsumoto, "Bit error rate performance analysis of optical cdma time-diversity links over gamma-gamma atmospheric turbulence channels," in *Wireless Communications and Networking Conference (WCNC)*, (Cancun, Quintana Roo), pp. 1932 – 1936, March 28-31 2011.

[37] Z. Wang, W.-D. Zhong, S. Fu, and C. Lin, "Performance comparison of different modulation formats over free-space optical (fso) turbulence links with space diversity reception technique," *IEEE Photonics Journal*, vol. 1, no.6, pp. 277 – 285, Dec., 22-31 2012.

[38] K. Wakafuji and T. Ohtsuki, "Performance analysis of atmospheric optical subcarrier multiplexing systems and atmospheric optical code division multiplexing systems," *2004 IEEE International Conference on Communications*, vol. 6, pp. 3336 – 3340, June 20-24 2004.

[39] T. A. Bhuiyan, M. Z. Hassan, S. S. Tanzil, S. Hayder, and S. Majumder, "Performance improvement of im-dd free space optical cdma (attenuated by strong atmospheric turbulence) with maximal ratio combining," in *Computational Intelligence and Communication Networks (CICN)*, (Bhopal), pp. 513 – 518, Nov. 26-28 2010.

[40] P. Kaur, V. K. Jain, and S. Kar, "Performance analysis of fso array receivers in presence of atmospheric turbulence," *IEEE Photonics Technology Letters*, vol. 26, no. 12, pp. 1165 – 1168, June 15 2014.

[41] H. Kaushal, V.K.Jain, and S. Kar, "Improvement of ground to satellite fso link performance using transmit diversity in weak atmospheric turbulence," in *Intelligent and Advanced Systems (ICIAS)*, (Kuala Lumpur, Malaysia), pp. 1–6, June 15-17 2010.

[42] H. Kazemi and M. Uysal, "Performance analysis of mimo free-space optical communication systems with selection combining," in *Signal Processing and Communications Applications Conference (SIU)*, (Haspolat), pp. 1–4, April 24-26 2013.

[43] M. Uysal, J. T. Li, and M. Yu, "Error rate performance analysis of coded free-space optical links over gamma-gamma atmospheric turbulence channels," *IEEE Transactions on Wireless Communications*, vol. 5, no.6, pp. 1229–1233, June 2006.

[44] E. Bayaki, R. Schober, and R. K. Mallik, "Performance analysis of mimo free–space optical systems in gamma–gamma fading," *IEEE Transactions on Communications*, vol. 57, no.11, pp. 3415–3424, Nov. 2009.

[45] N. Letzepis and A. G. i Fàbregas, "Outage probability of the gaussian mimo free-space optical channel with ppm," *IEEE Transactions on Communications*, vol. 57, no.12, pp. 3682–3690, Dec. 2009.

[46] N. Letzepis and A. G. i Fàbregas, "Transmission analysis of ofdm-based wireless services over turbulent radio-on-fso links modeled by gamma–gamma distribution," *IEEE Photonics*, vol. 2, no.3, pp. 510–520, June 2010.

[47] A. PROKEŠ, "Modeling of atmospheric turbulence effect on terrestrial fso link," *RADIOENGINEERING*, vol. 18, no.1, pp. 42–47, April 2009.

[48] M. Uysal, S. M. Navidpour, and J. T. Li, "Error rate performance of coded free-space optical links over strong turbulence channels," *IEEE COMMUNICATIONS LETTERS*, vol. 8, no.10, pp. 635–637, Oct. 2004.

[49] R. Miglani and M. Singh, "Performance evaluation of free space optical link using mid and far infrared wavelengths in turbulent atmospheric conditions," in *4th International Workshop on Fiber Optics in Access Network (FOAN)*, (Almaty), pp. 31–35, Sept. 11-12 2013.

[50] V. K. Dwivedi, P. Kumar, and G. Singh, "Performance analysis of ofdm communication system over correlated nakagami-m fading channel," in *Recent Advances in Microwave Theory and Applications, 2008. MICROWAVE 2008*, (Jaipur), pp. 536 – 539, Nov. 21-24 2008.

[51] A. Goldsmith, *Wireless Communications*. Cambridge University Press, 2005.

[52] H. Elgala, R. Mesleh, and H. Haas, "Non-linearity effects and predistortion in optical ofdm wireless transmission using leds," *Inderscience International Journal of Ultra Wideband Communications and Systems (IJUWBCS)*, vol. 1, no. 2, p. 143–150, 2009.

[53] S. Dimitrov, R. Mesleh, M. C. H. Haas, M. Olbert, and E. Bassow, "On the sir of a cellular infrared opticalwireless system for an aircraft," *IEEE Journal on Selected Areas in Communications (IEEE JSAC)*, vol. 27, no. 9, p. 1623–1638, Dec. 2009.

[54] C. Shannon, "Mathematical theory of communication," *Bell System Technical Journal*, vol. 27, p. 379–423 and 623–656, Jul. and Oct. 1984.

[55] R.-J. Essiambre, G. Kramer, P. Winzer, G. Foschini, and B. Goebel, "Capacity limits of optical fibre networks," *IEEE/OSA Journal on Lightwave Technology (IEEE/OSA JLT)*, vol. 28, no. 4, p. 662–701, Feb. 15 2010.

[56] S. Hranilovic and F. Kschischang, "Capacity bounds for power- and band-limited optical intensity channels corrupted by gaussian noise," *IEEE Transactions on Information Theory*, vol. 50, no. 5, p. 784–795, May 2004.

[57] C. Shannon, "Communication in the presence of noise," *in Proc. of the IRE*, vol. 37, no. 1, pp. 10–21, Jan. 1949.

[58] A. Farid and S. Hranilovic, "Capacity of optical intensity channels with peak and average power constraints," in *in Proc. of IEEE International Conference on Communications (IEEE ICC 2009)*, (Dresden, Germany), pp. 1–5, June14-18 2009.

[59] A. Farid and S. Hranilovic, "Capacity bounds for wireless optical intensity channels with gaussian noise," *IEEE Transactions on Information Theory*, vol. 56, no. 12, p. 6066–6077, Dec. 2010.

[60] R. You and J. Kahn, "Upper-bounding the capacity of optical im/dd channels with multiple-subcarrier modulation and fixed bias using trigonometric moment space method," *IEEE Transactions on Information Theory*, vol. 48, no. 2, p. 514–523, Feb. 2002.

[61] X. Li, J. Vucic, V. Jungnickel, and J. Armstrong, "On the capacity of intensity-modulated direct-detection systems and the information rate of aco-ofdm for indoor optical wireless applications," *IEEE Trans. on Commun.*, vol. 60, no.3, pp. 799–809, Mar. 2012.

[62] X. Li, R. Mardling, and J. Armstrong, "Channel capacity of im/dd optical communication systems and of aco-ofdm," in *ICC2007*, (Glasgow), pp. 2128 – 2133, June 24-28 2007.

[63] J. Bussgang, "Cross correlation function of amplitude-distorted gaussian signals," in *Research Laboratory for Electronics, Massachusetts Institute of Technology, Cambridge, MA, Technical Report 216*, Mar. 1952.

[64] R. Rice, "A useful theorem for nonlinear devices having gaussian inputs," *Information Theory, IRE Transactions*, vol. 19, no.2, pp. 69–72, June 1958.

[65] M. Sharma, D. Chadha, and V. Chandra, "Capacity evaluation of mimo-ofdm free space optical communication system," in *India Conference (INDICON), 2013 Annual IEEE*, (Mumbai), pp. 1–4, Dec. 13-15 2013.

[66] M. F. Siyau, R. Ormondroyd, and S. L. Ling

[67] B. Sklar, *Digital Communications*. McGraw-Hill, 1995.

[68] B. Sklar, *Digital Communications Fundamentals and Applications*. Prentice Hall PTR, 2001.

[69] A. R. Shah, R. C. J. Hsu, A. Tarighat, A. H. Sayed, and B. Jalali, "Coherent optical mimo (comimo)," *J. Lightw. Tech.*, vol. 23, no.8, pp. 2410 – 2419, Aug. 2005.

[70] N. Cvijetic, S. G. Wilson, and M. Brandt-Pearce, "Receiver optimization in turbulent free-space optical mimo channels with apds and q-ary ppm," *IEEE Photonics Technology Letters*, vol. 19, no.2, pp. 103–105, Jan. 2007.

[71] T. A. Tsiftsis, H. G. Sandalidis, G. K. Karagiannidis, and M. Uysal, "Optical wireless links with spatial diversity over strong atmospheric turbulence channels," *IEEE Trans. on Wireless Commun.*, vol. 8, no.2, pp. 951– 957, Feb. 2009.

[72] Q. T. Zhang, "Probability of error for equal-gain combiners over rayleigh channels," *IEEE Trans. on Commun.*, vol. 45, no.3, pp. 270–273, Mar. 1997.

[73] M. K. Simon and M. S. Alouini, *Digital Communication Over Fading Channels*. John Wiley & Sons, 2000.

[74] M. Charma, D. Chadha, and V. Chandra, "Performance analysis of spatially multiplexed mimo-ofdm free space optical communication system," in *Signal Processing and Communications (SPCOM)*, (Bangalore), pp. 1–5, July 22-25 2014.

[75] P. Uthansakuand and M. E. Bialkows, "Multipath signal effect on the capacity of mimo, mimo-ofdm and spread mimo-ofdm," in *Microwaves, Radar and Wireless Communications, 2004. MIKON-2004. 15th International Conference*, vol. 3, pp. 989 – 992, May 17-19 2004.

[76] Y. S. Cho, J. Kim, W. Y. Yang, and C. G. Kang, *MIMO-OFDM Wireless Communications with MATLAB*. John Wiley and Sons, 2010.

[77] F. Benkhelifa, Z. Rezki, and M.-S. Alouini, "Low snr capacity of fso links over gamma-gamma atmospheric turbulence channels," *IEEE Communications Letters*, vol. 17, no. 6, p. 1264–1267, June 2013.

[78] M.M.Kamruzzaman, "Performance of turbo coded wireless link for sisoofdm, simo-ofdm, miso-ofdm and mimo-ofdm system," in *Computer and Information Technology (ICCIT)*, pp. 185 – 190, Dec. 22-24 2011.

[79] Y. Zhu, T. R. Fischer, and B. Belzer, "Ofdm-constrained channel capacity estimates of the simo shallow underwater communication channel," in *Information Sciences and Systems (CISS)*, pp. 1–6, Mar. 21-243 2012.

[80] H. feng (Francis) Lu, "Optimal code constructions for simo-ofdm frequency selective fading channels," in *Information Theory for Wireless Networks, 2007 IEEE Information Theory Workshop*, (Solstrand), pp. 1–5, July 1-6 2007.

[81] V. K. V. Gottumukkala and H. Minn, "Ergodic capacity analysis of miso/simo-ofdm with arbitrary antenna and channel tap correlation," *IEEE Transactions on Vehicular Technology*, vol. 62, no.7, pp. 3062–3068, Sept. 2013.

APPENDIX: SAMPLE MATLAB CODES

Analytical MATLAB file

```
%close all
clear all
warning off all
clc
tic;

M=64;
N=2048;
EbNodB=[0:20];
EbNo = 10.^(EbNodBu./10);
sigma_n = sqrt(0.01);
No = 2*sigma_n^2;
Eb = EbNo*No;
sigma_s = sqrt(Eb*log2(M)/8);
[ac, Nc, aw, Nw] = gain_noise(sigma_n, sigma_s);

for p = 1:length(sigma_s)
    dc(p) = quadgk(@(s)2./sigma_s(p).*phi(s./sigma_s(p)).*(1-
Q(s./(sigma_n*sqrt(2)))), 0, Inf);
end

a_aver =(dc.*ac + (1-dc).*aw);
N_aver = (dc.*Nc + (1-dc).*Nw);

SNR =(a_aver.^2.*Eb./(N_aver));
ber1=0;
k=log2(M);
 for a=1:log2(sqrt(M))
    for b=0:((1-2^(-a))*sqrt(M)-1)
        ber1=ber1+(-1)^(floor(b*2^(a-1)/sqrt(M)))*(2^(a-1)-
floor(b*2^(a-1)/sqrt(M)+0.5))*qfunc((2*b+1)*sqrt(3*k/((M-
1))*SNR));
    end
end
ber=2/(sqrt(M)*log2(sqrt(M)))*ber1;


toc;
semilogy(EbNodB,ber);
axis([0 20 1e-4 1])
```

Gain Noise Function

```
function [ac, Nc, aw, Nw] = gain_noise(sigma_n, sigma_s)

Func = @(s,x) 1./(sigma_n).*phi((x-abs(s))./sigma_n).*(1-
Q(x./sigma_n));
Prc = @(s) quadgk(@(x) Func(s,x), -Inf, Inf);
Ec = @(s) sign(s).*quadgk(@(x) x.*Func(s,x), -Inf, Inf);
Vc = @(s) quadgk(@(x) (x.^2).*Func(s,x), -Inf, Inf);

Funw = @(s,x) 1./(sigma_n).*phi(x./sigma_n).*(1-Q((x-
abs(s))./sigma_n));
Prw = @(s) quadgk(@(x) Funw(s,x), -Inf, Inf);
Ew = @(s) -sign(s).*quadgk(@(x) x.*Funw(s,x), -Inf, Inf);
Vw = @(s) quadgk(@(x) (x.^2).*Funw(s,x), -Inf, Inf);

ac = zeros(1,length(sigma_s));
yc = zeros(1,length(sigma_s));
vca = zeros(1,length(sigma_s));

aw = zeros(1,length(sigma_s));
yw = zeros(1,length(sigma_s));
vwa = zeros(1,length(sigma_s));

acc = 100;
hwait=waitbar(0,'waiting...');%waitbar
for p = 1:length(sigma_s)

    delta = (sigma_s(p)/acc);
    UB = (5*sigma_s(p));

    for s = 0:delta:UB

        phis = 2*phi(s./sigma_s(p))./sigma_s(p);

        if Prc(s)>0.5
            if Prc(s+delta)<(10^-8)
               break;
            end
        end

        fc = Ec(s)./Prc(s);
        vc = Vc(s)./Prc(s)-fc^2;

        ac(p) = ac(p) + s.*fc.*phis.*delta./(sigma_s(p).^2);
        yc(p) = yc(p) + (fc.^2).*phis.*delta;
        vca(p) = vca(p) + vc.*phis.*delta;

        if Prw(s)< 10^-80
            continue;
        end
```

```
fw = Ew(s)./Prw(s);
        vw = Vw(s)./Prw(s)-fw^2;

        aw(p) = aw(p) + s.*fw.*phis.*delta./(sigma_s(p).^2);
        yw(p) = yw(p) + (fw.^2).*phis.*delta;
        vwa(p) = vwa(p) + vw.*phis.*delta;
    end

    yc(p) = yc(p)-(ac(p).^2).*(sigma_s(p).^2);
    yw(p) = yw(p)-(aw(p).^2).*(sigma_s(p).^2);


str=['dealing...',num2str(floor(p/length(sigma_s)*100)),'%'];
    waitbar(p/length(sigma_s),hwait,str);

end
close(hwait);

Nc = (yc+vca);
Nw = (yw+vwa);

end
```

MACO-OFDM Simulations Code

```
clear all;
clc;

EbNodB    = 0 : 25;  % ACO-OFDM bit energy-to-AWGN ratio
N         = 64 % IFFT/FFT size
N1        = N/4; % 1/4 of the FFT size (1/4 of data)
no_frames = 10000;


Mset = [4]; % M-QAM
BER  = zeros( length( Mset ), length( EbNodB ) );
for k = 1 : length( Mset )
    M            = Mset(k);
    xt_all       = zeros( 1, N * no_frames);
    x_unipol     = zeros( 1, 2 * N * no_frames);
    xt_noise     = zeros( 1, 2 * N * no_frames);
    xt_rec_all   = zeros( 1, N * no_frames);
    xr_unipol    = zeros( 1, N * no_frames);
    xf_all       = zeros( 1, N1 * no_frames);
    x_rec_final  = zeros( 1, N1 * no_frames);

    %Generation of random integers
    data = randi( [ 0 M-1 ], 1, N1 * no_frames );

    % QAM modulation
    mod_data = qammod( data, M,0,'gray' )/sqrt(1);
    re_x = zeros( 1, N );

    % OFDM frame mapping
    for i = 1 : no_frames
        x                       = mod_data( 1 + ( i - 1 ) *
N1 : i * N1 );   % taking N/4 of the data in one OFDM frame
        re_x( 2 : 2 : N / 2 )   = x;          % mapping the
data on odd subcarriers
        re_x( N : -2 : N/2 + 1 ) = conj(x);    % mapping
hermitian symmetry on the other half of the subcarriers
        xt                      = sqrt(N) * ifft( re_x, N );
% applying IFFT
        xt_all( 1 + ( i - 1 ) * N : i * N ) = xt;
    end

    % Unipolar encoding
    for i = 1 : length( xt_all )
        if xt_all(i) > 0
            x_unipol( 2 * i - 1 ) = xt_all(i);
            x_unipol( 2 * i ) = 0;
        else if xt_all(i) < 0
                x_unipol( 2 * i - 1 ) = 0;
                x_unipol( 2 * i )     = - xt_all(i);
```

```
            end
        end
    end

    y=zeros(1,2*N);
for h=1:no_frames
    x=x_unipol(1+(h-1)*2*N:h*2*N);
    n=1;
    for u=1:2:length(x)
    x_unipol_positive(n)=x(u);
    x_unipol_negative(n)=x(u+1);
    n=n+1;
    end
    x_unipol2(1+(h-1)*2*N:h*2*N)=[x_unipol_positive
x_unipol_negative];
end


    % Add noise
    EbNo   = 10.^( EbNodB ./ 10 ); % ACO-OFDM bit energy-to-
AWGN ratio
    U_EbNo = 2 * EbNo;             % U-ACO-OFDM bit energy-to-
AWGN ratio
    EsNo   = U_EbNo *log2(M) / 8; % average symbol energy to
noise ratio --> EsNo = ( average(sigma_s)/sigma_n_r )^2 = (
sigma_x^2 / 2 )/sigma_n_r^2
    EsNodB = 10 .* log10 ( EsNo )+log10(1);
    EsNo=10.^(EsNodB./10);

    %hwait = waitbar( 0, 'waiting...' );  % waitbar
    for g = 1 : length( EbNodB )
        noiseStandardDeviation = sqrt(  var( x_unipol2 ) /
EsNo(g) );
        noiseSamples           = randn( 1, 2 * N * no_frames
);
        noiseSamples           = noiseStandardDeviation *
noiseSamples;
        xt_noise               = x_unipol2 + noiseSamples;

        % receiver
        xr_unipol = xt_noise;
        xr_unipol( xt_noise < 0 ) = 0;        % clipping the
negative values

        for t=1:no_frames
  x= xr_unipol(1+(t-1)*2*N:t*2*N);
  n=1;
  for u=1:N
     if x(u)>=x(u+N)
  xt_noise1(n)=x(u);
      else
```

```
            xt_noise1(n)=-x(u+N);
        end
        n=n+1;
    end
    xt_rec(1+(t-1)*N:t*N)=xt_noise1;
end



    for s=1:no_frames
        xrr=zeros(1,N)
         for m=1:N/2
     xrr=xt_rec(1+(s-1)*N:s*N);
     if xrr(m)>xrr(m+N/2)
     xt_rec_all(m+(s-1)*N)=(xrr(m)-xrr(m+N/2))/2;
     xt_rec_all(m+N/2+(s-1)*N)=-(xrr(m)-xrr(m+N/2))/2;
     else
         xt_rec_all(m+(s-1)*N)=-(-xrr(m)+xrr(m+N/2))/2;
     xt_rec_all(m+N/2+(s-1)*N)=(-xrr(m)+xrr(m+N/2))/2;
         end
     end
 end



          % OFDM demapping
          for i = 1 : no_frames
              xf = ( 1 / sqrt(N) ) * fft( xt_rec_all( 1 + ( i -
1 ) * N : i * N ), N );
              xf_all( 1 + ( i - 1 ) * N1 : i * N1 ) = xf( 2 : 2
: N/2 );
          end

          % QAM demodulation
          x_rec_final = qamdemod( xf_all*sqrt(1), M,0,'gray' );
          BER( k, g ) = biterr( x_rec_final, data ) / ( log2(M)
* N1 * no_frames );

      end
      end

figure;
semilogy( EbNodB, BER( 1, : ), 'b*-', 'LineWidth', 2,
'MarkerSize', 6  );
axis( [ 0 25 1e-4 1 ] );
grid;
xlabel( 'MACO OFDM bit energy-to-AWGN ratio,
{\itE_b}/{\itN_0}' );
ylabel( 'Bit-error rate, BER' );
```